YJEQ AND BACTERIAL RIBOSOME ASSEMBLY

UNDERSTANDING RIBOSOME ASSEMBLY: NEW APPROACHES TO DETERMINING THE FUNCTION OF *ESCHERICHIA COLI* YJEQ

By

BY GEORDIE F.S. STEWART, HONOURS ARTS SC.

A Thesis Submitted to the School of Graduate Studies in Partial Fulfillment of the Requirements for the Degree Doctor of Philosophy

McMaster University

DOCTOR OF PHILOSHPY (2015) McMaster University
(Biochemistry and Biomedical Sciences) Hamilton, Ontario

TITLE: **Understanding Ribosome Assembly: New Approaches To Determining The Function of *Escherichia Coli* YjeQ**

AUTHOR: Geordie F.S. Stewart Honours Arts Sc. (McMaster University)

SUPERVISOR: Dr. Eric D. Brown

NUMBER OF PAGES: xiii, 159

LAY ABSTRACT

In all cells, translation is carried out by ribosomes, large molecules that mediate the interpretation of the genetic code. These cellular interpreters are absolutely required for protein synthesis in bacteria and thus, are necessary for life. Like proteins, ribosomes themselves must also be synthesized, a process known as ribosome biogenesis. The ribosome consists of myriad RNA and protein components and is perhaps the single most complex machine in cells. Nevertheless, cells can build these enormous molecules in less than two minutes. This is made possible by a team of helper proteins, such as the bacterial assembly factor YjeQ. The function of this protein has evaded researchers, but there is growing evidence that it facilitates a key stage in the assembly process. Our work provides new detail into how this protein influences ribosome biogenesis, and how this in turn affects the overall health and proliferation of bacterial cells.

ABSTRACT

As the gateway to translation, ribosome biogenesis is a core cellular process that is highly efficient, accurate and regulated. This is made possible in part by a suite of ancillary proteins with diverse but poorly understood functions. One such factor, the *Escherichia coli* GTPase YjeQ, is suspected of playing a critical role in the assembly of the 30S ribosomal subunit. Here we demonstrate that the absence of this factor *in vivo* leads to an accumulation of a late-stage immature 30S subunit species. While these precursors lack several ribosomal proteins and feature a number of conformational abnormalities, they are competent for maturation, suggesting that they represent an assembly intermediate. We further demonstrate that YjeQ accelerates the maturation of these precursors *in vivo*. In addition, we explore the role of YjeQ through genetic interaction studies and substantiate a functional connection with the putative assembly factor RbfA.

A linear correlation between growth rate and ribosomal content has been observed for multiple wild-type microbes. We have examined this relationship in the Δ*yjeQ* strain and found there to be a significant increase in the total cellular ribosomal material in comparison to the wild-type. This phenotype is not wholly exclusive to perturbations in biogenesis. Indeed, linear correlations and elevated levels of ribosomal content are also observed for several translation mutants. The degree of elevation, however, is marginal in comparison to that seen in the biogenesis mutant. Our work explores this phenomenon and the possibility of exploiting it to identify and further characterize perturbations in the ribosome assembly process.

ACKNOWLEDGEMENTS

I wish to extend my sincere thanks to my mentor and supervisor Dr. Eric Brown, both for the opportunity to conduct this research and for his continued guidance and support in all things. I also thank committee members Joaquin Ortega, Marie Elliot and Justin Nodwell for their insight, consideration and challenge. I owe a debt of gratitude to all of my collaborators for sharing their research passions with me and guiding my curiosity. I thank the entire Brown Lab, past and present, as well as the labs of Dr. Ortega, Dr. Scott and Dr. Emili. Special thanks also goes to all of the members of the Ribosome Biogenesis group, Dr. Ahmad Jomaa and Dr. Matthew Scott for their creativity and sage advice on all things ribosomal. To the researchers tirelessly dissecting the ribosome assembly process – a hearty cheers and thanks. Keep the faith.

I kindly thank my parents, grandparents, sisters, relatives, friends and musicians who have all been key players throughout this process.

Lastly, I thank my partner in crime and all else, Erin, for her support, grace, brilliance and fortitude. She lent me the energy to keep going long after the last gradient. PLM.

TABLE OF CONTENTS

LIST OF FIGURES

Chapter 1

Chapter 2

Chapter 3

Chapter 4

Supplementary Figures

LIST OF TABLES

Chapter 1

Supplementary

ABBREVIATIONS AND SYMBOLS

16S	rRNA transcript component of the 30S subunit
17S	Precursor form of 16S rRNA
23S	Large rRNA component of the 50S subunit
30S	Small Ribosomal Subunit
3D	Three dimensional
50S	Large Ribosomal Subunit
5S	Small rRNA component of the 50S subunit
A	Adenine
Å	Angstroms
A-site	Aminoacyl-site
Amp	Ampicillin
Anti-SD	Anti-Shine-Delgarno Sequence
Ara	D-Arabinose
BME	Beta-mercaptoethanol
C	Cytosine
C-terminus	Carboxyl-terminus
cAA	M63 media supplemented with casamino acids
cryo-EM	Cryo-electron microscopy
E-site	Exit-site
EDTA	Ethylenediaminetetraacetic acid
EF	Elongation Factor
ESI-TOF	Electro-spray ionization time-of-flight
eV	Electronvolt
F	rRNA processing rate (P) divided by growth rate λ^{-h}
FASTA	FAST-All scripts for protein sequences
Fru	Fructose
GDP	Guanosine diphosphate
Glu	Glucose
Gly	Glycerol
GMP-PNP	5'-Guanylyl imidodiphosphate
GTP	Guanosine triphosphate
h44	Helix 44 of 30S subunit
IF	Initiation factor
iTRAQ	Isobaric tag for relative and absolute quantitation
Kan	Kanamycin
kt	Translational capacity
L-	Large subunit protein
LB	Luria-Bertani
m/z	Mass-to-charge ratio

M63	M63 minimal media
MALDI	Matrix-assisted laser desorption/ionization
Man	Manose
ML	Maximum-likelihood
MOPS	3-(N-morpholino)propansulfonic acid
mRNA	Messenger RNA
MS	Mass spectrometry
N-terminus	Amino-terminus
NT	Nucleotide
OB-fold	Oligonucleotide/oligosaccharide binding fold
OD600	Optical Density of culture at 600 nm
P	rRNA processing rate
p_{conc}	protein concentration (μg/OD_{600})
P-loop	Phosphate-binding loop
P-site	Peptidyl-site
Pre	Precursor
PTC	Peptidyltransferase center
r	RNA/Protein (mass/mass)
r_0	Basal level of non-translating RNA/Protein
r_{nf}	Non-functional ribosomal material in excess or r_0
R-protein	Ribosomal protein
RDM	Rich Defined Media
RNA	Ribonucleic Acid
RNA*conc*	Concentration of RNA (μg/OD_{600})
rrn	rRNA operon
rRNA	Ribosomal RNA
S-	Small subunit protein
SD	Shine-Delgarno Sequence
SDS-PAGE	Sodium dodecyl sulphate polyacrylamide gel electrophoresis
Spec	Spectinomycin
TOF	Time-of-flight
Tris	2-amino-2-hyrdoxymethyl-propane-1,2-diol
tRNA	Transfer RNA
V_{max}	Maximum enzymatic rate possible under Michaelis-Menten kinetics at saturating substrate concentrations
Zn-finger	Zinc-finger
Δ	Mutant
λ^{-h}	Specific growth rate
$\lambda_O{}^{-h}$	Observed specific growth rates
$\lambda_P{}^{-h}$	Predicted specific growth rates

DECLARATION OF ACADEMIC ACHIEVEMENT

Experiments highlighted in this thesis were designed and performed by myself under the mentorship of Dr. Eric Brown, except where stated in the preface of each chapter. Portions of Chapter 2 were designed and executed in collaboration with the lab of Dr. Joaquin Ortega, including the structural work, which was performed by Ahmad Jomaa. Dr. Matthew Scott served an advisory role in the design of experiments in Chapter 3. All committee members provided input over the course of study that guided project implementation.

CHAPTER 1. Introduction

1.1 ANTIBOTICS

1.1.1 Origins of the 'Wonder Drug'

Antibiotics are arguably one of the most successful therapeutic classes in the history of medicine. The famously serendipitous discovery of penicillin by Alexander Fleming and the development of early sulfa drugs by Gerhard Domagk revolutionized the treatment of infectious diseases caused by bacteria, many of which had been intractable for much of human existence [1, 2]. Likewise, seminal work conducted by Paul Ehrlich had profound implications for clinical practices and set the tone for the future of drug discovery. His search for the proverbial "magic bullet," a chemical capable of selectively targeting a pathogenic agent in a host, laid the foundations for chemical screening and defined a drug discovery paradigm that has persisted to present day [3].

The work by these early pioneers at the dawn of the antibiotic era paved the way for a golden age of drug discovery between 1940-1960, which saw the development and clinical introduction of the vast majority of antibiotics in use today [4]. The forty years that followed, however, were marred by stagnant development, with only one wholly new class of antibiotic being introduced. Only recently has there been renewed momentum in antibiotic discovery with a number of distinct classes emerging since 2000, including the oxazolidinones, lipopeptides, mutilins amongst others [5, 6].

1.1.2 The Threat of Microbial Resistance

Despite the string of therapeutic successes, nearly 75 years after the introduction of penicillin to the clinic bacterial infections are still a grave concern to global healthcare

(reviewed in [7]). The widespread emergence of microbial resistance is to blame; as pathogens have acquired the means to subvert antibiotic mechanisms, they have greatly undermined the therapeutic utility of nearly all clinically-relevant drugs (reviewed in [8]).

Resistance is by no means a new phenomenon, having evolved alongside and in response to antibiotic agents developed by bacteria that sought to fend off their microbial neighbours. Thus, the antibiotic resistance we encounter today is a legacy of microbial warfare that has been ongoing for millennia [9, 10]. It is no surprise then that resistance to our clinical repertoire has emerged, as it is the natural progression that follows the advent of any antimicrobial agent. The problem of microbial resistance, however, has been substantially compounded by the extensive and at times irresponsible use of antibiotics worldwide [7].

Mutation is the fundamental source of resistance. Antibiotics exert a selective pressure on microbes that favours those organisms with mutations conferring resistance. Thus, antibiotics have become victims of their own success as widespread use has cultivated an environment driving Darwinian selection of resistant pathogens [7]. With the emergence of seemingly pan-resistant pathogens, its has been postulated we may be on the verge of a post-antibiotic era, a gloomy scenario where the proliferation of resistance will render our therapeutic stockpiles ineffective [7]. In the context of this grizzly image, the impact of the hiatus in discovery is especially pronounced. Calls for action to stem the tide of resistance espouse responsible use and express an urgent need for innovation. One approach in responding to such calls will be to strengthen and diversify our catalogue of therapeutics. New drugs will require new targets.

1.1.3 The Ribosome as an Antibiotic Target

The ribosome is that cellular component, universal to biology, responsible for the interpretation of genetic code and its subsequent translation to the proteins that drive life. Generally speaking, the structure and function of this nucleoprotein is broadly conserved; two subunits of unequal size, comprised of multiple rRNAs and proteins, serve to catalyze peptide formation as dictated by mRNA transcripts [11]. The ribosomal active sites are remarkably similar across all three taxonomic domains and translation follows the same universal key to equate codons with their respective amino acids [12-14]. Despite many common attributes, however, the bacterial ribosome, and the process by which it achieves translation, differs from of that of eukaryotes in many respects [15-18]. It is these differences that have made selective targeting of this organelle possible and rendered it a cornerstone of our antimicrobial strategies.

As the center of protein synthesis, the ribosome is a vital and ubiquitous piece of cellular machinery. For this reason, bacterial ribosomes have long been an important focus of therapeutic research, with inhibitors of translation representing a major component of our antibiotic arsenal [18]. Indeed, out of the twelve major classes of antibiotics, seven target the ribosome [4]. This includes antibiotics of the following classes: tetracyclines, aminoglycosides, macrolides, chloramphenicol, streptogramins, oxazolidinones and mutilins [15, 19]. Collectively, these make up ~20% of annual global antibiotic consumption, with the first three classes playing a major role in modern clinical settings. This wealth of therapeutics, however, represents only a narrow range of ribosomal targets and, as such, a limited number of resistance mechanisms have

effectively undermined the clinical utility of drugs that disrupt bacterial protein synthesis [18, 20]. Thus, new means of perturbing ribosome function are needed if bacterial translation is to remain a useful antimicrobial target.

1.2. THE PROKARYOTIC RIBOSOME

1.2.1 Ribosome Structure and Function

The 70S bacterial ribosome consists of two distinct subunits, termed 30S and 50S in reference to their sedimentation coefficients [21]. The 30S, or small subunit, features 21 ribosomal proteins (r-proteins) and a singular strand of 16S rRNA that is 1542 nucleotides (nt) in length. The 50S large subunit is comprised of 34 proteins and both a 5S (120 nt) and 23S (2904 nt) strand of rRNA. These two subunits come together to form the functional 70S ribosome. The vast majority of this project has focused on the 30S subunit rather than the 50S subunit, and so special attention will be given to its structure, assembly and function.

The new millennium bore witness to the first high-resolution x-ray crystal structures of the 70S bacterial ribosome [22-27]. This work was eventually awarded the 2009 Nobel Prize in Chemistry, underscoring the magnitude of this achievement. The initial models and those that followed provided fresh insight into the architecture of the individual subunits and their corresponding functional sites (Figure 1.1). In addition, these structures revealed new levels of detail surrounding subunit association and interaction, including important points of subunit contact, such as the ‘inter-subunit’ bridges [26, 28].

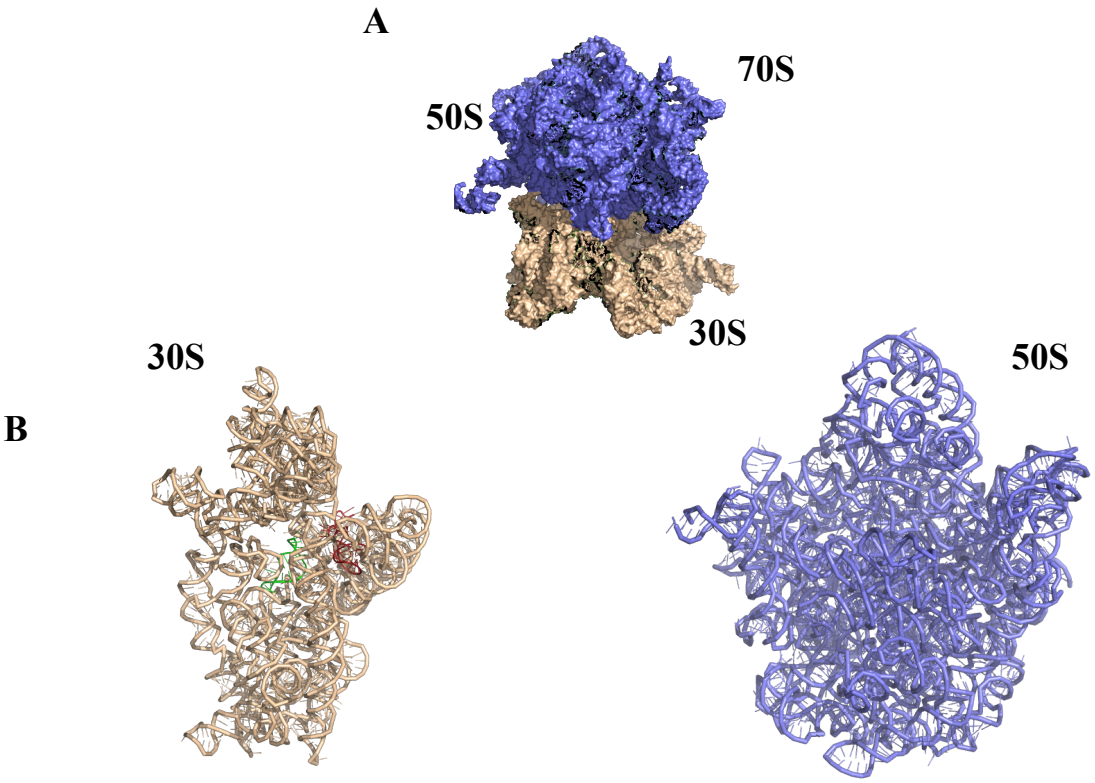

Figure 1.1: X-Ray crystal structure of RNA elements in the prokaryotic ribosome. A) *The figure shows a surface representation of the rRNA components of the 70S ribosome. The 23S and 5S rRNA transcripts are coloured in blue. The 16S rRNA transcript of the small subunit is coloured in beige. rRNA defines the general structure of the ribosome.* ***B)*** *A view of the subunit interfaces for the 30S and 50S subunits. The 5' and 3' terminal sequences of 16S rRNA discussed throughout are coloured in red and green respectively. This figure was created using MacPymol version 1.7.4.3 in conjunction with the structure published by Schuwirth et al. [27]. PDB ID 4V4Q.*

rRNA provides the scaffold that defines subunit structure (Figure 1.1) [24]. In general, most r-proteins are located on exterior, solvent-facing regions. As such, the functional core of both subunits is composed almost entirely of rRNA [24, 27]. Folding of the 16S rRNA subdivides the small subunit into four distinct globular subdomains. These include the body (5' domain), the platform (central domain) and the 3' major and minor domains. The compartmentalization of each of these regions enables independent folding and assembly [29-32]. The four subdomains coalesce around the decoding center of the

30S subunit. The 50S subunit is comprised of seven domains, six of which stem from the 23S rRNA [22]. 5S rRNA forms the seventh domain [33]. Unlike the 30S subdomains, these regions are not independent, but instead form a rigid half-dome structure. When viewed from the subunit interface, the 50S ribosome displays three extensions: The L1 stalk, the central protuberance and the L7/L11 stalk [27]. The large subunit houses the peptidyl transferase center (PTC), the region that catalyzes the formation of peptide bonds and mediates protein elongation [34, 35].

The functional regions of both subunits are located near their mutual interface. This environment is almost exclusively composed of rRNA, a testament to the enzymatic capabilities of this molecule [36]. The process of translation is carried out across three sites spanning both subunits: the A-site (aminoacycl), the P-site (peptidyl) and the E-site (exit) [37]. The 30S and 50S subunits have distinct functions in translation: the former facilitates mRNA binding and decoding while the later recruits tRNA and catalyzes peptide bond formation in the growing amino acid chain. The initial association of mRNA with the 30S subunit is facilitated by base pairing between the Shine-Delgarno (SD) sequence upstream of the translational start site on incoming mRNA and a complimentary sequence (anti-SD) housed on 16S rRNA [38].

Charged tRNA associates with both the small and large subunits, entering the ribosome at the A-site. Here, codon-anticodon matching between the mRNA transcript and incoming tRNA facilitates the incorporation of the appropriate amino acid into the growing peptide [39-41]. The decoding center is thought to validate this base pairing, qualifying the spatial geometry of cognate codon-anticodon complexes [42, 43]. The

correct geometry leads to conformational changes in the universally conserved 16S rRNA residues A1492, A1493 (of helix 44) and G530 that propagate translation [44-46]. Non-cognate base pairing leads to the expulsion of charged tRNA. This 'proofreading' process is subsequently followed by peptide bond formation between the growing protein and the incoming amino acid in the PTC of the 50S subunit. Not surprisingly, these key functional regions are targets of a number of antibiotic classes [15].

The process of translation is also mediated by a host of ancillary proteins including initiation factors (IF1, IF2, IF3), elongation factors (EF-Tu, EF-G, EF-P), termination factors (RF1, RF2, RF3) and ribosome recycling factors (RRF1, EF-G) [47-50]. These non-ribosomal proteins act in concert with the enzymatic abilities of the 70S ribosome to efficiently and accurately guide protein synthesis.

1.3 BACTERIAL RIBOSOME ASSEMBLY

While the processes involved in bacterial translation have been extensively studied and targeted by therapeutics, ribosome assembly has remained largely unexploited, owing to a limited knowledge of its *in vivo* mechanism [51]. In recent years, the expansion of our understanding of this process has created momentum for research into the feasibility and therapeutic potential of inhibiting biogenesis. In the current environment of microbial resistance, ribosome assembly may offer a promising new avenue for antibiotic development wholly distinct from protein translation.

In rapidly growing organisms like *Escherichia coli*, up to 40% of a cell's total energy can be invested in the ribosome-mediated interpretation of mRNA and protein synthesis [21]. This demand on resources necessitates strict regulation of translational

activities. For bacteria, the assembly of functional ribosomes represents a key component of this regulation and thus must be both highly efficient and tightly controlled [21, 52-54]. Considering the size and mosaicity of the mature ribosome, with over 50 proteins and 4500 nucleotides making up the final product, biogenesis is no small task [21].

1.3.1 *In vitro* Assembly

Seminal experiments by the Nomura research group demonstrated that 30S subunits could be assembled from purified ribosomal components, albeit under non-physiological conditions [55-57]. Likewise, the Nierhaus group demonstrated *in vitro* reconstitution of the large subunit [58-60]. This work established the order of r-protein binding and dependency by systematically examining the influence of individual proteins on assembly times. These results led to the formulation of the first assembly maps, which describe the prescriptive hierarchy of protein addition in building subunits (30S assembly map in Figure 1.2). Nearly half a decade later this model remains largely unchanged, though additional studies have provided further information regarding dependency, binding order and binding rates [61, 62]. In these maps, ribosomal proteins are classified into one of three categories reflecting their binding dependencies. Primary binders are those proteins that can bind directly to rRNA. Secondary binders require one or more primary r-proteins. Likewise, tertiary binders are dependent on the presence of secondary r-proteins [55, 57, 63]. In general, primary binders tend to coalesce around the 5' end of the 16S rRNA while tertiary proteins are more heavily concentrated at the 3' end [32, 64]. This is reflective of *in vivo* assembly, where proteins are added to nascent rRNA as it is transcribed in a 5' to 3' fashion (discussed in further detail below).

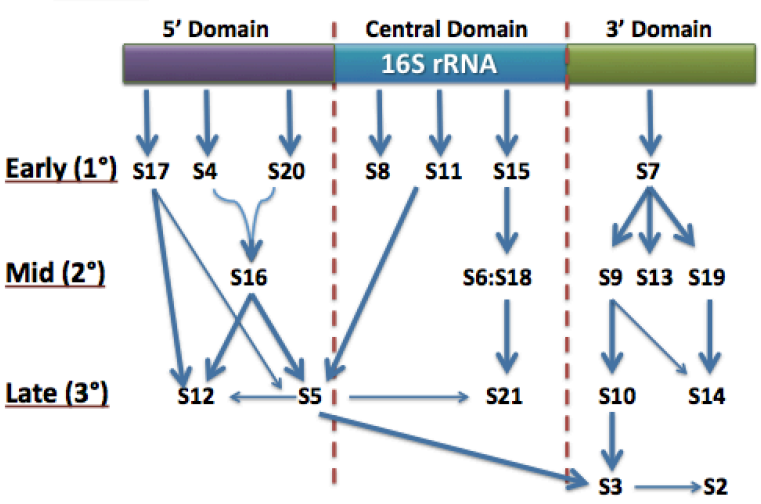

Figure 1.2: The Nomura assembly map. *The figure depicts the refined map of 30S r-protein binding order and dependency as determined by the Nomura research group. The arrows indicate a dependent relationship. The incorporation of early (1°) binders is dependent only on 16S rRNA. Mid and late stage binders (2° and 3°) require the presence of one or more of the early proteins. In vivo subunit assembly follows this hierarchy of protein addition in a 5' to 3' fashion [32, 57, 61, 63, 64].*

An assembly map has also been established for the large subunit; however, the hierarchy gleaned is far more complicated that that of its small counterpart [58-60, 65]. Reconstitution of functional 50S subunits from purified components is possible but requires conditions far from physiological. *In vitro* assembly occurs via three intermediates [58, 66]. The transition between these intermediates is dictated by the complement of proteins present as well as a series of shifts in temperature and magnesium concentration [58, 67].

That full functional subunits can assemble autonomously is a testament to the level of information encoded in rRNA and r-proteins. Much of the ribosomal scaffolding is dictated by the secondary structure of the individual rRNA transcripts. Many r-proteins

are thought to complement the intrinsic folding process by acting as chaperones, stabilizing proper confirmations and blocking aberrant ones (Reviewed in [21, 68]). Recent studies have demonstrated that subunit assembly does not follow a single linear and successive path. Instead, assembly occurs simultaneously at multiple sites along the rRNA transcripts [69-71]. As such, subunit maturation can proceed via multiple pathways populated with numerous stable, yet often non-native, intermediates [62, 72]. This necessitates an iterative approach to folding so that these intermediates ultimately converge on the proper confirmation. Ribosomal proteins are thought to play an important role in this process by guiding the assembling ribosome to intermediates capable of final maturation.

1.3.2 *In vivo* Assembly

In vivo assembly begins with the transcription of the *rrn* operon, which houses ribosomal RNA constituents and tRNAs (Reviewed in [21, 54, 68, 73, 74]). Many bacteria possess multiple copies of this operon (as many as 15), likely to support the high demand for protein synthesis that accompanies rapid growth and cell division [75]. There are seven nearly identical operons in *E. coli* (*rrn*A-E, G, H), from which all rRNA is transcribed (Reviewed in [68, 73]). Each operon codes for the three RNA transcripts necessary to manufacture a ribosome (16S, 23S, 5S) and one or two tRNAs. In addition, each operon features two tandem promoter sequences, P1 and P2, which govern expression [68, 73]. These promoter sequences are both exceptionally strong and highly regulated, allowing for tight responses to changes in environment and nutrient conditions [76-78].

Ribosomal RNA is transcribed as a single molecule, which subsequently undergoes successive rounds of processing to yield the mature forms of 16S, 23S and 5S (Figure 1.3) (Reviewed in [21, 68]).

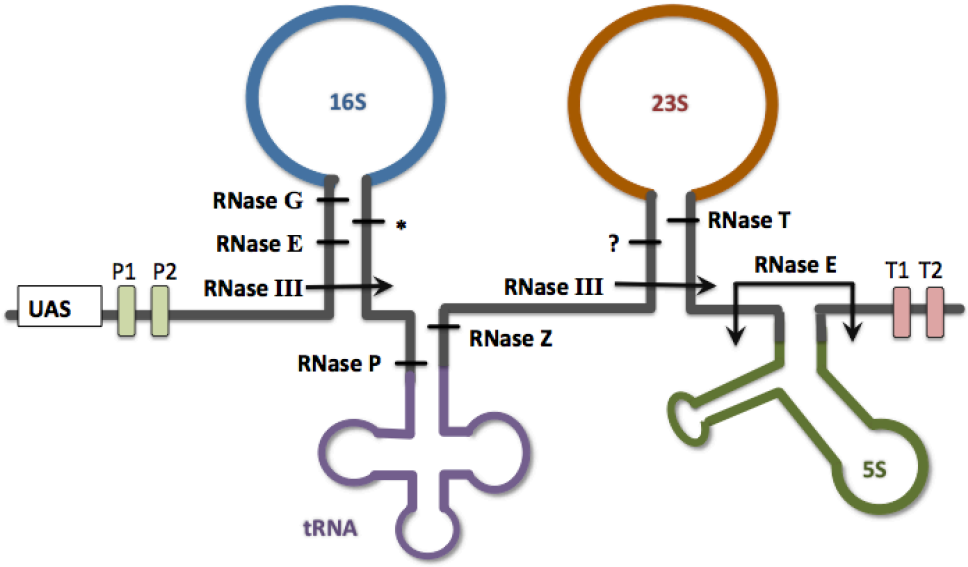

Figure 1.3: Processing of the primary RNA transcript in E. coli. *All of the RNA that makes up the ribosome is initially transcribed as one continuous molecule. The individual transcripts are released and processed by the coordinated action of several RNases. Cleavage sites are marked with dashes and labeled with their respective nucleases. The site marked with an asterisk (*) is thought to be processed by multiple enzymes (RNase II, RNase R, PNPase, RNase PH) [79]. The site labeled with a question mark (?) is cleaved by an unknown nuclease.*

First, cleavage by endonuclease RNase III releases precursor forms of each transcript [80-83]. These precursors are then modified by a series of nucleases to become mature transcripts. The immature 16S precursor, commonly termed 17S rRNA, features an additional 115 and 33 nucleotides (nt) at its 5' and 3' ends 3' ends, respectively. The 5' extension is trimmed by the coordinated action of RNase E, which cleaves the first 49

nt upstream of the precursor sequence, and RNase G, which cleaves the remaining 66 nt [80, 81, 84]. The enzyme responsible for processing the 3' trailer sequence has been elusive for many years. However, a recent study demonstrated that multiple processive exoribonucleases are capable of trimming this extension, including RNase II, RNase R and PNPase (* in Figure 1.3) [79]. In the absence of all three of these factors, processing may still occur by the action of RNase PH, albeit at a slower rate. If all four enzymes are absent, however, 3' maturation cannot occur [79]. Interestingly, failure to process the 3' end results in the accumulation of full 17S precursors, suggesting that 3' processing is a prerequisite for maturation of the 5' end. It has been suggested that the 5' and 3' precursor sequences base pair during assembly and that this pairing may act to prevent association of the 30S and 50S subunits either directly through steric hindrance or by maintaining an unfavorable conformation in the small subunit [25, 85]. The theory follows then that 3' processing by one of the exoribonucleases mentioned above eliminates this base pairing, releasing the single stranded 5' end so that it can in turn be processed [79]. Ultimately, this maturation step enables association of the free subunits.

The 23S precursor is fully functional and can be found in actively translating ribosomes despite the presence of additional nucleotides at the 5' and 3' termini (7 or 9 nt at the 5' and 3 or 5 nt at the 3') [83]. Nevertheless, these sequences are usually removed during maturation; RNase T trims the 3' terminus while a second, as of yet unidentified RNase is suspected to process the 5' end [86, 87].

The ribosome is built progressively on the nascent rRNA as it is transcribed, such that the progress of RNA production dictates the assembly of the ribosome [21, 51, 68].

Primary r-proteins begin to bind the 5' terminus as soon as it is transcribed, thereby facilitating the adoption of proper secondary and tertiary structure. The *E. coli* chromosome encodes 55 ribosomal proteins organized into 21 operons (Reviewed in [68, 88]) . The expression of these proteins is self-regulated; free ribosomal proteins bind to sites on their respective operons and repress transcription. When rRNA is abundant in cells, free r-protein concentrations are low as they are bound up in ribosomal subunits. When r-protein concentrations exceed rRNA in the cytoplasm, the free r-proteins will bind to down-regulate their own expression (Reviewed in [68]). This feedback mechanism, termed "translational coupling," gives rise to a robust system of control governing the production of ribosomal constituents. Consequently, the rate of RNA synthesis is directly correlated with ribosome levels [53, 89].

1.4 A DIVERSE COLLECTION OF RIBOSOME ASSEMBLY FACTORS

Though *in vitro* construction of the total ribosomal complex is possible, it requires lengthy incubations under non-physiological conditions [57, 58]. In contrast, rapidly proliferating *E. coli* produce functional ribosomes in 2-3 minutes [90]. Constructing a fully functional 70S ribosome within this time frame is suspected to require a host of ancillary factors. Indeed, in eukaryotes, more than 200 auxiliary proteins are known to be involved in ribosome biogenesis [91]. Though the assembly process in bacteria is less well characterized, a diverse and growing repertoire of proteins facilitating biogenesis exists (Figure 1.4, Table 1) [21, 68, 71, 92-94]. These auxiliary factors represent potential targets for small molecules that may provide a convenient and effective means by which to perturb the assembly process [51, 95].

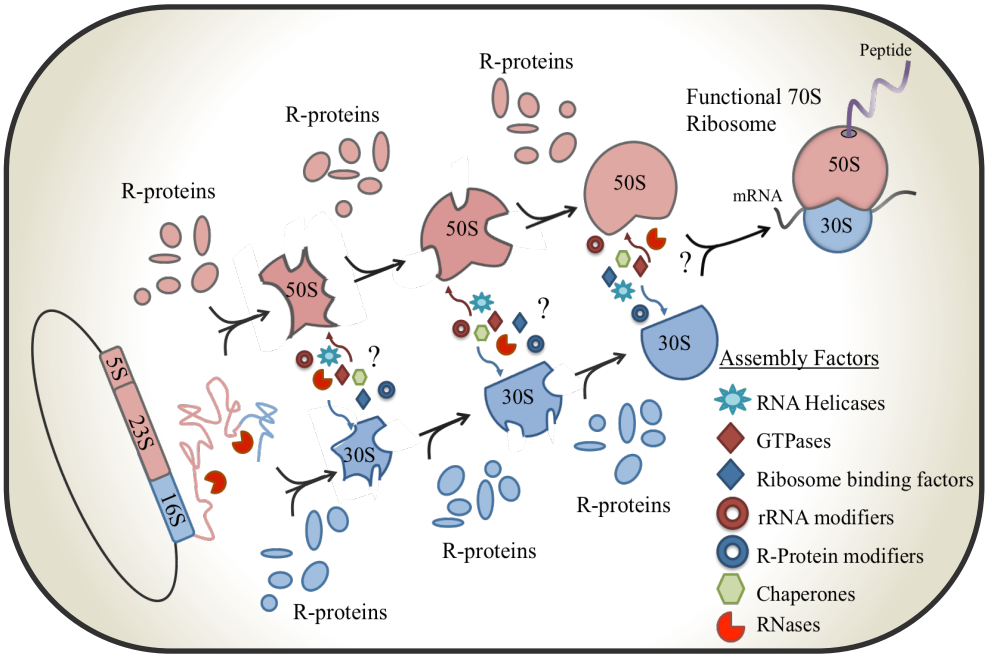

Figure 1.4: In vivo bacterial ribosome assembly. *In bacteria the assembly of the ribosome begins with the transcription of ribosomal RNA (16S, 23S and 5S). In addition to processing and folding of the rRNA, ribosomal proteins are added in sequence to the nascent transcripts. The end result of this process is the production of the 30S and 50S subunits, which subsequently associate to form a mature 70S ribosome. In vivo, the whole process occurs in just a few minutes. The mechanisms underlying this assembly and maturation are not well understood. A series of factors mediating the assembly process have been identified, however, their precise functions and temporal placement in the production line are not known. The emerging list of assembly protein is diverse, featuring RNases, GTPases, helicases, chaperones and modifying enzymes as well as a collection of RNA binding proteins.*

More than 50 trans-acting factors of diverse function, including RNases, chaperones and modification enzymes, have been implicated in biogenesis of the 30S subunit in bacteria [21, 71, 92, 94, 96-98]. Though the specific functions of some of these factors have been determined, there is a subset of proteins for which a cellular role and mechanism have been elusive [21, 99, 100]. This list of enigmatic factors includes the putative maturation factors RimM, RimP and RbfA, as well as the highly conserved GTPases, Era and YjeQ (RsgA) (Table 1).

1.1.1 Modifying Proteins

Ribosomal RNA undergoes extensive post-transcriptional modification. This includes both methylation as well as pseudo-uridinlyation. In *E. coli* this amounts to 24 methylated nucleosides (ten on 16S rRNA, 14 on 23 rRNA), as well as 10 pseudo-uridines (one on 16S RNA, nine on 23S rRNA) (Reviewed in [21, 101, 102]. In general, these modifications are thought to provide structural support to flexible ribosomal regions so as to maintain the optimal conformation for ribosome function [103]. Many of these modifications are located in functionally important regions; however, the enzymes responsible for them are largely dispensable. Notable exceptions include *rluD*, *ksgA*, *rrmJ* and *rlmA*, all of which have severe deletion phenotypes [98, 102]. Interestingly, the latter is essential for growth despite the fact that the modification it catalyzes is not, suggesting that is plays an additional role critical to viability [103]. Eleven ribosomal proteins can undergo modification via the addition of acetyl, methyl, methylthiol and glutamyl groups [104-106]. The function of most of these additions is not immediately obvious. Of the seven known enzymes responsible for r-protein modification only two, RimJ and PrmB, have discernible dispensability phenotypes [106, 107]. The factors responsible for the four remaining r-protein modifications have yet to be identified.

1.1.2 Helicases

Not surprisingly, several helicases have been found to play an important role in ribosome biogenesis. These factors facilitate proper folding through their ability to unwind rRNA (Reviewed in [21]). As the ribosome is built, nascent rRNA can adopt

unfavorable conformations that prevent further assembly. Helicases are thought to reverse this mis-folding in an effort to guide RNA to its correct state [94, 108]. The majority of helicases suspected to be involved in assembly belong to the DEAD-box family of ATPases, which use the hydrolysis of ATP to drive the unwinding of RNA. Two helicases of import to biogenesis, SrmB and CsdA, appear to play crucial roles in 50S subunit assembly [109, 110]. The absence of the former leads to an accumulation of a 50S precursor species that lacks ribosomal protein L13. Strains lacking SrmB also accumulate 17S rRNA, suggesting that the absence of this factor also impedes 30S subunit maturation [109]. Deletion of the gene encoding CsdA also gives rise to immature 50S subunits that lack late-stage r-proteins [110]. Both factors have been found to interact with their respective immature subunits, suggesting that they play a role in advancing these species to the mature form [110, 111].

1.1.3 Chaperones

Chaperones also appear to play an important role in ribosome assembly, particularly when temperatures deviate from the ideal. The DnaK/DnaJ/GrpE suite of chaperones has been found to govern protein folding and appears to aid in ribosome biogenesis [21, 96, 97]. At low temperatures, the deletion of either *dnaK or dnaJ* gives rise to a slow growth defect [112]. In addition, exposure to heat stress when these factors are absent results in the accumulation of both 30S precursors and 50S precursors. The temperature-sensitive nature of these defects points to a role for these proteins in overcoming energy barriers at restrictive temperatures [21]. This is reminiscent of the

temperatures-shifts required for *in vitro* reconstitution of ribosomal subunits. A second chaperone, GroEL/GroES, is also suspected of participating in assembly. This complex has been shown to facilitate the maturation of 50S precursors [113]. In addition, overexpression of GroEL/GroES suppresses the heat-sensitive ribosomal defect of dnaK/dnaJ-null strain [113]. This mitigating interaction suggests a level of functional overlap, further implicating both of these chaperones in ribosomal assembly.

1.1.4 Enigmatic Proteins: Maturation Factors and GTPases

For many modifying factors, such as the RNases and methylases, a general function is well established. The modifying activity of these proteins has provided convenient means by which to examine their interaction with, and specific influence on, the ribosome. There has been a great deal of success in mapping the residues and regions that these factors target. The challenge has been to clarify the role that these modifications play, if any, in ribosome biogenesis. The same cannot be said for the collection of so-called 'enigmatic factors' for which function remains elusive [95, 99, 100]. These proteins have been challenging to study, as they do not exert an obvious effect on ribosomes.

This list of enigmatic factors includes a number of multi-domain GTPases (30S: YjeQ, Era and 50S: ObgE, EngA, YihA) as well as a number of proteins that comprise only a single RNA binding domain (Reviewed in [21, 68, 71]). The latter include 30S maturation factors RimM, RbfA and RimP as well as 50S-binding proteins YhbY and YihI. While the specific function of these factors is not clear, there is a growing body of

evidence drawing on biochemical, genetic and structural studies that implicate each of these proteins in subunit maturation. Here, I briefly review the lines of evidence supporting a subset of factors believed to be involved in 30S biogenesis (RimM, RbfA, and Era). I then provide a comprehensive overview of YjeQ, the putative 30S assembly factor that was the primary focus of our work.

RimM

RimM is a non-essential protein, yet its deletion results in one of the most severe slow-growth phenotypes seen with any biogenesis factor [114, 115]. The absence of this protein leads to an accumulation of 17S rRNA and free subunits in cells [116]. RimM has been shown to bind the 30S subunit and is thought to interact with the 3' helices h31 and h33b of 16S rRNA as well as r-proteins S13 and S19 [114]. Recent work monitoring factor-mediated r-protein binding rates suggests that this factor accelerates the addition of S9, S19, S10 and S3 to 16S rRNA [70]. All four of these proteins are situated in the 3' domain and are proximal to the 3' 17S rRNA leader sequences [23]. *In vivo* footprinting work further suggests that this factor chaperones formation of the 3' end of 16S rRNA by mediating proper folding of helices 31 and 43 [117]. Collectively, this all points to a role in subunit assembly that is ultimately necessary for efficient processing of precursor rRNA, specifically at the 3' terminus.

RbfA

Like RimM, Ribosome Biding Factor A (RbfA) is a small single-domain protein with RNA binding motifs [118, 119]. This protein was first flagged as a 30S assembly factor because its overexpression suppresses a cold-sensitive C23U mutation in the 5' end

of 16S rRNA [118, 119]. Interestingly, overexpression of RbfA partially suppresses the slow-growth defects in a *rimM*-null strain, reinforcing their mutual involvement in 30S assembly [116]. This factor has been shown to stably bind the mature 30S subunit [119, 120]. In addition, recent studies have demonstrated that RbfA is also able to bind immature 30S ribosomal species, suggesting it may associate and remain with the assembling subunit through multiple stages of maturation [121].

Cryo-EM (cryo-electron microscopy) structural studies of RbfA in complex with the mature 30S subunits place its binding site near the 5' terminus of 16S rRNA of the small subunit, overlapping regions of the A and P sites that accommodate tRNA [120]. Association with this region appears to alter the 3' minor domain by displacing helices 44 and 45, which are adjacent to the leader sequences of precursor 17S rRNA. As such, RbfA is suspected to influence the maturation of the 3' domain and consequently, facilitate the processing of immature rRNA. Deletion of *rbfA* leads to an accumulation of 17S rRNA, free 30S and 50S subunits as well as a slow-growth phenotype [119, 122]. A subpopulation of 30S subunits in this strain is immature and features defects reminiscent of the immature subunits found in a *rimM*-null [117]. This includes missing tertiary r-proteins (S2, S3 and S21) as well as non-native conformations in the 3' major domain and helix 44 [117]. However, subtle differences between the immature ribosomal species from these two strains provide insight into their respective functions. *In vivo* characterization of the ribosomal intermediates suggests RbfA may play a role at multiples stages of assembly, promoting proper folding of the 5' domain early in the pathway and then chaperoning the formation of the central pseudoknot downstream [117].

Era

The broadly conserved GTPase Era (*E. coli* Ras-like protein) is one of only four known essential trans-acting ribosome biogenesis factors in *E. coli* (Reviewed in [21, 51, 68, 99, 100]. Depletion of this protein gives rise to assembly defects similar to *rimM* and *rbfA* deletions: accumulation of 17S rRNA and an increase in free subunits accompanied by a decrease in 70S ribosomes [123]. *In vitro* binding studies suggest that Era binds both 30S subunits as well as naked 16S rRNA, implicating it in small subunit function [124]. A cryo-EM structure of Era in complex with a mature 30S subunit substantiated this interaction and mapped its binding to the 3' terminus of 16S rRNA [124]. Interestingly*, in vitro* studies examining the influence of this factor on r-protein binding suggest Era expedites the addition of both 5' domain binders (S5 and S12) as well r-proteins that occupy the central (S11) and 3' domain (S19) [70]. Thus, this protein appears to influence the maturation of multiple domains at temporally divergent stages of assembly. As such, it has been suggested that Era may serve a high-level role in subunit assembly, possibly facilitating a maturation event with broad impact. Genetic interaction has been observed amongst Era and other putative assembly factors including RbfA and YjeQ [125, 126].

Common Phenotypes, Common Challenges

Dispensability studies have highlighted the importance of several biogenesis factors to cellular fitness and revealed a collection of common phenotypes indicative of involvement in subunit assembly and maturation (Table 1.1). For example, mutations in each of the aforementioned factors affect the processing of premature 17S rRNA [92-94, 96], a hallmark of perturbation in subunit maturation. Other dispensability phenotypes

shared by these factors include altered ribosome profile and sensitivity to cold temperatures. These phenotypes represent the primary indicators of factors involved in 30S biogenesis and, in addition to suggesting functional overlap, have been useful in assigning general putative roles [92]. Despite their utility, however, these phenotypes do not describe specific function.

Gene	Function	Dispensability Phenotypes			Interacts with	Cold sensitivity
		Growth	RNA	Ribosome Profile		
Era	GTPase	Essential	↑17S	↓ 70S, ↑30S & 50S	30S	✔
RbfA	Unknown	Slow growth	↑17S	↓ 70S, ↑30S & 50S	30S	✔
RimM	Unknown	Slow growth	↑17S	↓ 70S, ↑30S & 50S	30S	✔
RimP	Unknown	Slow growth	↑ 17S	↓ 70S, ↑30S	30S	✔
YjeQ / RsgA	GTPase	Slow growth	↑ 17S	↓ 70S, ↑30S & 50S	30S	✔

Table 1.1: Enigmatic factors with putative roles in 30S subunit biogenesis *[70, 116, 119, 121-133]. Discussed in detail in the main text.*

It is no small wonder then that modern efforts to delineate the assembly process have turned to structural studies enabling molecular resolution of factor-ribosome interaction. Advances in cryo-EM techniques and the development of rapid footprinting methods have provided means by which to analyze the assembling ribosome in resolutions not previously possible. These techniques will no doubt be key to further exploration of the assembly process; however, the technically demanding nature of these methods currently limits their use, especially in the context of high-throughput studies.

1.1.5 *Escherichia Coli* YjeQ

At the outset of this PhD thesis, the study of the YjeQ protein was still in its infancy. The impetus for the pursuit of this factor was initially grounded in a search for novel antibiotic targets amongst enigmatic and poorly-characterized GTPases of unknown function [99]. Our focus quickly shifted to the field of ribosome assembly as evidence amassed implicating this particular factor in ribosomal activities. Our group thus endeavored to further characterize YjeQ in an effort to adjudicate its potential as a therapeutic target and, more broadly, to contribute to the understanding of bacterial ribosome assembly. The following section details knowledge of YjeQ function and presents its gradual characterization as a backdrop for the studies that followed as part of this research project.

Structural Features

The 39 kDa *Escherichia coli* protein YjeQ represents a subfamily of orthologous P-loop GTPases broadly conserved in bacteria but absent in eukaryotes [134, 135]. These GTPases are comprised of 3 domains: an N-terminal oligonucleotide/oligosaccharide-binding fold (OB-fold) domain, a unique circularly permuted GTPase motif, and a C-terminal zinc-binding domain (Zn) [135, 136]. The OB-fold found in this family is present in many RNA-binding proteins, including translation factors and proteins involved in mRNA metabolism [136]. These observations were the provenance of the hypothesis that YjeQ plays a role in ribosome function. Campaigns to elucidate the function of this protein have provided further evidence supporting this notion and have

implicated YjeQ in ribosome biogenesis, specifically in 30S subunit assembly and maturation (discussed below).

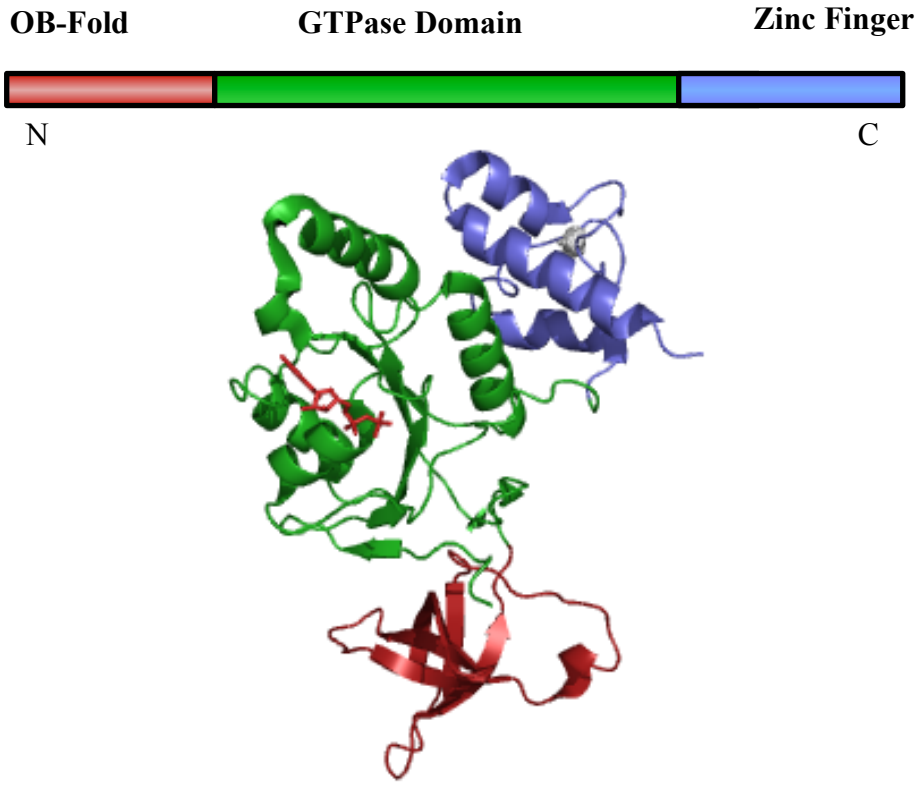

Figure 1.5: The structure of YjeQ. *The figure depicts X-Ray crystal structure of YjeQ from Thermatoga maritima refined to a resolution of 2.8 Å. The protein is shown in complex with a single molecule of GDP (red). The N-terminal OB-fold (dark red), the GTPase Domain (green) and the Zinc Finger (blue) of YjeQ have been highlighted. The figure was constructed with MacPymol version 1.7.4.3 using the atomic coordinates from the structure solved by Shin, et al. [137]. PDB ID 1U0L.*

Kinetic Properties

As a GTPase, YjeQ catalyzes the hydrolysis of GTP to GDP and inorganic phosphate. Detailed pre-steady state kinetic studies have revealed that catalysis is rapid, occurring at a rate of 100 molecules hydrolyzed per second (100 S^{-1}) [127]. Despite this rapid catalytic activity, YjeQ has a low steady state turnover of 8 h^{-1}. The deviation

between enzymatic potential and turnover is consistent with a slow, rate-limiting release of products [127]. Two active site residues in the GTPase domain, namely the lysine and serine at position 220 and 221, have been shown to be critical to the proteins catalytic activity. A double mutant harbouring substitutions at both of these residues (K220A, S221A) was found to drastically reduce the proteins V_{max} (~5% of wild-type) [127]. In contrast, a large truncation of the N-terminal OB-fold (removal of the first 113 residues) had little bearing on intrinsic GTPase activity, suggesting that this domain serves a functional role distinct from intrinsic GTP hydrolysis [127, 138].

Interaction with the 30S subunit

Association of YjeQ with the ribosome, particularly with the 30S subunit and 70S ribosome, has been shown to significantly stimulate the intrinsic GTPase activity of this protein (160 fold and 100 fold, respectively) [132, 138]. Both rRNA and protein components of the 30S ribosomal subunit are required for this stimulation and studies have suggested that YjeQ preferentially interacts and with fully mature 16S-containing ribosomes [132, 138]. In the presence of a non-hydrolyzable GTP analogue, GMP-PNP, YjeQ tightly binds 30S ribosomal subunits derived from wild-type cells [130, 138].

Multiple studies have illustrated that antibiotics targeting the A-site of the 30S subunit, such as members of the aminoglycoside class, inhibit the ribosome-stimulated GTPase activity of YjeQ [132, 139]. However, there have been conflicting observations regarding formation of the YjeQ-30S complex in the presence of these molecules. Himeno, et al. reported that aminoglycosides inhibit the association of YjeQ with the 30S subunit; it has been suggested that these antibiotics directly block interaction, thereby

preventing stimulation of GTP catalysis [132]. This implies that YjeQ and aminoglycosides bind similar locales in the vicinity of the A-site. In contrast, Campbell, et al. reported that while A-site antibiotics do inhibit stimulation of GTPase activity, they not prevent the formation of the YjeQ-30S complex [139]. An alternative hypothesis has been put forward suggesting that YjeQ binds at a region distal to the A-site, and that the observed inhibition of stimulation was of an allosteric nature. These conflicting theories highlight the necessity for further study to accurately determine the binding site of YjeQ and uncover its interaction with the 30S subunit.

Dispensability

Though dispensable, YjeQ is critically important to overall cellular fitness in *Escherichia coli*, *Bacillus subtilis* and *Staphylococcus aureus* [128, 132, 139]. Infection models in mice have demonstrated that this factor is required for full virulence of *Staphylococcus aureus*, which further emphasizes the importance of the gene product in cell viability [128]. Deletion studies have also revealed a collection of phenotypic defects implicating YjeQ in ribosome function, specifically in 30S subunit assembly and maturation. These include an altered ribosome profile featuring an accumulation of free 30S and 50S subunits (Supplementary Figure 1.1), as well as an increase in levels of unprocessed 17S rRNA. Both phenotypes are indicative of subunit immaturity [126, 139]. While these phenotypes are a hallmark for aberrant ribosome assembly, they can arise indirectly due to perturbation in a number of cellular processes. Further clarification of this factor's putative role in ribosome assembly requires an exploration of its linkage to the assembly process. This includes detailed characterization of the immature subunits

that arise from the deletion of the *yjeQ* gene as well as the proteins direct influence on these phenotypic defects.

Genetic interaction

A previous study of epistasis amongst ribosome-related factors revealed multiple proteins with genetic connection to YjeQ [126]. This work examined the influence of additional gene deletions on the growth rate and ribosomal profile of a *yjeQ*-null strain and uncovered interactions with multiple ribosome-associated factors including proteins involved in translation (*ssrA, tgt, trmU, trmE*) and ribosome assembly (*ksgA, rim, rluD*). In addition, the overexpression of several essential ribosome-related proteins was found to suppress the deleterious effects that arise when YjeQ is absent [126]. Both the essential translational component IF2 (initiation factor 2, *infB*) and the putative assembly factor Era (*E. Coli* Ras-like GTPase A, *era)* were found to partially ameliorate the slow-grow defect and aberrant ribosome profile in a *yjeQ*-null when overexpressed [126]. All of these interactions point to a role in ribosome function and provide opportunity for detailed study of their functional relationships.

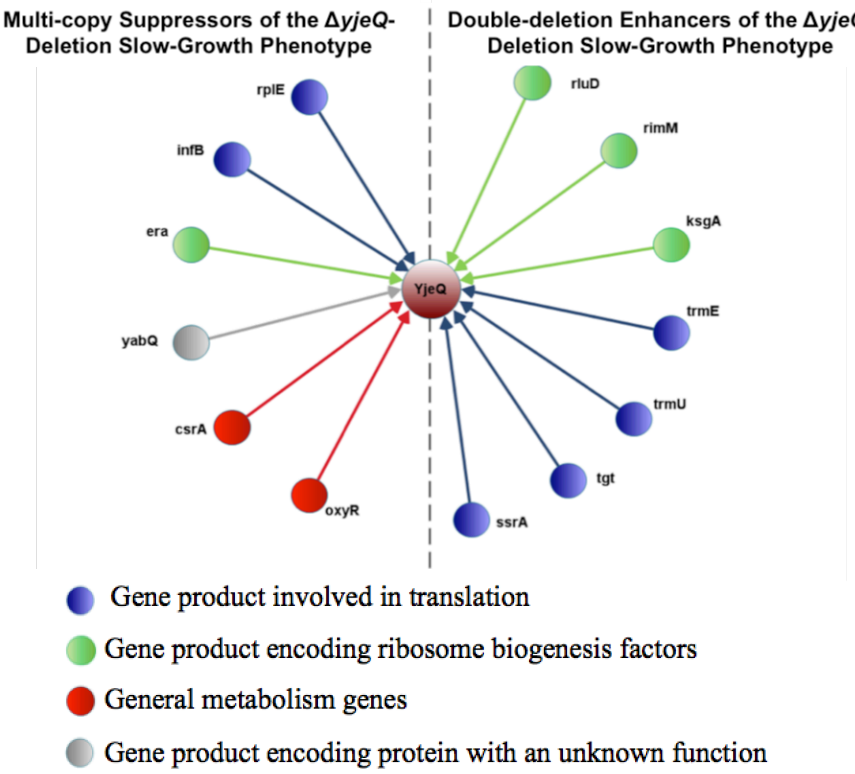

Figure 1.6: Genetic interaction with the ΔyjeQ deletion. *The figure depicts the interaction map developed by Campbell, et al. Multicopy supressors of the ΔyjeQ deletion strain are featured on the left hand side. Gene deletions that enhance the growth and ribosomal defects of the ΔyjeQ strain are on the right. The functional categories represented include genes involved in translation, biogenesis and metabolism as well as a gene of unknown function [126].*

1.5 PROJECT OBJECTIVES

A major focus of our research has been characterizing the function of YjeQ in ribosome assembly. However, the motivation underpinning this study has always been centered on exploring its potential as a therapeutic target. This required a deeper understanding of this factor's specific function within the broad context of bacterial survival. The developing image we have of its role in bacterial physiology depicts a

bacteria-specific protein that, though dispensable, is important for ribosome assembly and ultimately, cellular proliferation. As such, it is representative of a number of assembly factors and provides a platform by which we can assess the therapeutic potential of these would-be targets.

The work herein sought to further clarify the assembly process. This took the form of both a detailed investigation of YjeQ function through biochemical and structural means, as well as a study of the broader relationship between biogenesis defects and cell proliferation. Given the limits of phenotypes available to the field, we also endeavored to develop new tools with which to characterize perturbations in biogenesis. Ultimately, these efforts augmented our repertoire of assembly assays, which in turn were applied to further scrutinize our understanding of the role YjeQ plays in ribosome production. Chapters 2 through 4 of this thesis document these efforts as follows:

1.6 THESIS ORGANIZATION

Chapter 2: Understanding the role of YjeQ in 30S Subunit Maturation

- Exploring the composition of immature 30S subunits in a *yjeQ*-null
- Determining the cellular fate of immature 30S subunits
- Examining factor-mediated repair
- Determining the 30S binding site of YjeQ

Chapter 3. New Tools for Studying Biogenesis

- Development of new assays capable of uniquely identifying perturbations in biogenesis
- Study of the relationship between cell growth and ribosome biogenesis

Chapter 4. Exploring Genetic Interactions

- A detailed exploration of genetic interactions previously identified by Campbell et al. [126].

CHAPTER 2. The Role of YjeQ in 30S Subunit Maturation

2.1 AUTHOR'S PREFACE

This chapter contains experiments conducted as a part of two published manuscripts as well a third manuscript in preparation at the time of writing. The contributions and full citations for each are outlined below.

Section 2.3.1 Characterizing the Immature Subunits in the *ΔyjeQ* Deletion Strain

This section highlights work that contributed to the manuscript featured in reference [140]. All cryo-EM structural work was performed by Dr. Jomaa, Dr. Ortega and Dr. Martin-Benito. Proteomics were conducted by Dr. Zielke and Dr. Maddock. All RNA work and sample preperation for structural/proteins studies was completed by myself as a graduate student in the lab of Dr. Eric Brown. Dr. Ortega, Dr. Brown, Dr. Jomaa and I were all involved in analysis, interpreation and mansucript production. The full citation is as follows:

> Jomaa, A., Stewart, GFS., Martin-Benito, J., Zielke, R., Campbell, T., Maddock, JR., Brown, ED., Ortega, J. (2011) Understanding Ribosome Assembly: the Structure of *in vivo* Assembled Immature 30S Subunits Revealed by Cryo-electron Microscopy, *RNA*. **17**, 697-709.

Section 2.3.2 The Fate of the Immature Subunit

All work was designed and performed by myself in consultation with Dr. Eric Brown. The arabinose-inducible mutant (Δ*yjeQ*-ara) was created by Tracey Campbell in consultation with Dr. Brown. These studies were in preparation for publication at the time of thesis submission.

Section 2.3.1 Co-structure of YjeQ in Complex with Mature 30S Subunits

Work in this section was featured in the manuscript in reference [130]. All cryo-EM structural studies were performed by Dr. Jomaa, Dr. Mears and Dr. Ortega. Protein and occupancy work was performed by myself in consultation with Dr. Eric Brown and Dr. Ortega. Mass spectrometry for protein identification was performed by Inga Kireeva. The full citation is as follows:

> Jomaa, A., Stewart, G., Mears, JA., Kireeva, I., Brown, ED., Ortega, J. (2011) Cryo-electron microscopy structure of the 30S subunit in complex with the YjeQ biogensis factor, *RNA*. **17**, 2026-2038.

2.2 INTRODUCTION

One of the central focuses of this PhD thesis was an exploration of the role played by the putative ribosome assembly factor YjeQ. At the outset of our research there was a growing body of data implicating YjeQ in ribosome function, however, conclusive evidence of this protein's influence on the ribosome was elusive and its functional niche was only vaguely defined. Multiple studies have demonstrated that the absence of YjeQ leads to abnormal ribosome profiles that accumulate free 30S and 50S subunits (Supplementary Figure 1.1) [126, 139]. While this is a hallmark for perturbation in ribosome assembly, there is little detail as to how the absence of YjeQ gives rise to this phenotype. Naturally, further delineation of the role this enigmatic factor plays in assembly called for an examination of its influence on and interaction with its putative substrate, the 30S ribosome.

Until recently, most studies examining biogenesis relied heavily on biochemical and genetic assays to interrogate function. However, in the wake of the first 3D models of the ribosome there was new opportunity to explore the assembly process using structural methods. This provided a new avenue by which to examine in detail the relationship between ribosomal structure and the action of ancillary assembly factors.

Our research involved participation in a multi-lab collaboration to characterize 30S ribosomal subunits in a strain lacking the YjeQ protein. This involved an in-depth analysis of the RNA and protein constituents that make up the small ribosomal subunit as well as an examination of subunit structure. Comparison of 30S ribosomes derived from the wild-type and *ΔyjeQ* strains revealed several variations in structure and composition

that suggest the mutant strain harbors a late-stage immature 30S subunit species [140]. The structure, detailed below, represents one of the first published 3D reconstructions of an immature ribosomal species and highlights a number of conformational aberrations in the mutant. Further biochemical study by our group has indicated that the Δ*yjeQ* precursor subunit is relatively long-lived but nonetheless competent for maturation. Thus, the species we have characterized is suspected to be an example of a *bona fide* assembly intermediate. In addition, we have illustrated that maturation of the precursor species is accelerated in the presence of YjeQ and that this influence occurs downstream of precursor formation.

One of the strongest lines of evidence implicating YjeQ in ribosome function is its interaction with the 30S subunit. There has been tremendous work documenting the stringency of this interaction as well as its bearing on the enzyme kinetics of YjeQ-catalyzed GTP hydrolysis. However, as discussed in Chapter 1, a concrete binding site has been elusive. We have developed a 3D co-structure of YjeQ in complex with the 30S subunit to clarify this interaction.

2.3 RESULTS

2.3.1 Characterizing Immature Subunits in a *ΔyjeQ* Deletion Strain

Precursor RNA in the yjeQ-null

Total RNA was extracted and purified from both wild-type and *ΔyjeQ* strains and resolved by gel electrophoresis (Figure 2.1 B). Visualization of the RNA species revealed a decrease in the relative level of fully processed 16S rRNA in the Δ*yjeQ* strain in comparison to the wild-type. In addition, two other species of rRNA were found to be

abundant when YjeQ is absent: a slower migrating 16S precursor and a faster migrating species suspected to be a truncation product. We investigated the identity of these species via northern blot analysis, using radiolabeled oligonucleotides complimentary to the 5' and 3' terminal regions of 17S rRNA (Figure 2.1 C). Both probes were found to bind to the precursor sequence found in the *yjeQ*-null, indicating that the slower migrating species was in fact fully unprocessed 17S rRNA. The faster migrating species did not pair with either terminal probe; however, it did bind a control oligonucleotide complimentary to an internal sequence of 16S rRNA. As such, it is suspected that this rRNA species is likely a breakdown product originating from either the 17S precursor or mature 16S rRNA. Work by Hase et al. suggests that this rRNA species is a 3' truncation of mature 16S rRNA [141]. The mechanism by which this species emerges remains unclear, as does the functionality of the corresponding 30S subunits. Elevated levels of 17S rRNA are indicative of defects in subunit maturation and corroborate the altered ribosome profile previously observed for the *ΔyjeQ* deletion strain. As such, these findings lend credence to the hypothesis that YjeQ plays a role in 30S subunit assembly.

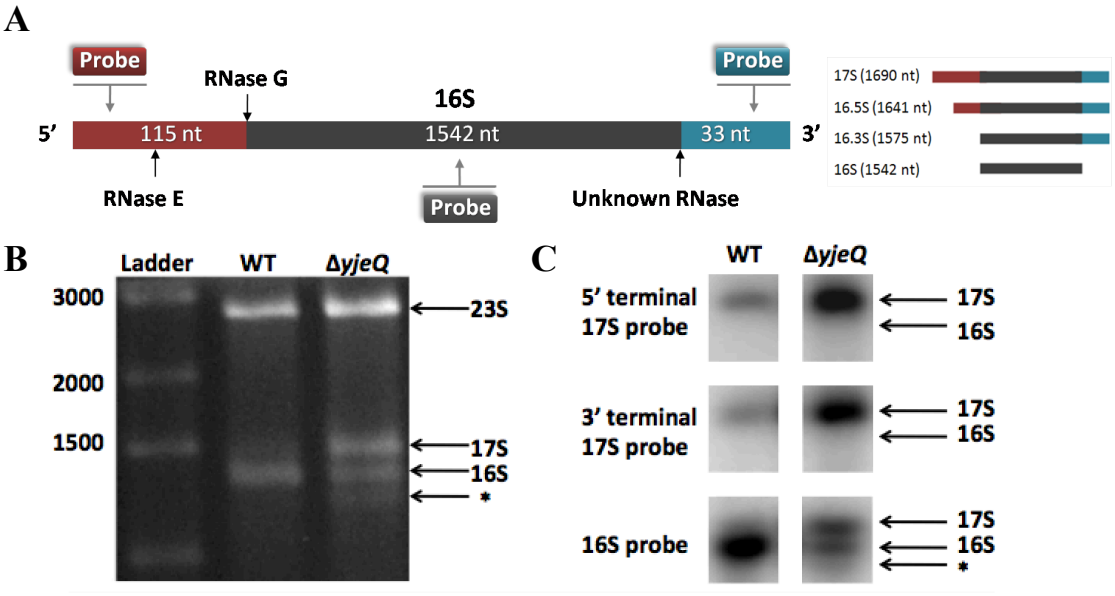

Figure 2.1: Deletion of yjeQ leads to the accumulation of precursor rRNA. A) *Schematic outlining 17S rRNA maturation, cleavage sites and the intermediates resulting from successive ribonuclease cleavage. The target location for the radiolabeled probes is indicated.* ***B)*** *Electrophoretic analysis of rRNA derived from the wild-type and yjeQ-null strain cell extracts. The wild-type gel pattern exhibited only two bands with migration corresponding to mature 16S and 23S rRNA. Two additional bands were observed in the ΔyjeQ deletion strain corresponding to a precursor form of 16S rRNA (17S label) and a previously identified species suspected to be a degradation product (asterisk, *).* ***C)*** *The identity of the precursor 16S rRNA found in the yjeQ-null strain was confirmed by northern blot analysis using radiolabeled DNA sequence specific probes directed at the 5' and 3' terminal sequences of 17S rRNA. Hybridization of these probes with the rRNA precursor derived from the yjeQ deletion cell extract indicated that the species was indeed full 17S rRNA. Mobility of the 16S rRNA and 17S rRNA is indicated. Figure modified from Jomaa et al.* [140].

Protein complement of the immature subunit

The protein composition of immature 17S-containing ribosomes was examined using iTRAQ (isobaric tag for relative and absolute quantification) mass spectrometry [142]. This technique provides for the identification and relative quantification of subunit proteins, enabling the detection of variation in the protein complements of subunits

derived from wild-type and *ΔyjeQ* cells. As the majority of mature 16S rRNA is harboured within the functional 70S ribosomes, it was suspected that the 30S peak of the *ΔyjeQ* deletion would be primarily comprised of immature 17S-containing subunits. As such, ribosomes from both strains were purified under non-dissociating conditions (10 mM magnesium acetate) and the 30S peak was collected for proteomic analysis. A double duplex isobaric labeling experiment was performed to characterize the proteins in the purified 30S subunits. We successfully identified 1207 peptides that represented 41 distinct proteins. Each species was identified by a minimum of two peptides with 95% confidence. All 21 small subunit proteins were successfully identified along with 11 50S subunit proteins and nine additional non-ribosomal proteins. The presence of the latter suggests a small level of contamination, with the 50S r-proteins arising due to incomplete resolution of subunits in the ribosome profile. Nevertheless, we were able to perform comparative analysis of the relative quantities of each protein species in 30S subunits derived from the wild-type (predominantly mature, 16S) and the *ΔyjeQ* deletion strain (predominantly immature, 17S). These quantities, expressed as a ratio *ΔyjeQ*:WT, can be found in Figure 2.2. Though the protein content of both 30S subunit samples was found to be similar, our analysis did reveal a subset of r-proteins that were significantly underrepresented in the Δ*yjeQ* 30S sample, including S21, S1 and S2. All three of these r-proteins are known to bind the 30S subunit in the late stages of assembly, suggesting that the immature species from the *yjeQ*-null may represent a 30S subunit in the terminal stages of maturation. Several other r-proteins were marginally underrepresented in the

immature *ΔyjeQ*-derived 30S subunit. These included tertiary late-stage binders S3 and S5, secondary binders S13 and S16, as well as primary r-proteins S7, S8 and S11.

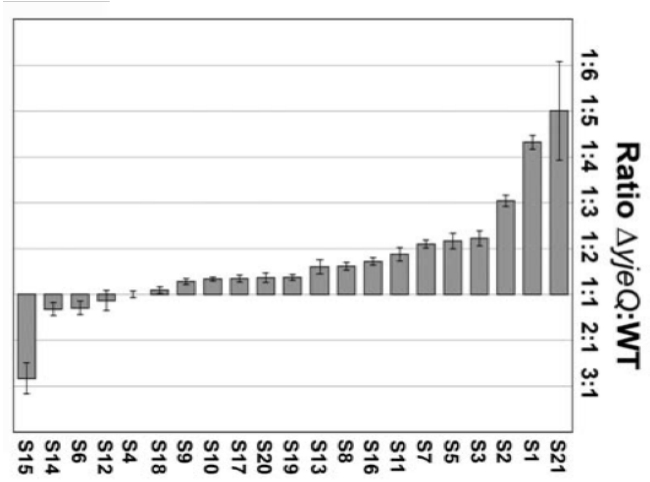

Figure 2.2: iTRAQ analysis of r-protein content in 30S subunits derived from the ΔyjeQ deletion strain. *The graph illustrates the level of 30S r-protein content in the ΔyjeQ deletion strain relative to 30S r-protein content in the wild-type. Relative levels for each protein are expressed as a ratio of ΔyjeQ:WT. Ratios were derived from the average of two replicate experiments. Only peptides that were capable of indicating a protein with ≥95% confidence were used to determine these ratios. Error bars represent the standard error of the mean for each protein ratio. The late stage r-proteins S21, S2 and S1 are significantly underrepresented in ΔyjeQ 30S subunit. Figure modified from Jomaa et al. [140].*

Structure of the immature 30S subunit

We obtained three-dimensional reconstructions of 30S subunits purified from the wild-type and Δ*yjeQ* strains using cryo-electron microscopy (cryo-EM) (Figure 2.3). Purification of these subunits was achieved via sucrose gradient ultracentrifugation and fractionation. As the immature species co-migrates with free 30S subunits during centrifugation, purification of a heterogeneous sample was unavoidable. As such, a

supervised classification method was employed to eliminate projections of mature 30S subunits in the Δ*yjeQ*-derived samples [143, 144]. The remaining projections were used to develop the structure of the immature subunit, which was refined to a resolution of 11.6 angstroms. A homogenous preparation of 30S mature subunits derived from the wild-type strain was used for comparative purposes. The resulting structures both feature all major landmarks of the 30S subunit, suggesting that the species derived from the Δ*yjeQ* strain was largely mature. However, comparative analysis did reveal a series of distinct differences (Figure 2.3).

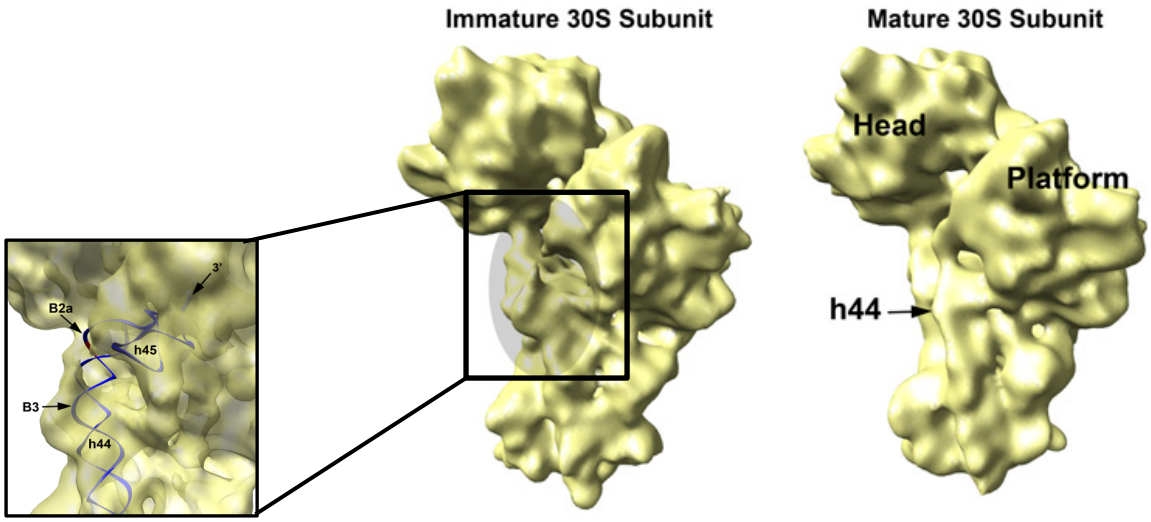

Figure 2.3: The structure of the immature 30S subunit derived from ΔyjeQ cells*. The cryo-EM maps of the both wild-type and ΔyjeQ subunits are shown. These two species represent immature and mature subunits respectively. Both 30S subunits are oriented to provide a view of the ribosomal interface. The framed area in the immature species highlights the region around helix 44 and the decoding center. These features are distorted in the EM map of the immature 30S subunit purified from ΔyjeQ cells. The inset features a magnification of this region with helix 44 and 45 from the X-ray structure of the wild-type 30S subunit fit into the cryo-EM map of the immature subunit to illustrate the variation between the two species of subunits. Main landmarks of the 30S subunit are indicated. Landmark abbreviations are: h44 (helix 44), h45 (helix 45), B2a (Bridge 2a), B3 (Bridge 3) and 3' (3' terminus of the 16S rRNA molecule). Figure modified from Jomaa et al. [140].*

The most profound variation observed was the distortion of the 3' minor domain, specifically helix 44, a central component of the decoding center and an important locale for inter-subunit contact. In agreement with the iTRAQ results, decreased density was observed in the mutant subunit in the region usually occupied by r-protein S2.

Collectively, these findings depict an image of a structurally immature 30S subunit that accumulates as a result of the deletion of *yjeQ*. However, this work did not clarify whether this immature species constitutes an authentic assembly intermediate on the path to maturation or an off-pathway species bound for degradation. Determining which of these two fates await the immature species will aid in narrowing the scope of future interaction studies.

2.3.2 The Fate of the Immature Subunit in a Δ*yjeQ* Deletion Strain

Persistence of the ribosomal defect

The defects in ribosome assembly observed in the *yjeQ*-null strain are suspected to be the underlying cause of its slow growth. To more clearly define this relationship, we performed a series of experiments to assess these defects with respect to growth and the presence of the YjeQ protein. To this end, we examined the distribution of ribosomal subunit species over time, using 17S rRNA as proxy for immature 30S subunits. The conversion of precursor 17S rRNA to 16S rRNA is thought to be one of the final stages in subunit maturation and the formation of a functional 70S ribosome [145]. Indeed, previous studies suggest that this event occurs in polysomes, with the processing taking place once the small and large subunits are associated [145]. Thus in most cases, the

emergence of 16S rRNA can be considered indicative of the formation of fully mature functional 70S ribosomes.

Wild-type and *yjeQ*-null (MG1655) cultures were grown at 37°C for 10 hours and aliquots of cells were harvested at 60 minute intervals over the course of growth. Total RNA was subsequently extracted and purified from each sample and resolved by electrophoresis. As expected, rRNA isolated from the wild-type strain was primarily comprised of mature 23S and 16S rRNA (Figure 2.4, top panel). This remained the case throughout exponential and stationary phase. In contrast, rRNA extracted from the Δ*yjeQ* strain contained large quantities of immature precursor 17S rRNA (Figure 2.4, middle panel). The level of 17S rRNA remained constant throughout exponential growth. A robust decrease in the level of 17S rRNA was observed only as cultures entered and continued through the stationary growth phase approximately 10 hours after inoculation. Once cells have entered into stationary growth phase the demand for new ribosomes is drastically reduced [146]. Thus, the eventual reduction of 17S rRNA in the Δ*yjeQ*-deletion strain is suspected to result from a deceleration in growth and a corresponding decrease in ribosome production rather than a compensatory mechanism.

A conditional *ΔyjeQ* deletion strain (*ΔyjeQ*-ara) was used to assess the capacity of YjeQ to repair assembly defects and rescue cell growth. This strain lacks a copy of *yjeQ* at its native locus but features an ectopic copy of the gene placed under the control of the araBAD promoter (*yjeQ*::kan; *araBAD*::*yjeQ*-amp). Reintroduction of the protein into depleted cells by induction (2 %, after 4 hours of growth) resulted in a rapid and robust decrease in 17S rRNA levels (Figure 2.4, bottom panel). Within one hour of

complementation, the rRNA profile of the conditional deletion cells resembled that of wild-type cells. This observation does not directly implicate YjeQ in the processing of 17S rRNA, however, it does indicate that the defect in processing is rapidly reversible when YjeQ is present.

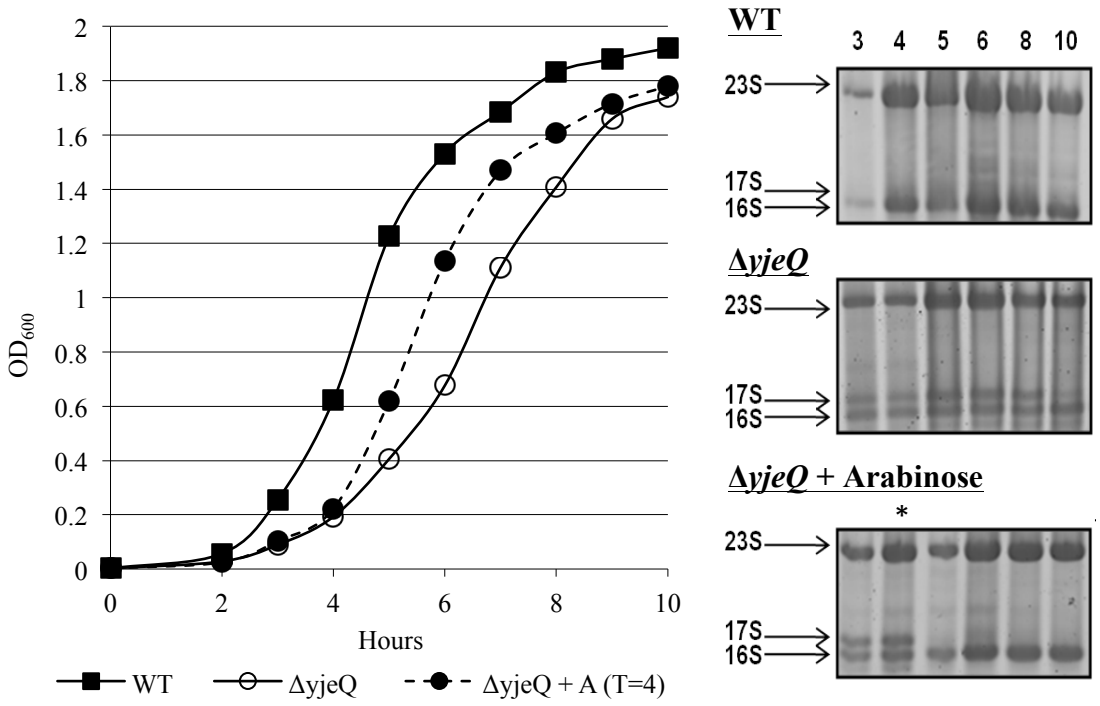

Figure 2.4: Profiling of ΔyjeQ cellular rRNA with respect to growth at 37°C. A) *The figure shows growth curves (OD_{600}) and rRNA profiling for wild-type MG1655 (top panel), ΔyjeQ (middle panel), and a ΔyjeQ mutant strain complemented with expression from the araBad locus (bottom panel). Cultures were grown for 10 hours at 37°C. Growth (OD_{600}) and rRNA profile was monitored each hour until the strains reached stationary phase. In the wild-type, 16S rRNA is predominant over the course of growth. In the yjeQ-deletion there is an increased abundance of precursor rRNA. The relative levels of 16S and 17S rRNA remained constant until late exponential/early stationary growth phase when a decrease in 17S rRNA was observed (lane 6). Expression of YjeQ was induced after 4 hours of growth (*). Prior to induction, the RNA profile and growth curve resembled that of the yjeQ-null. At 5 hours the RNA profile is nearly wild-type and the growth rate increases substantially.*

Monitoring the immature subunit via pulse-chase

While our structural and compositional analysis shed light on the characteristics of the immature 30S subunit, it did not provide insight as to the eventual fate of this ribosomal species in cells. We hypothesized two possibilities: these subunits represented either a dead-end by-product of defective assembly bound for degradation and recycling, or, they were in fact an assembly intermediate, en route to maturation and incorporation into functional 70S ribosomes.

Pulse-chase labeling techniques using ^{14}C-uridine, in combination with gel electrophoresis, were employed to monitor the maturation of rRNA in *ΔyjeQ* cells. This enabled us to track the progress of a discreet population of ribosomes over time with 16S/17S rRNA species serving as proxies for mature/immature subunits respectively. An off-pathway or dead-end species would not be expected to undergo further maturation. In this scenario, 17S rRNA should remain in cells for a significant period of time, only disappearing once subunits undergo degradation and recycling. In contrast, a true assembly intermediate competent for maturation will eventually yield mature 30S subunits, and ultimately, functional ribosomes. This maturation can be identified by the stoichiometric conversion of 17S rRNA to 16S rRNA over time. These hypothetical outcomes are depicted in Figure 2.5

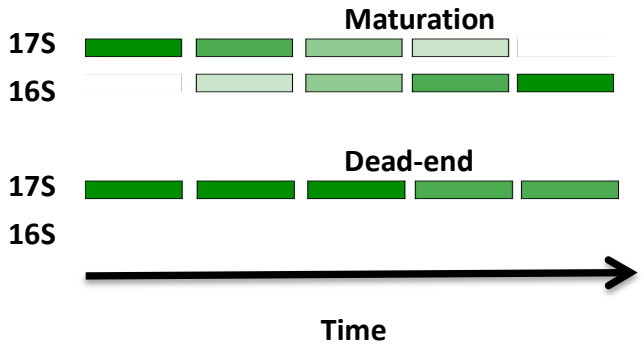

Figure 2.5: Possible outcomes of the pulse-chase maturation experiment for the ΔyjeQ strain. *The green bands depict labeled 17S and 16S rRNA levels in cells over time. In the top scenario, the immature species undergoes further maturation resulting in a decrease in 17S rRNA and a concomitant increase in 16S rRNA. In the bottom scenario, the immature rRNA is part of a dead-end product and will instead eventually disappear due to degradation.*

Wild-type and Δ*yjeQ*-ara cultures were grown to early exponential growth phase in a rich media (Rich Defined Media supplemented with glucose, Teknova). Cells were then exposed to a brief 'pulse' (5 minutes) of ^{14}C-uridine in order to label rRNA. Following this incubation, cultures were treated with an excess of unlabeled uridine to quench the initial radiolabel. Cells were then incubated for at least one doubling of optical density (OD_{600}). Aliquots (0.5 ml) were harvested at regular intervals (WT=1 minutes, KO=10 minutes) by centrifugation and fast-frozen in a dry ice-ethanol bath. Total RNA was then isolated, purified and resolved by electrophoresis. The rRNA was subsequently transferred to a nitrocellulose membrane and the radiolabeled RNA was imaged using a multimode reader in combination with a phosphor screen.

Imaging of radiolabeled rRNA from the wild-type illustrated the rapid disappearance of a band corresponding to 17S rRNA and the concomitant emergence of a second band representing mature 16S rRNA (Figure 2.6 A). These results confirm that the

conversion of the immature species to the mature form occurs quickly in wild-type cells; nearly all of the labeled 17S rRNA was mature within approximately six minutes of the initial pulse. This time-course for maturation is significantly less than the doubling-time for wild-type cells grown in these conditions (~ 22 minutes). In contrast, radiolabeled precursor rRNA derived from the Δ*yjeQ* strain remained unprocessed for substantially longer (Figure 2.6 B). Significant quantities of 17S rRNA persisted even after 60 minutes of growth (approximately 1.5 doublings). There was however a clear stoichiometric emergence of 16S rRNA as 17S levels waned over the full 90-minute course. This suggests that the majority of precursor subunits did proceed to a mature form.

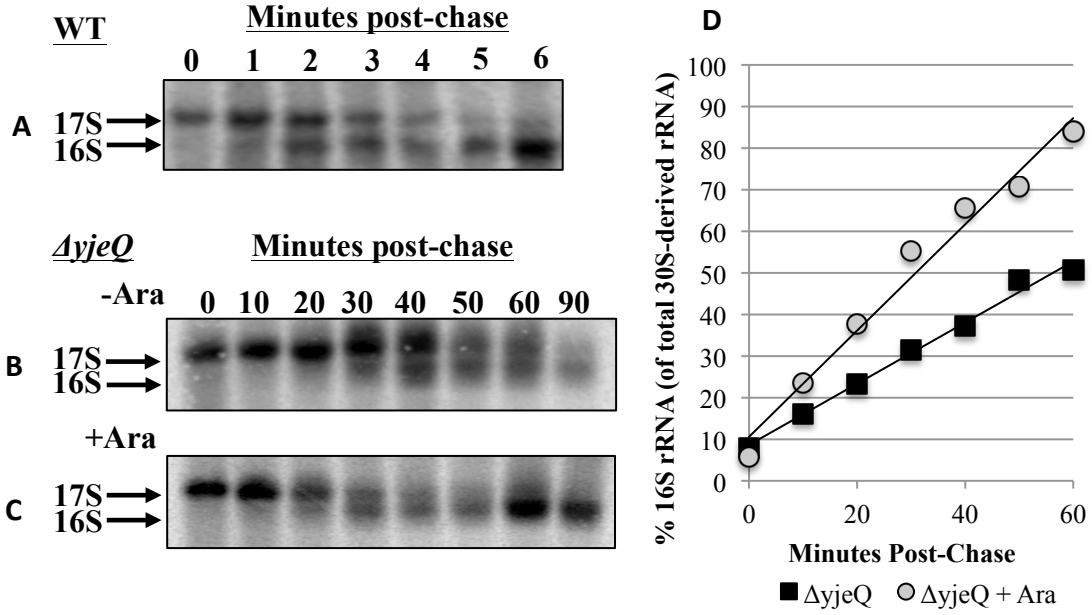

Figure 2.6: Pulse-chase reveals processing of 17S rRNA in the ΔyjeQ deletion strain. *Cells were grown at 37°C with shaking and were pulsed with 0.1 µCi/ml of ^{14}C-labeled uridine for 5 minutes. The culture was subsequently chased with an excess of non-labeled uridine (100 µg/ml). Samples were harvested at regular intervals throughout growth (wt = 1 minute, ΔyjeQ =10 minutes) and total RNA was isolated and resolved by electrophoresis. Samples were subsequently transferred to a nitrocellulose membrane and the label was visualized using phosphor screens in combination with a Typhoon™ multimode imager.* ***A)*** *Radiogram of labeled 30S-rRNA from the wild-type strain. The*

radiolabel reveals a nearly homogenous population of precursor 17S rRNA at the beginning of the time course. This species is readily processed as is indicated by the appearance of 16S rRNA. After ten minutes of growth (approximately half of a doubling), nearly all of the rRNA present is of the mature form. ***B)*** *Radiogram of labeled 30S-rRNA in the ΔyjeQ deletion strain. Initially, only 17S rRNA is detected and this precursor persists for substantially longer than in the wild-type (>40 minutes). After 90 minutes of growth (approximately two doublings) nearly all 17S precursor rRNA has been converted to mature 16S form.* ***C)*** *Radiogram of labeled 30S-rRNA in the ΔyjeQ strain complemented with YjeQ under araBAD control. Arabinose was added immediately following the chase (0 minutes). Precursor rRNA persists beyond the wild-type duration; however, conversion appears to be accelerated by the presence of YjeQ. After 50 minutes, nearly all rRNA is of the mature form.* ***D)*** *A plot tracking the percentage of small subunit rRNA that is 16S rRNA (16S/(16S+17S)) over time. The levels of rRNA species were quantified using ImageQuant version 5.2. The percentage of 16S rRNA in cells increases in an approximately linear fashion over a 60-minute time course. Accumulation of the mature species is faster in the complemented deletion strain.*

We next examined whether or not these immature subunits were susceptible to factor-mediated maturation. To this end, we made use of the aforementioned strain harbouring an arabinose-inducible copy of YjeQ (*ΔyjeQ*-ara). Once again, a pulse-chase approach was employed to follow the progress of a distinct generation of ribosomes over time. The method remained the same as that described above except that the expression of YjeQ was induced with 1% arabinose following the pulse phase (0 minutes post-chase). At the beginning of the time-course the labeled rRNA is exclusively 17S precursor. As time progresses there is a decrease in 17S rRNA and a corresponding increase in 16S rRNA. Once again, this suggests the conversion of the immature subunit to its mature form. However, the reintroduction of YjeQ was found to accelerate this conversion as is illustrated in Figure 2.6 C. After 60 minutes, nearly all of the pulsed rRNA is mature 16S.

As this experiment visualizes a discreet subunit population, the accelerated appearance of 16S rRNA is not likely a result of upstream effects. All of the labeled

ribosomal subunits were synthesized prior to the induction of YjeQ, and thus, the enhanced rate of maturation observed, must in all likelihood, be factor-mediated. This does not imply a direct role in rRNA maturation, but rather that YjeQ may act downstream of the formation of this immature species, carrying the maturation of the subunits forward rather than facilitating the assembly of new functional ribosomes from scratch. If the immature subunits were a dead-end or stalled byproduct, then the presence of YjeQ would not accelerate their maturation. These observations, however, do not rule out the possibility of separate parallel assembly pathways that proceed independently of YjeQ. Ultimately, these data suggest that the immature species abundant in a *yjeQ*-null strain represents an assembly intermediate, or at the very least a precursor susceptible to further processing. YjeQ is able to accelerate the maturation process significantly and likely acts down stream of the precursor formation.

While the re-introduction of YjeQ to the assembly process accelerates the conversion of 17S rRNA to 16S rRNA, maturation still appears to take a considerable amount of time. In the wild-type, all rRNA is converted to the mature form in less than ten minutes. At two minutes approximately half of the material is 16S rRNA. However, in the complemented deletion the same level of processing takes upwards of 30 minutes. It is possible that this lag can be accounted for by the time needed to induce sufficient amounts of functional YjeQ. The Δ*yjeQ* cells have a substantial reservoir of immature subunits, having been grown with a defective assembly process for a number of generations. In a typical wild-type cell, the proportion of ribosomes undergoing assembly at any given time ranges from 2-5% [147]. This subpopulation is closer to 50% in the

mutant, as is evidenced by the significant proportion of 17S rRNA. Thus, the lag in processing time could simply be a consequence of the shear volume of immature subunits that must be processed. Higher expression of YjeQ with plasmids was not reliably tunable and therefore not an option, as this protein is toxic when present in high quantities.

2.3.3 Co-structure of YjeQ in Complex with a Mature 30S Subunit

In an effort to further clarify the function and mechanism of YjeQ, we sought to verify its binding site on the 30S subunit. As discussed in Chapter 1, previous studies illustrate that the association of YjeQ with the mature 30S ribosome is inhibited by aminoglycosides, which bind in the A-site of the small subunit [132, 139]. Whether or not this inhibition is the result of overlapping binding locales is not clear. We thus endeavored to visualize YjeQ in complex with the mature 30S subunit using cryo-EM so as to ascertain details of this interaction.

Formation of the YjeQ-30S complex

Obtaining an accurate and high-resolution co-structure of YjeQ bound to the 30S subunit was dependent on achieving maximal occupancy of YjeQ in the complex [130]. To this end, occupancy was examined for multiple incubations of YjeQ and 30S in various ratios. Briefly, purified recombinant protein was incubated with wild-type 30S subunits (1 μM) in ratios of 1:1 and 5:1 at 30°C for one hour. GMP-PNP, a non-hydrolysable analogue of GTP, was included in this mixture in excess (1 mM). Thus, the complex was formed with YjeQ adopting its GTP-bound state. Following incubation, the ribosomal subunits were pelleted by ultracentrifugation on a 20% sucrose cushion in buffer A (20 mM Tris-HCl at pH 7.5, 10.5 mM magnesium acetate, 100 mM NH_4Cl, 0.5

mM EDTA, and 3 mM 2-mercaptoethanol). Ribosomal pellets were then resuspended in buffer A and both the pellet resuspensions and supernatant were separated by SDS-PAGE, stained with Coomassie brilliant blue, and examined for the presence of YjeQ (Figure 2.7). The occupancy level of YjeQ in the complex was estimated by quantifying the amount of YjeQ that co-pelleted with ribosomes. Quantification was performed using Imagequant version 5.2 (Molecular Dynamics). Using the previously established stoichiometry of 1:1, an occupancy level of 70% was determined when YjeQ was in excess 5-fold [130].

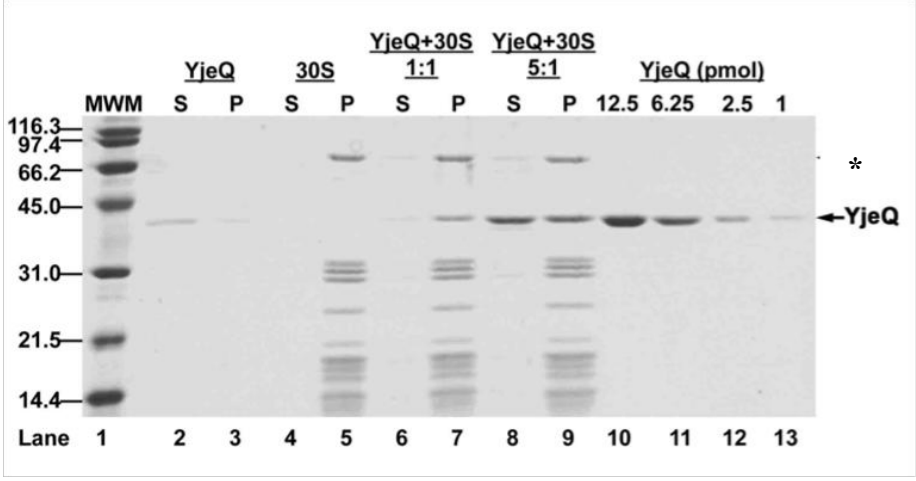

Figure 2.7: Assembly of the 30S-YjeQ complex*. Purified YjeQ was incubated with 30S subunits in ratios of 1:1 (lanes 6-7, 2.5 pmol) and 5:1 (lanes 8-9, 12.5 pmol) in the presence of GMP-PNP. Following incubation, samples were overlaid onto a sucrose cushion and pelleted by ultracentrifugation. Pelleted material was resuspended and both the supernatant (S) and pellet (P) were resolved by SDS-PAGE and stained with Coomassie brilliant blue. The lanes are as follows 1: molecular weight marker, 2-3: YjeQ + GMP- PNP, 4-5: 30S + GMP-PNP, 6-7: YjeQ + GMP-PNP + 30S (1:1), 8-9: YjeQ + GMP-PNP + 30S (5:1), 10-13: known quantities of YjeQ (1- 12.5 pmol). The position of YjeQ in the gel is indicated. A contaminating protein co-purifying with the 30S subunits is indicated with an asterisk (*). This protein was identified as S1 by mass spectrometry. The occupancy of the YjeQ-30S complex was assessed by quantifying the amount of YjeQ that co-pelleted with ribosomes in each reaction using the lanes with known quantities of YjeQ (lanes 10-13). The fraction of YjeQ that pellets in the absence of ribosomes (25%) (lane 3) was subtracted from that quantified in the reaction pellet (lanes 7 and 9). Using the previously determined binding ratio of 1:1, occupancy for both 1:1 and 5:1 incubations was found to be approximately 70%. Modified from Jomma et al.* [130].

A large contaminating protein was found to pellet with the 30S subunits (top band, ~70 kDa of SDS-Page gel). This protein was identified as S1 using mass spectrometry (see methods). Previous reports suggest that S1 dissociates from the 30S subunits when purified under high-salt conditions [148]. However, SDS-page analysis suggests that our purification method was unable to strip the 30S subunits of this r-protein. When bound, S1 occupies a region between the head and platform of the 30S subunit [149]. As shown below, our cryo-EM map does not feature a density corresponding S1 in this region. As such, we expect that sample treatment in preparation for cryo-EM studies ultimately lead to the dissociation of this protein from the ribosomal complex. Regardless, the binding site of S1 does not overlap with the proposed binding site of YjeQ, and thus, it did not interfere with our ability to reliably identify the presence of YjeQ in the complex.

The Co-Structure of YjeQ with Wild-Type 30S Subunits

A co-structure of YjeQ in complex with the 30S subunit was obtained using cryo-EM. The three-dimensional reconstruction, in conjunction with difference mapping, reveals an additional density in the upper region of helix 44, which closely maps to the X-ray structure of YjeQ (Figure 2.8). This region of binding, proximal to the A-site, lends credence to hypothesis that aminoglycosides inhibit YjeQ binding in a direct fashion. This structure is also in agreement with previous footprinting studies by Kimura et al. that suggest YjeQ binds near the A-site [150]. A portion of the density attributable to helix 44 and 45 was absent from our structure, suggesting that the presence of YjeQ displaces these regions. Our difference maps also highlighted additional density in the neighborhood of S12, which could correspond to a portion of helices 44 or 45 in their

new location (Supplementary Figure 1.2). The primary interaction appears to be mediated by the N-terminal OB-fold of YjeQ, which contacts 16S rRNA of the 30S subunit through helix 23b and 24a in the platform (Supplementary Figure 1.2). This agrees with previous reports indicating that the OB-fold is essential for YjeQ-30S interaction. The zinc-finger domain appears to be located near the upper region of helix 44, possibly inducing a displacement in this helix when binding. This positions YjeQ in proximity to the 3' end of 16S rRNA, suggesting it may play a role in the maturation and folding of this site.

Our co-structure was assembled using YjeQ in its GTP-bound state. The X-ray structure used for modeling, however, depicted the GDP-bound form. Nevertheless, the X-ray structure fit the additional density in our 3D reconstruction remarkably well, suggesting that YjeQ does not undergo a significant conformational change upon GTP hydrolysis. This is rather surprising given that the function of many GTPases is defined by large changes in conformation that accompany substrate binding and product release. The *ras*-like bacterial GTPase EF-Tu (elongation factor thermo unstable), a protein involved in facilitating recruitment of aminoacycl-tRNA to the ribosome during elongation, exemplifies this link between substantial rearrangement and activity. Further study will be needed to clarify the difference between the GTP and GDP-bound forms of YjeQ and how the subtle conformational change contributes to ribosome function.

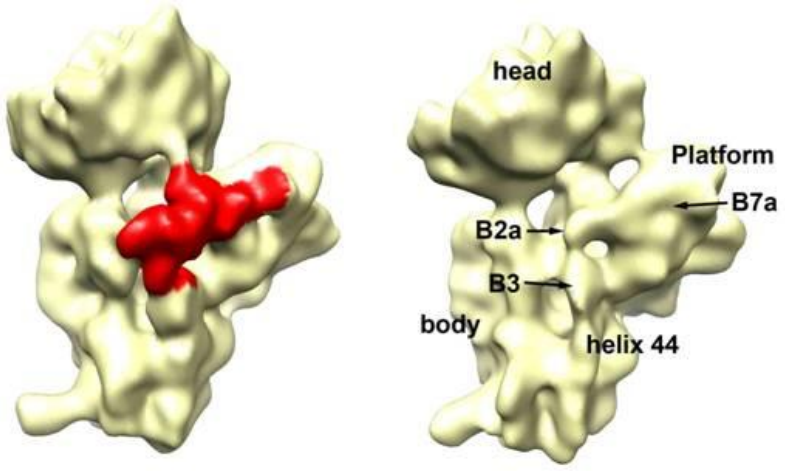

Figure 2.8. Cryo-EM structure of the 30S-YjeQ complex. *Cryo-EM map of the 30S-YjeQ complex adjacent to a control reconstruction of free wild-type 30S subunits. The head, platform, body and helix 44 are indicated. The inter-subunit bridges B2a, B3 and B7A that are covered upon YjeQ binding are also highlighted. The additional density representing the YjeQ protein has been colored in red. Modified from Jomma et al.* [130].

An alternate Co-structure

A second group has developed a 3D structure of the GTP-bound form of YjeQ in complex with the 30S subunit [151]. This model places YjeQ in the vicinity of the binding-region we identified; however, there are several distinct differences. Once again the OB fold is interpreted as playing a critical role in association, but in this alternative structure it is found to contact helices 18 and 44 as well as protein S12 (versus helices 23b and 24a in our model) [151]. In addition, the zinc finger is nearly inverted with respect to our placement of it, contacting helices 29-31 of the head (versus helix 44 in our structure) [151]. Thus, these co-structures differ markedly, and as a result, bear divergent functional and mechanistic interpretations. Resolution of this conundrum will require further analysis characterizing specific residues involved in YjeQ-30S association. Ultimately, however, both structures provide corroborative evidence supporting YejQ

interaction near the A-site of the 30S subunit. Interestingly, both co-structures also suggest that the binding of this factor has very little impact on the conformational arrangement of the mature small subunit. It is worth considering that the presence of YjeQ might influence the conformation of the immature subunit, as it is both less stable and functionally immature. The presence of YjeQ may induce structural rearrangements in this species that facilitate processing and maturation.

2.4 DISCUSSION

The absence of YjeQ leads to an accumulation of immature 30S subunits containing unprocessed 17S rRNA and lacking late-binding ribosomal proteins [140]. That this subunit species is nearly mature and competent for further processing suggests that YjeQ may play a role in the final stages of 30S assembly and/or association with the 50S subunit. The immature subunit species also features distortion in key functional regions, providing insight into the functional abatement and defective subunit association affiliated with the absence of this protein.

Generally, it is thought that processing of the 5' and 3' ends of pre-16S rRNA precedes formation of the 70S ribosome. Indeed, it has been suggested that this cleavage could be one of the final stages in subunit maturation and that failure in this regard could serve to prevent premature subunit association [117, 121, 129, 133, 140, 152]. As such, it is possible that YjeQ plays a direct or assistive role in this process. However, there have been several reports documenting instances of 70S ribosomes containing fully unprocessed 17S rRNA [80, 117, 132, 145, 152]. A second model accommodating these observations posits that processing occurs within the 70S ribosome or on polysomes. In

this scenario, the prevalence of free subunits in the *ΔyjeQ* strain would not be directly attributable to the presence of the leader sequences. Instead, the reduction of 70S ribosomes would be a consequence of an additional defect, arising from the absence of YjeQ and preventing the stable association of subunits.

The precursor sequences in the Δ*yjeQ*-derived 30S subunit are accompanied by abnormal architecture in the decoding center of the 30S subunit [140]. It is probable that this defect renders the immature species unable to properly accommodate mRNA and participate in the formation of the translation complex. Thus, the distortion of this region may be sufficient to prevent subunit association and therefore, be the underlying cause of the altered ribosome profile in strains devoid of YjeQ. Formation of a functional decoding center may in fact be a pre-requisite for 17S rRNA processing, regardless of whether the cleavage occurs on the free 30S subunit or within the 70S complex. As such, YjeQ could potentially function upstream of 17S rRNA cleavage, perhaps mediating proper folding of this region.

Understanding the role of YjeQ in the final stages of maturation hinges on a deeper understanding of the connection between the formation of the decoding center and the presence of 17S rRNA. While this region may be able to adopt its native functional arrangement independently of the presence of 17S rRNA, there are multiple lines of evidence suggesting that precursor sequences may play a critical role in mediating proper folding [153-155]. Therefore, it is plausible that these sequences remain an integral part of the assembly process until the small subunit is able to associate with its large

counterpart. YjeQ may serve in this regard acting as checkpoint protein to verify completion of a certain stage of assembly.

Interestingly, the regions of variation in the immature subunit are proximal to the proposed binding site of YjeQ [130, 140]. It is tempting to postulate that that this protein may play a direct role in facilitating the proper formation of this functionally critical region, however, there is little evidence of YjeQ interacting with this unfinished ribosomal species. Rather, binding and GTPase stimulation studies suggest that YjeQ interacts strongest with fully mature 30S subunits [121, 132, 138]. This does not preclude the possibility of direct influence on the immature subunit; however, it does raise the question as to how the absence of this protein gives rise to an unfinished species with which it does not interact. This is especially paradoxical in light of our pulse-chase work that suggests YjeQ functions downstream of this precursor and directly influences its progression. Our experiments illustrate factor-mediated acceleration of 17S rRNA processing and, presumably, final subunit maturation. As such, it is anticipated that YjeQ does indeed directly act on this immature subunit.

There is a growing body of evidence implicating RbfA in 30S assembly; however, the specific role of this protein has also been elusive. Like YjeQ, the absence of this factor leads to telltale ribosomal defects including an accumulation of free 30S and 50S subunits as well as 17S rRNA [116, 122]. Cryo-EM studies have illustrated that this factor binds the 30S subunit near the interface, its presence leading to conformational shifts in the 3' minor domain of 16S rRNA [120]. As such, YjeQ and RbfA appear to occupy proximal regions on the 30S subunits near the decoding center. However, studies

suggest that RbfA strongly binds immature 30S subunits, while YjeQ seems to associate primarily with the mature form [121].

A study by Goto and colleagues builds on these observations and suggests functional interplay between these two proteins [121]. A series of mutations in *rbfA* were found to suppress the deletion of *yjeQ*. In addition, this work observed that YjeQ stimulates the dissociation of RbfA from the 30S subunit. Likewise, it was found that the presence of RbfA on the 30S subunit promotes the binding of YjeQ. A model emerged from this work suggesting that RbfA binds the immature 30S subunit and promotes the processing of precursor rRNA sequences. Following these events, YjeQ then binds to the now-processed small subunit and acts to dissociate RbfA [121]. The presence of 17S rRNA in both deletion strains is ultimately a result of perturbation of RbfA function. When RbfA is absent, 17S rRNA processing is substantially slower, giving rise to the immature subunit. When YjeQ is absent, RbfA remains bound to the 30S subunit inhibiting the final stages of maturation. Thus, the dispensability of YjeQ is dependent on whether or not RbfA is performing its cellular task. The absence of RbfA renders YjeQ a fully non-essential protein.

This model hinges on the premise that YjeQ only interacts with mature 30S subunits. Thus, it fails to reconcile the exclusive association of YjeQ with mature subunits with the observation that deletion of this factor gives rise to immature 17S-containing ribosomes. In our view, the presence of 17S rRNA in the *yjeQ*-null strain is in conflict with the notion that the ribosomal defect in this strain is strictly due to a failure to remove RbfA. An alternative possibility is that RbfA and YjeQ both bind the immature

subunit in sequence (or simultaneously), the former inducing conformational rearrangements that recruit the latter. YjeQ in turn plays a role (either directly or indirectly) in facilitating maturation and 17S rRNA processing. Further analysis of the interaction of YjeQ with the immature 30S subunit is required to interrogate these models.

2.5 MATERIALS AND METHODS

In this section I document all the materials and methods for the studies above. For posterity, I have opted to include published methods in full where applicable. The individuals responsible for each experiment are included in parenthesis at the beginning of each section. The corresponding supervisors were also involved in experiment execution.

2.5.1 Characterizing the Immature Subunits in the *ΔyjeQ* Deletion Strain

(Adapted with modification from Jomaa et al. [140])

Isolation and analysis of cellular rRNA (Author)

Overnight cultures of *E. coli ΔyjeQ* (EB1140) and the parental strain (EB344) were sub-cultured in LB media (1:10000 dilution) and grown with shaking at 37°C to an optical OD_{600} of 0.2. Subsequently, 1 ml of culture was pelleted by centrifugation at 5,000 *g* for 10 minutes in an Eppendorf 5424 microcentrifuge. Cell pellets were resuspended in 100 µl of lysis buffer (Tris-HCl pH 8.0, 10 mg/ml lysozyme, 1 mg/ml proteinase K, 0.15 mM calcium acetate). Lysis mixtures were incubated at 22°C for 10 minutes with shaking. Ribosomal RNA was then purified from cells using an RNeasy® Mini Kit (Qiagen) according to the manufacture's protocols. Purified RNA was incubated with an

equal volume of RNA loading buffer (50% w/v urea. 10% w/v sucrose, 1 x TBE) for 10 minutes at 75°C. Samples were loaded onto a modified agarose gel comprised of 0.7% agarose and 0.9% Synergel^{TM} (Diversified Biotech, Boston, MA). RNA was separated by electrophoresis for 4 hours at 4.5 V/cm. Gels were stained with ethidium bromide and visualized under UV light.

Northern hybridization analysis was performed for both the 5' and 3' precursor sequences of the 17S rRNA to determine its identity. Samples were transferred to Hybond-N^+ charged nylon membranes (GE Healthcare) under alkaline conditions (0.1 M NaOH, 3M NaCl) using the standard capillary method. Membranes were incubated at 32 °C in 50 ml of prehybridization buffer (0.5 M sodium phosphate pH 7.2, 7% (w/v) SDS, 1 mM EDTA pH7.0) for two hours. Single stranded DNA probes complimentary to the 5' or 3' terminal precursor sequences (Sigma Canada) were labeled with ^{32}P using T4 polynucleotide kinase (Fermentas). The sequence of the 5' probe was 5'-TTAAGAATCCGTATCTTCGAGTGCCCACA-3' and the sequence of the 3' probe was 5'-TGTGTGAGCACTACAAAGTACGCTTCTTTAAGGTAA GG-3.'

Purification of 30S ribosomal subunits (Author)

Purified 30S subunits from *Escherichia coli* Δ*yjeQ* (EB1140) and BW25113 parental (EB334) strains were prepared using centrifugation over sucrose cushions and gradients as previously described [138]. For each strain, one litre of Luria-Bertani broth (LB) was inoculated with 10 ml of a saturated overnight culture. Cultures were grown at 37°C to an OD_{600} of 0.2. Cells were cooled down to 4°C and all subsequent steps were conducted at this temperature. Cultures were harvested by centrifugation at 8,500 x g for

15 min and the cell pellet was resuspended in buffer A (20 mM Tris-HCl pH 7.5, 10.5 mM magnesium acetate, 100 mM NH_4Cl, 0.5 mM EDTA and 3mM 2-mercaptoethanol). Cell lysis was performed by three consecutive passes of the cell suspensions through a French pressure cell at 20,000 lb/in^2. The cell lysate was spun at 30,000 g for 45 min to clear cell debris. Recovered supernatant (S30 fraction) was overlaid on an equal volume of 1.1 M sucrose cushion made up in buffer B (20 mM Tris-HCL pH 7.5, 10.5 mM magnesium acetated, 500 mM NH_4CL, 0.5 mM EDTA and 3mM 2-mercaptoehtanol) and centrifuged at 100,000 x g for 16 hours. The ribosomal pellet was gently washed and sucrose removed by resuspension in buffer C (10 mM Tris-HCl pH 7.5, 10.5 mM magnesium acetate, 100 mM NH_4Cl, 0.5 mM EDTA and 7 mM 2-mercaptoethanol. The crude ribosomes were pelleted at 100,000 x g for 16 hours.

To obtain the 30S fraction from the *E. coli* Δ*yjeQ* strain, the crude ribosome pellet was resuspended in buffer E (10 mM Tris-HCl pH 7.5, 10 mM magnesium acetate, 60 mM NH_4Cl, 3 mM 2-mercaptoethanol) (non-dissociating conditions). In the case of the 30S fraction from the parental strain, the crude ribosome pellet was resuspended in buffer F (10 mM Tris-HCl pH7.5, 1.1 mM magnesium acetate, 60 mM NH_4Cl, 3mM 2-mercaptoethanol (dissociating conditions). In both cases, a portion of the subunit suspension (50-60 A_{260} units) was layered onto a 32 ml 10-30% (wt/vol) sucrose gradient made up in buffer E (for non-dissociating conditions) or F (for dissociating conditions) and centrifuged at 43,000 *g* for 16 hours using a Beckman SW32 Ti rotor. Gradients were fractionated using an AKTAprime™ purification system (GE HealthCare) in combination with a Brandel fractionator and particle peaks were monitored by absorbance at A_{260}. The

30S ribosomal subunits were then recovered by centrifugation at 100,000 x *g* for 16 hours and the pellet was resuspended in Buffer E (10 mM Tris-HCl pH 7.5, 10 mM magnesium acetate, 60 mM NH_4Cl, 3 mM 2-mercaptoethanol) and stored at - 80°C until further use. Quantification of the 30S subunits was accomplished by absorbance at 260 nm (1 A_{260} unit is equivalent to 69 pmol of 30S).

iTRAQ Proteomic Analysis (Dr. Zielke, Dr. Maddock)

Biological replicates of 30S particles from *Escherichia coli* Δ*yjeQ* (EB1140) and BW25113 parental (EB334) strains were purified separately using non-dissociating conditions and analyzed independently. Total protein was measured using a 2D Quant kit (GE Healthcare). A total of 25 mg from each 30S subunit preparation was precipitated with 80% ice-cold acetone and washed twice with 100% acetone. The pellet was resuspended in 21 ml 0.5 M triethylammonium bicarbonate (TEAB), 0.01% SDS and proteins were reduced with Tris(2-carboxyethyl)phosphine (TCEP), cysteines were blocked with methylmethanethiosulfate (MMTS) and digested with trypsin as described previously [156]. Labeling with the iTRAQ reagents was according to the manufacturer's recommendations (Applied Biosystems). For each biological replicate, the peptides derived from the parental and Δ*yjeQ* 30S subunits were labeled with two different iTRAQ reagents. The iTRAQ reagents 115 and 117 were used to label tryptic peptides from independently isolated Δ*yjeQ* 30S subunits preparations and 114 and 116 were used to label tryptic peptides from independently isolated parental 30S subunits. The iTRAQ reagent was reconstituted in ethanol and added directly to the protein digest (70% ethanol, final concentration). The mixture was incubated at room temperature for 1 hour and the

reaction was stopped by adding 250 ml of 0.1% trifluoroacetic acid (TFA, Fisher Sci, USA). Reaction mixtures from both labeling experiments were combined, dried by lyophilization and stored at -20°C.

iTRAQ-labeled peptides were resuspended in buffer A (5mM KH_2PO_4 pH 2.7, 30% acetonitrile) and applied to a strong cation exchange chromatography (SCX) using a Paradigm MG4 HPLC system (Michrom BioResources, Inc. Auburn, CA, USA) on a packed Polysulfoethyl aspartaminde column; 200 × 2.1 mm; 5 µm; 200 Å (Poly LC, Inc., Columbia, MD, USA). Peptides were eluted using a linear gradient with B (buffer A with 500 mM KCl) using an flow rate of 200 µl/min over 50 min. Two-min fractions were collected throughout and pooled into twelve fractions. For RP-HPLC-MS analysis, fractions were dried and redissolved in 45 ml of 0.1% TFA, desalted and concentrated on a reversed-phase cartridge (Zorbax C18) calibrated with 0.1% TFA as described previously (Chen et al., 2006). Peptides were eluted with a linear gradient using 0.1% TFA with 90% acetonitrile using a flow rate of 4 ml/min for 90 min and spotted at 20 seconds intervals onto a stainless steel MALDI target plate (192 wells; Applied Biosystems).

The MS and MS/MS spectra were acquired on an Applied Biosystems 4800 Proteomics Analyzer (TOF/TOF) (Applied Biosystems/MDX Sciex, Foster City, CA) in positive ion reflection mode (selected mass range of 800-3000 *m/z*) with a 200 Hz Nd:YAG laser operating at 355 nm. Accelerating voltage was 20 kV with 450 ns delay. For MS/MS spectra, the collision energy was 6 keV and the collision gas was air. The instrument was calibrated using a default mixture of 7 peptides. Typical MS spectra were

obtained with the minimum possible laser energy in order to maintain the best resolution. MS/MS spectra were collected for up to 12 of most intense MS peaks (minimum signal-to-noise ratio of 60) from each well.

The peak lists were generated from the acquired MS/MS spectra with the Protein Pilot software (Applied Biosystem, version 3.0) using default parameters. Acquired MS/MS spectra were searched against a concatenated (forward and reverse) *E. coli* K12 protein sequence database downloaded as a FASTA file from UniProtKB/Swiss-Prot (http://www.uniprot.org/taxonomy/complete-proteomes) on April 10th, 2008. The Protein Pilot software with default settings and the Paragon search engine (Applied Biosystems, version 3.0) was the software used to perform all the database searches. Proteins were identified with 1% local false discovery rate calculated by a module built-in the software.

Peptides for which one or more of the iTRAQ values were absent and proteins identified by only a single distinct peptide were discarded. Peak areas for all of the reporter ions (m/z 114.1, 115.1, 116.1, and 117.1) were extracted and automatically corrected using Protein Pilot (Applied Biosystems, version 3.0). The MS/MS data obtained were deposited into TRANCHE (https://proteomecommons.org/tranche/) with the Tranche Hash:dDZes+9slItFdCPmF8YepUC7GZEGcVekFr284mjTK4lsoEtAC1HZ ThAr5WcXUfce+J eZ1BYon2HV3tLR42W0aBiwCFsAAAAAAGmUKQ==.

The Δ*yjeQ*:WT (wild type) and WT: Δ*yjeQ* protein ratios as well as the p-values were generated with the Protein Pilot Software. The ratios in Figure 2.2 were generated manually, as we have done previously [156, 157]. In this case, only peptides that identify proteins with ≥95% confidence were used for the calculation. Peptide ratios for each

replicate (115/114 and 117/116) were combined and then averaged. To obtain protein ratios, the average from all peptide ratios was obtained after removal of outliers using a Grubbs test (http://www.graphpad.com/quickcalcs/Grubbs1.cfm). The entire dataset was normalized at the level of the proteins by adjusting the median of the protein ratio to 1:1.

Cryo-EM Structure (Dr. Jomaa, Dr. Ortega)

For cryo-EM, holey carbon grids (400 mesh copper) containing an additional continuous thin (5-10 nm) layer of carbon were previously washed with acetone vapor for 15 min and glow discharge in air for 30 seconds [158]. Then, 3.5 µL aliquots containing 30S subunits purified from Δ*yjeQ* or wild type cells were applied to the grid for one min. The 30S subunits were in Buffer E and at a concentration of ~60 nM. Grids were blotted for 7 s and vitrified by rapidly plunging into liquid ethane at -180°C with a Vitrobot^{TM} (FEI). Data acquisition was performed under low dose conditions (~10 $e^-/Å^2$) on a JEOL 2010F FEG microscope operated at 200 kV with a Gatan 914 side- entry cryo-holder and at a nominal magnification of 50,000x. A total number of 72 and 29 electron micrographs were collected from the samples containing 30S subunits purified from Δ*yjeQ* and wild type cells, respectively. The defocus range of the images was from - 0.65 to -3.9 mm. The micrographs were digitized with a step size of 12.7 µm in a Nikon Supercool Scan 9000 producing images with a sampling value of 2.54 Å/pixel.

Projections representing 30S subunits purified from Δ*yjeQ* and wild type cells were picked using Boxer [159]. Contrast transfer function of the micrographs was estimated using CTFFIND software [160] and corrected using Xmipp software package [161] Image classification was performed using supervised [143, 144] and 3D maximum

likelihood-based [162, 163] methods.

The 3D reconstructions were calculated using 3D projection alignment procedures as implemented in the Xmipp software package [161]. The reference map used to refine the 3D reconstruction of both the mature and immature 30S subunit was the X-ray structure of the *E. coli* 30S subunit (PDB ID: 2Z4K) low-pass filtered to 25Å resolution [164]. In each refinement, sets of projections were calculated from the reference map using an angular spacing that ranged from 15° to 2° during the multiple cycles of refinement. The correct handedness of the structures was imposed by the X-ray crystal structure of the 30S subunit from *E. coli* (PDB ID: 2Z4K). Resolution of the cryo-EM maps was estimated by calculating two maps following the last cycle of refinement from the even and odd numbered particles. Then Fourier shell correlation was calculated between both maps and the resolution was estimated using a FSC value of 0.5. These values were used to low-pass filter the refined cryo-EM maps. Difference maps between the immature and mature 30S subunit structures were calculated using Xmipp software package [161].To this end, maps were subtracted after alignment of the two structures and normalization to a comparable grayscale.

Docking of X-ray crystallographic structures and structure visualization (Dr. Jomaa)

Fitting of the X-ray crystallographic structure of the *E. coli* 30S subunit (PDB ID: 2Z4K) [164] was performed using rigid-body fitting of the entire X- ray structure of the 30S subunit onto the EM maps as implemented in the Situs software [165]. Visualization of the fitted atomic structure and the cryo-EM density maps and difference maps was done with UCSF Chimera software [166].

Accession Numbers

The EM maps of the immature 30S subunit purified from Δ*yjeQ E. coli* cells and the mature 30S subunit purified from wild type *E. coli* cells have been deposited in the Electron Microscopy Data Bank (EMDB IDs: 1774 and 1775).

The Fate of the Immature Subunit in a Δ*yjeQ* Deletion Strain

Persistence of the Ribosomal Defect (Author)

All strains used in this work, MG1655 wild-type *and ΔyjeQ*-ara (Δ*yjeQ::pBAD-yjeQ)*, were sourced from the strain collection of Dr. Eric Brown, McMaster University, having been created previously by Campbell et al. [128, 139]. The RNA profile of the Δ*yjeQ-ara* strain was examined over the course of 10 hours of growth to study the persistence of non-functional immature 30S subunits. Starter cultures (5 ml, LB) were incubated for 16 hours at 37°C with shaking (250 rpm). Cells were then sub-cultured at 37°C with shaking (250 rpm) in fresh LB media and supplemented with arabinose (2 %) after four hours of growth. Aliquots of cells (1 ml) were harvested by centrifugation (5000 g, 5 minutes, Eppendorf 5424 microcentrifuge) every hour throughout exponential growth and fast frozen in a dry ice/ethanol bath. Total rRNA was then isolated using the RNeasy Mini Kit as per the manufactures instructions (Qiagen), incubated with custom loading buffer (50% w/v urea. 10% w/v sucrose, 1 x TBE) and resolved by agarose (2.1%, Bioshop) gel electrophoresis (2% gel, 4 hours at 4.5 V/cm). The rRNA species were then stained with RedSafe™ (FroggaBio) and visualized using a Typhoon™ multimode imager (GE).

Pulse-Chase Studies

Strains were grown overnight at 37°C in LB media. Cells were subsequently diluted (1 in 10,000) in fresh RDM-Glucose media and grown in a 37°C water bath with aeration (250 rpm). At an OD_{600} ~ 0.1-0.2, ^{14}C-labeled uridine was added to the growing culture (final concentration of 0.1 μCi/ml). After five minutes of exposure to this 'pulse,' unlabeled uridine was added to the culture to a final concentration 500 ug/ml (1000-fold greater concentration than the pulse). Cells were harvested (200 μl) at regular intervals (WT every two minutes, Δ*yjeQ* every five minutes) and fast frozen in a dry ice/ethanol bath. Samples were harvested over a full doubling of the cell population. Frozen samples were subsequently pelleted by centrifugation for 10 minutes at 4°C in an Eppendorf 5424 microcentrifuge. Total rRNA was extracted from each sample using the Qiagen RNeasy kit as per the manufactures protocol. Purified RNA was then incubated with custom loading buffer (50% [w/v] urea, 10% [w/v] sucrose, 1× TBE) and resolved via gel electrophoresis. rRNA was subsequently transferred to a charged nitrocellulose membrane (Hybond N+, GE Healthcare) with an alkaline buffer (0.1 M NaOH, 3M NaCl) using the standard capillary method. Membranes were rinsed in 6x SSC buffer (0.3 M sodium citrate, 3M NaCl) and then exposed to a phosphor screen for 72 hours. Following exposure, the radiolabeled samples were imaged on a Typhoon™ multimode imager (GE). Quantification of labeled rRNA bands was performed using ImageQuant, version 5.2 (Molecular Dynamics) with the rolling average of the region surrounding the band used for background correction.

Co-structure of YjeQ in Complex with a Mature 30S Subunit
(Adapted with modification from Jomaa et al. [130]).

Construction of YjeQ overexpression clone (Dr. Daigle)

Gateway Recombination Cloning technology (Invitrogen) was used to construct full-length YjeQ featuring an N-terminal His_6 affinity purification tag cleavable by TEV protease [127]. Briefly, the *yjeQ* gene was amplified from *E. coli* MG1655 genomic DNA using the polymerase chain reaction. PCR was performed using VENT DNA polymerase (New England Biolabs) and the following primers: 59-G G GGG ACA AGT TTG **TAC AAA AAA GCA GGC TTA** GAT TAC GAT ATC CCA ACG ACC GAA AAC CTG TAT TTT CAG *GGC AGT AAA AAT AAA CTC TCC AAA GGC-39 and 59-CGC GGA TCC TCA GTC ATC CGT ATC AGA AAA G-39, where the recombination sites, coding sequence, and cleavage sites are denoted by bold letters, underlining, and an asterisk, respectively. The amplified product was inserted into the pDONR201 (Invitrogen) vector as per the manufacturer's protocol and subsequently cloned into the pDEST17 (Invitrogen) destination vector that encodes six histidine residues at the N terminus of the insert. The resulting construct, pDEST17-YjeQ, was validated by sequencing (MOBIX, McMaster University).

Purification of YjeQ protein (Dr. Jomaa, Author)

YjeQ protein was expressed as an N-terminal His_6-tagged protein in *E. coli* BL21-AI competent cells transformed with the expression vector pDEST17-YjeQ (see above). One litre of cells was grown in LB medium at 37°C to OD_{600} = 0.6, and expression was induced with 0.2% L-arabinose. Cells were induced for 3 h at 37°C and harvested by centrifugation at 3700 g for 10 min. The cell pellet was washed with 13 PBS buffer (137

mM NaCl, 2.7 mM KCl, 8.1 mM Na_2HPO_4, 1.76 mM KH_2PO_4 at pH 7.4) and resuspended in 20 mL of lysis buffer (50 mM Tris-HCl at pH 8.0, 10% [w/v] sucrose, 100 mM NaCl). The cell suspension was passed through a French pressure cell at 20,000 lb/in^2 three consecutive times to lyse the cells. The lysate was spun at 30,000 g for 45 min to clear cell debris. NaCl was added to bring the concentration to 0.5 M, and the lysate was filtered with a 0.45-mm filter and added to a HiTrap Metal Che- lating column (GE Healthcare Life Sciences) equilibrated with 50 mM Tris-HCl (pH 8.0), 0.5 M NaCl, and 5% (v/v) glycerol. Nonspecifically bound proteins were washed with increasing concentrations of imidazole up to 90 mM. YjeQ was eluted with 240 mM imidazole. Purity of the fractions was monitored by SDS-PAGE. Fractions containing pure protein were pooled and dialyzed against 50 mM Tris-HCl (pH 8.0), 10% (v/v) glycerol (Amicon Concentrators). The N-terminal His_6-tag was removed by digestion with purified tobacco etch virus (TEV) protease. An amount of 0.74 mg of TEV was added to the pooled and dialyzed fractions containing YjeQ (40 mg). The total volume of the reaction was 10 mL, and the reaction mixture was incubated for 4 h at 16°C. The mixture was added to 1 mL of Ni-NTA agarose resin (QIAGEN) previously equilibrated with 50 mM Tris-HCl (pH 8.0), 0.5 M NaCl, and 5% (v/v) glycerol, and incubated on a rocking platform for 1 h at 4°C. The mixture was spun at 1400 g for 5 min, and the supernatant containing the untagged YjeQ protein was recovered, dialyzed against 50 mM Tris-HCl (pH 8.0), 10% (v/v) glycerol, and concentrated using a 10 kDa-cutoff filter (Amicon). The protein was frozen in liquid nitrogen and stored at -80°C.

Purification of the 30S ribosomal subunits and preparation of the 30S:YjeQ complex (Dr. Jomma, Author)

Purified 30S subunits from *E. coli* (BW25113) were prepared using centrifugations over sucrose cushions and gradients [138]. One liter of LB was inoculated with 10 mL of a saturated overnight culture. Cultures were grown at 37°C to an OD_{600} of 0.4 and cooled down to 4°C with all subsequent steps performed at this temperature. Harvesting of the cultures was done by centrifugation at 8500 g for 15 min, and the cell pellet was resuspended in buffer A (20 mM Tris-HCl at pH 7.5, 10.5 mM magnesium acetate, 100 mM NH_4Cl, 0.5 mM EDTA, and 3 mM 2-mercaptoethanol). Cell lysis was performed by three consecutive passes of the cell suspension through a French pressure cell at 20,000 lb/in^2. The cell lysate was spun at 30,000 g for 45 min to clear cell debris. Recovered supernatant (S30 fraction) was overlaid on an equal volume of 1.1 M sucrose cushion made up in buffer B (20 mM Tris-HCl at pH 7.5, 10.5 mM magnesium acetate, 500 mM NH_4Cl, 0.5 mM EDTA, and 3 mM 2-mercaptoethanol) and centrifuged at 100,000g for 16 h. The ribosomal pellet was gently washed, and sucrose was removed by resuspension in buffer C (10 mM Tris-HCl at pH 7.5, 10.5 mM magnesium acetate, 100 mM NH_4Cl, 0.5 mM EDTA, and 7 mM 2-mercaptoethanol). The crude ribosomes were pelleted at 100,000 g for 16 h. To obtain the 30S fraction, the crude ribosome pellet was resuspended in buffer F (10 mM Tris-Hcl at pH 7.5, 1.1 mM magnesium acetate, 60 mM NH_4Cl, 0.5 mM EDTA, and 2 mM 2-mercaptoethanol) (dissociating conditions). A portion of the subunit suspension (50–60 A_{260} units) was layered onto a 32-mL 10%–30% (w/v) sucrose gradient made up in buffer F and centrifuged at 43,000 g for 16 h

using a Beckman SW32 Ti rotor. Gradients were fractionated using an AKTAprime purification system (GE Healthcare), and the elution peaks corresponding to 30S and 50S particle peaks were monitored by absorbance at A_{260}. The 30S ribosomal subunits were then recovered by centrifugation at 100,000g for 16 h, and the pellet was resuspended in buffer E (10 mM Tris-HCl at pH 7.5, 10 mM magnesium acetate, 60 mM NH4Cl, 3 mM 2-mercaptoethanol), and stored at -80°C until further use. Quantification of the 30S subunits was accomplished by absorbance at 260 nm (1 A_{260} unit is equivalent to 69 pmol of 30S).

To determine the occupancy level of YjeQ in the 30S:YjeQ complex, a fivefold excess of freshly purified YjeQ protein was incubated with a 1 mM preparation of purified 30S subunits for 1 h at 30°C in the presence of 1 mM GMP-PNP in buffer E. The volume of the reaction was 50 μL. The reaction mixture was layered onto a 1.1 M sucrose cushion (volume 150 μL) made up in buffer E. The ribosomal subunits were pelleted by ultracentrifugation at 330,000 g for 4 h using a Beckman TLA-120.1 rotor, and the pellet was resuspended in 200 μL of buffer E. The supernatant and resuspended pellet of each sample (12 μL load volume) were resolved by SDS-PAGE and stained with Coomassie brilliant blue. The stained gel was subsequently photographed using a FluorChem FC3 system (Alpha Innotech). The occupancy level of YjeQ in the 30S:YjeQ complex was estimated by quantifying the amount of YjeQ that co-pelleted with ribosomes (2.5 pmol) in each reaction. The integrated pixel density of each YjeQ band was calculated using Imagequant, version 5.2 (Molecular Dynamics), with the local average of the region surrounding the band used for background correction. This yielded an optical density for

each band that was used to estimate the proportion of YjeQ found in the supernatant and pellet of each reaction. YjeQ protein (25%) was seen to pellet in the absence of ribosomes. Thus, to determine the amount of YjeQ that co-pelleted with 30S subunits, it was necessary to subtract this fraction from the YjeQ observed in the reaction pellets (lanes 7,9). The previously established 1:1 stoichiometry for the 30S:YjeQ was assumed to determine the occupancy level.

To assemble the complex for cryo-EM, a 50-μL reaction mixture in buffer E with 2 mM GMP-PNP was prepared by adding 30S subunits to a concentration of 1 mM and a fivefold excess of freshly purified YjeQ protein. The reaction was incubated for 1 h at 30°C and then diluted 100 times in buffer E containing 2 mM GMP-PNP before applying it to the EM grids.

Nanoscale microcapillary liquid chromatography electrospray ionization tandem mass-spectrometry (LC-MS/MS) (Dr. Kireeva, Author)

The protein gel bands were destained with 50 mM ammonium bicarbonate and water until clear, then rinsed with water several times to remove all color. The band was reduced with 10 mM DTT for 30 min at 56°C and alkylated with 100 mM iodoacet-amide for 15 min at room temperature in the dark. Protein in the band was digested in situ with 30 mL of (13 ng/mL) trypsin (Promega) in 50 mM ammonium bicarbonate overnight at 37°C, followed by peptide extraction with 30 mL of 5% formic acid, then 30 mL of acetonitrile. The pooled extracts were concentrated to <5 mL on a SpeedVac spinning concentrator and then brought up in 0.1% formic acid and 5% acetonitrile for protein identification by micro-flow liquid chromatography electrospray tandem mass

spectrometry (microLC-ESI-MS/MS) using a ThermoFisher LTQ- XL- Orbitrap Hybrid Mass Spectrometer (ThermoFisher) coupled to an Eksigent nanoLC-2D HPLC system (Eksigent). Chromatography was performed using 0.1% formic acid in both the A solvent (98% water, 2% acetonitrile) and B solvent (10% water, 80% acetonitrile, 10% isopropanol), and a 5% B to 95% B gradient over 30 min at 5 mL/min through an Eksigent capillary (CSP-3 C18 -100, 0.3 m 3 100 mm) column. The instrument method consisted of one MS full scan (200– 2000 m/z) in the Orbitrap mass analyzer, an automatic gain control target of 500,000 with a maximum ion injection of 500 msec, one microscan, and a resolution of 60,000. Three data-dependent MS/MS scans were performed in the linear ion trap using the three most intense ions at 35% normalized collision energy. The MS and MS/MS scans were obtained in parallel fashion. In MS/MS mode automatic gain control targets were 10,000 with a maximum ion injection time of 100 msec. A minimum ion intensity of 1000 was required to trigger an MS/ MS spectrum. The dynamic exclusion was applied using a maximum exclusion list of 500 with one repeat count with a repeat duration of 30 sec and exclusion duration of 45 sec. The lock-mass option was enabled for the FT full scans using the ambient air polydimethylcyclosiloxane (PCM) ion of m/z = 445.120024 or a common phthalate ion m/z = 391.284286 for real-time internal calibration. For database searching, tandem mass spectra were extracted by Proteome Discoverer 1.2. All MS/MS samples were analyzed using SEQUEST (ThermoFinnigan; version 27, revision 12) and X! Tandem (The Global Proteome Machine Organization; version 2006.04.01.2). Both search engines were set up to search the *E. coli* database, assuming trypsin digestion, allowing two missed cleavages,

and using a fragment ion mass tolerance of 0.5 Da and a parent ion tolerance of 0.02 Da. The iodoacetamide derivative of cysteine was specified as a fixed modification. Deamidation of asparagine and glutamine and oxidation of methionine were specified in X! Tandem as variable modifications. Oxidation of methionine was specified in SEQUEST as a variable modification.

Cryo-electron microscopy, image classification, and 3D reconstruction (Dr. Jomaa)

For cryo-EM, holey carbon grids (400 mesh copper) containing an additional continuous thin (5–10 nm) layer of carbon were previously washed with acetone vapor for 15 min and glow discharged in air for 30 sec [158]. Then, 3.5-mL aliquots of sample were applied to the grid for 1 min. Grids were blotted for 7 sec and vitrified by rapidly plunging into liquid ethane at -180°C with a Vitrobot (FEI). Data acquisition was performed under low dose conditions (z15 $e^{-}/Å^{2}$) on a JEOL 2010F FEG microscope operated at 200 kV with a Gatan 914 side-entry cryo-holder and at a nominal magnification of 50,0003. A total number of 121 electron micrographs were collected. The defocus range of the images was from -0.65 to -3.9 mm. The micrographs were digitized with a step size of 12.7 mm in a Nikon Supercool Scan 9000 producing images with a sampling value of 2.54 Å/pixel.

Particle projections from the electron micrographs were picked using Boxer [159]. Contrast transfer function of the micrographs was estimated using CTFFIND software [160] and corrected using the Xmipp software packager [161]. Image classification was performed using supervised methods [143, 144]. Detailed procedures regarding the classification method are included in the figure legend for Figure 2 of Jomma et al. [130].

From the total 73,896 projections collected, 16,228 showed a clear YjeQ density in our image classification procedure, and only those particles were subsequently used for the reconstruction of the 30S:YjeQ complex. The 3D reconstruction of the 30S:YjeQ complex was calculated using 3D projection alignment procedures as implemented in the Xmipp software package [161]. The reference map used to refine the 3D reconstruction was the X-ray structure of the *E. coli* 30S subunit (PDB ID: 2AVY) [27] low pass filtered to 25 Å resolution. In each refinement, sets of projections were calculated from the reference map using an angular spacing that ranged from 15° to 2° during the multiple cycles of refinement. The correct handedness of the structures was imposed by the X-ray crystal structure of the 30S subunit from *E. coli* (PDB ID: 2AVY). Resolution of the cryo-EM maps was estimated by calculating two maps following the last cycle of refinement from the even and odd numbered particles. The Fourier shell correlation was calculated between both maps and the resolution was estimated using an FSC value of 0.5. These values were used to low-pass filter the refined cryo-EM maps.

Construction of a pseudo-atomic model of the 30S:YjeQ complex (Dr. Jomaa)

To locate the YjeQ protein in the cryo-EM map of the 30S:YjeQ complex, a difference map between the control cryo-EM structure of the free 30S subunit (Fig. 3A, left panel) (low-pass filtered at the same resolution) and the YjeQ-bound 30S subunit was calculated. To this end, we scaled the two maps relative to each other by normalizing their average density and standard deviation values(s) to zero and one, respectively. Then, the two maps were super-imposed by maximizing the correlation coefficient and subtracted. The resulting difference map had an average density equal to zero and an *s* of

0.6. In the rendering only significant values (>2*s*) were displayed. The atomic structure of S. typhimurium YjeQ (PDB ID 2RCN) [167] was then docked as a single rigid body into the density of the obtained difference map covering the upper domain of helix 44 and platform in the 30S subunit. Subsequently, we applied small translational and rotational movements to each domain independently to optimize the fitting. Overlapping the obtained difference map containing the docked X-ray structure of YjeQ into the cryo-EM structure of the 30S:YjeQ complex and subsequent docking of the X-ray structure of the 30S subunit (PDB ID: 2AVY) [27] in the remaining density of the cryo-EM map allowed us to produce a pseudo-atomic model of the 30S:YjeQ complex. The same difference map analysis was repeated using two *E. coli* 30S subunit X-ray structures (PDB IDs: 2AW7 and 2AVY) [27]. In these two cases, the structures were first lowpass filtered to match the resolution of our 30S:YjeQ cryo-EM map and then fitted into the cryo-EM map of the 30S:YjeQ complex to perform the map subtraction and calculate the difference map. The CCC values to measure the fitting of the X-ray coordinates of YjeQ into the cryo-EM density were determined after conversion of the fitted atomic coordinates into a density map.

Flexible fitting refinement (Dr. Jomaa)

The starting model for the flexible fitting refinement was the atomic structures of the 30S subunit (PDB ID: 2AVY) and YjeQ (PDB ID: 2RCN) manually placed in the cryo-EM density of the 30S:YjeQ complex (see above). This assembly was divided into 26 distinct units (five 16S rRNA structural domains including the head, body, platform, helix 44, and helix 45 along with 20 ribosomal proteins and YjeQ) that were refined with

a flexible fitting algorithm using the YUP.scx module [168] of YUP [169]. The potential energy function included terms for the all-atom structures of the 30S:YjeQ complex that were represented as a Gaussian Network Model, terms for scoring the quality of the fit of the model to the density map, and volume exclusion terms. Specifically, the Gaussian Network was created from the initial structure, taking in any atom pairs that were within the cutoff distance of 4 Å. This prevented motions that would otherwise distort the starting structure, while allowing for flexibility between more isolated domains. The molecular dynamics simulation was carried out with a time step of 5 fsec. After an initial energy minimization, the model was heated from a low temperature to 10 K over 5000 steps and then held at 10 K over 20,000 steps. After equilibration, the annealing process was performed by reducing the temperature from 10 K to 1 K over ~50,000 steps, and the model was subjected to a final round of energy minimization. The final placement provides a pseudo-atomic model with stereochemical restraints that fits into the electron density map optimally.

Visualization of structures (Dr. Jomaa)

Visualization of the fitted YjeQ and 30S atomic structures and cryo-EM maps was done with UCSF Chimera software [166]. The electrostatic surface potential shown for YjeQ was also created using this software.

CHAPTER 3. New Tools for Studying Ribosome Biogenesis

3.1 AUTHOR'S PREFACE

This chapter contains experiments conducted as a part of a manuscript under construction at the time of the writing of this thesis. All experiments were designed and performed by myself in consultation with Dr. Eric Brown and Dr. Matthew Scott with input from my committee. All strains used for the study were sourced from the Brown lab strain databank except for the SmR and SmP mutants, which were provided by Dr. Matthew Scott.

3.2 INTRODUCTION

There is a paucity of descriptive phenotypes with which to study ribosome biogenesis. The hallmarks of disturbed assembly (altered ribosome profile, abundant precursor rRNA) are common to a number of biogenesis factors (Table 1.1). As such, they have limited utility in assessing specific functional roles. Furthermore, these phenotypes are not unique to defects in ribosome biogenesis. They can arise from multiple and sometimes seemingly unrelated sources. For example, inhibition of protein translation by chloramphenicol, an antibiotic targeting the 50S subunit, results in the accumulation of 17S rRNA and immature 30S subunits, two phenotypes associated with defects in 30S subunit biogenesis [51, 170].

This phenotypic overlap represents a central hindrance to the progression of the field, namely, the inability to conclusively determine if factors are directly involved in biogenesis or in translation. The interconnectedness of these two processes makes it challenging to study them independently. Perturbation of either system can affect the other, often through complex feedback pathways (Reviewed in [21, 51, 68, 74]). The problem is compounded by the fact that associated dispensability phenotypes can often correspond to both functional niches. Clearly, a convenient assay capable of definitively indicating direct perturbation of biogenesis would be a significant asset to the study of ribosome assembly. Such an assay would not only aid in identifying novel biogenesis factors and detailing the role of current putatives, but could also prove useful as a tool in screening for small-molecule inhibitors of the ribosome assembly process.

One of the aims of our work has been to design and validate such an assay. To this end, we have employed the putative biogenesis factor YjeQ as the vanguard protein in developing new tools for dissecting the assembly process. While a single assay capable of readily distinguishing between perturbations in biogenesis and translation has been elusive, these efforts have yielded a collection of new approaches that have proven useful to understanding ribosome assembly in the context of cellular health.

Growth Rate-Dependent Control

Proliferation is intimately linked with gene expression, which in turn depends on the ribosomal content of a cell [171-173]. As there is an upper limit to the rate at which individual ribosomes can translate, cells must rely on the modulation of ribosome quantity to meet demands for protein synthesis [146, 173-176]. Faster growth requires increased gene expression, which necessitates more ribosomes. Likewise, slower growth demands less protein synthesis and therefore, fewer ribosomes. Thus, proliferation is a function of cellular ribosome levels [177]. Indeed, for exponentially growing *E. coli,* ribosomal content is linearly correlated with growth rate [89, 172, 177, 178]. This phenomenon, termed growth rate-dependent control, has been observed in a number of microbes, suggesting a degree of universality [179].

In a study by Scott et al., a systems biology approach was used to examine the relationship between cell growth rate and gene expression [179]. Expanding on early studies, this group examined the effect of growth rate, dictated by the nutritional content of media, on the ribosomal material in wild-type cells and translation mutants. It is commonly held that ribosomal material in cell is reflected by the ratio of total RNA to

total protein [89, 173, 177, 179]. This ratio is henceforth denoted as *r*. In agreement with previous studies, the authors observed a linear correlation between specific growth rate λ (λ = ln(2)/doubling time) and ribosomal content (*r*) in wild-type *E. coli* (Figure 3.1). This correlation is described by the linear equation:

$$r = r_o + \lambda/k_t \qquad \text{eqn. 3.1}$$

Here r_o is the vertical intercept and k_t is the inverse of the slope. The latter reflects the translational capacity of the organism [179]. Scott and co-workers also examined the relationship between growth rate λ and *r* for two translation mutants denoted streptomycin resistant (SmR) and streptomycin pseudo-dependent (SmP), as well as the corresponding parent strain Xac (Figure 3.1B) [179]. Both SmR and SmP mutant strains feature alterations in ribosomal protein S12 that yield hyper-proofreading ribosomes with reduced rates of translation (Figure 3.1 B inset) [180]. Linear correlations between λ and *r* were observed for all three strains; however, both translation mutants yielded trends with steeper slopes (Figure 3.1 B). The increase in slope indicates a decreased translational capacity in the mutant strains (lower k_t values). Collectively, these experiments illustrate that the translational efficiency of a ribosome determines the quantity of ribosomes required for a certain growth rate. That is, to achieve the same growth rate as a wild-type strain with efficient ribosomes, a mutant strain harboring inefficient ribosomes requires more ribosomal material (Supplemental Figure 3.1).

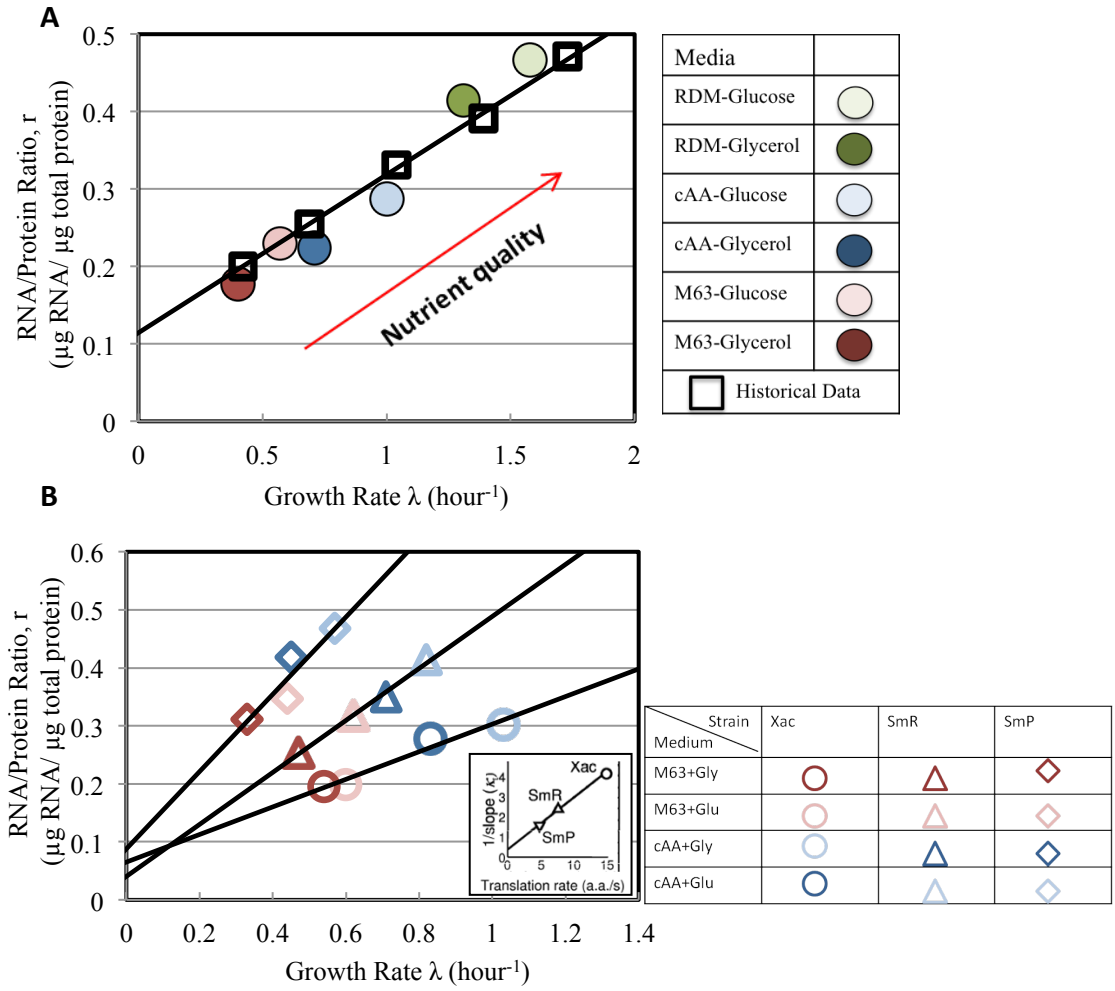

Figure 3.1: Correlation of the RNA/Protein ratio (r) with growth rate (λ) for various strains of E. coli. A) *A plot of RNA/Protein (r) with respect to specific growth rate λ^{-h} for two wild-type strains of E. coli. The growth rate is modulated using media of different nutritional value (figure legend). Solid circles represent recent data collected by Scott, et al. and open squares (black) are taken from historical experiments by Bremer et al. [146, 179]. Both data sets show a linear correlation between r and λ with a similar slope and common vertical intercept. The value of r at this vertical intercept (λ = 0) is hypothesized to reflect the basal level of non-functional ribosomal material in cells.* ***B)*** *A plot of r with respect to λ for two translation mutants (SmR, SmP) and their parent strain (Xac). Growth rate was modulated with various nutrients. For each strain a linear correlation between r and λ was observed, with each trendline having a common vertical intercept. The slope of this correlation was steeper for both translation mutants, suggesting the translational capacity (k_t) of the strains was reduced. Inset: Linear correlation of k_t values for Xac, SmR and SmP with respect to the measured rate of translation in each strain. Modified from Scott et al. [179].*

Implications for Studying Biogenesis

Of significant interest to our research group was the observation that the vertical intercept (r_o) for each curve in the study above was not zero. It can be seen in Figure 3.1 that at a theoretical growth rate of zero some quantity of ribosomal content ($r_o \approx 0.1$) was predicted to exist. Scott and co-workers interpreted this as the basal level of ribosomal material not directly contributing to protein synthesis, including both assembling subunits as well as non-functional ribosomal entities [173, 179]. This phenomenon is made more significant by the fact that the trendlines for all three strains studied, namely, the wild-type and two translation mutants, had approximately the same intercept; they had the same basal level of non-functional ribosomes. Indeed, previous studies suggest that the proportion of ribosomal material not involved in translation is constant regardless of growth rate [68, 147, 173]. This phenomenon could be telling in the context of ribosome assembly where defects are anticipated to affect this ratio (Supplementary Figure 3.1). Mutations in several ancillary biogenesis factors, including YjeQ, have been shown to increase the levels of non-functional ribosomal material in cells in the form of immature subunits [51, 114, 116, 117, 122, 124-126, 129, 132, 133]. Thus, it became our working hypothesis that disruptions in ribosome assembly would alter the correlation between growth rate and ribosomal content, elevating total ribosomal material (r) at each growth rate as a result of the higher level of r_o (the proportion of non-functional material). Figure 3.2 depicts the predictions of this hypothesis.

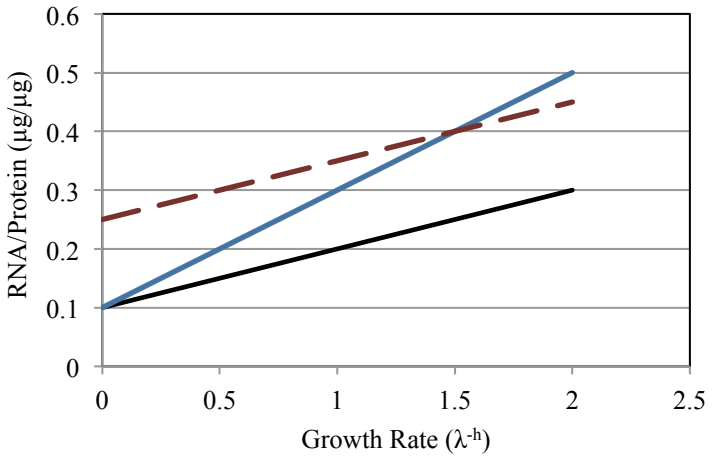

Figure 3.2: Hypothetical dependence of growth rate on ribosome content in a biogenesis mutant. *Linear correlations between RNA/Protein (r) and growth rate (λ^{-h}) were observed to have a common non-zero vertical intercept in a wild-type strain (solid black line) and a translation mutant (solid blue line) [179]. In both these strains non-functional ribosomal material represents a minor fraction of the total ribosomal content of the cell and is indicated by the vertical intercept ($r \approx 0.1$ at $\lambda = 0$). Biogenesis mutants (dashed red line) have been shown to have significant levels of immature, and thus, non-functional ribosomal material. It was hypothesized that this would manifest in an elevated vertical intercept when the linear correlation between r and λ was examined.*

3.3 RESULTS

3.3.1 Growth Rate and Ribosome Content in a Δ*yjeQ* Strain

Growth rate-dependence of ribosome quantity

We examined the relationship between ribosomal content (*r*) and growth rate (λ) in a strain lacking the putative biogenesis factor YjeQ (MG1655 background). Our methodology was adapted from the work by Scott et al. and is detailed in the Materials and Methods section of this chapter. Briefly, media of varying nutritional quality were used to modulate growth rate and ribosomal content was estimated from total RNA/total protein (*r,* µg/µg) (Supplementary Figure 3.2). As can be seen in Figure 3.3 A, we observed a linear correlation between λ and *r* for our wild-type control strain (black line, circles). The slope (and therefore k_t) was similar to that observed historically and also

reported by Scott et al. [146, 173, 179]. In addition, the vertical intercept was non-zero ($r \approx 0.1$).

A linear correlation between λ and r was also observed for the Δ*yjeQ* mutant strain (Figure 3.3 red line, squares and Supplementary Figure 3.3 hashed line). The trend had a substantially steeper slope (lower $k_{t)}$ than the wild-type. This suggests a greater quantity of ribosomal material in the cells, especially at faster growth rates; $r_{\Delta yjeQ}$ was approximately double r_{wt} in rich media (RDM-Glucose). Interestingly, our Δ*yjeQ* trend revealed a negative y-intercept (r_o). Multiple iterations of this experiment produced the same result. This observation was inconsistent with our hypothesis that a perturbation of biogenesis should increase the non-functional ribosomal material in cells and manifest in an elevated vertical intercept r_o. Our previous work with Δ*yjeQ* cells, however, indicates that this is in fact the case; there is an elevated level of non-functional 17S-containing 30S precursors in strains lacking YjeQ. This disparity suggests that the r_o intercept no longer depicts non-functional material in a ribosome biogenesis mutant. Indeed, a negative level of ribosomal material has no meaning in the real world, as cellular growth cannot occur without ribosomes.

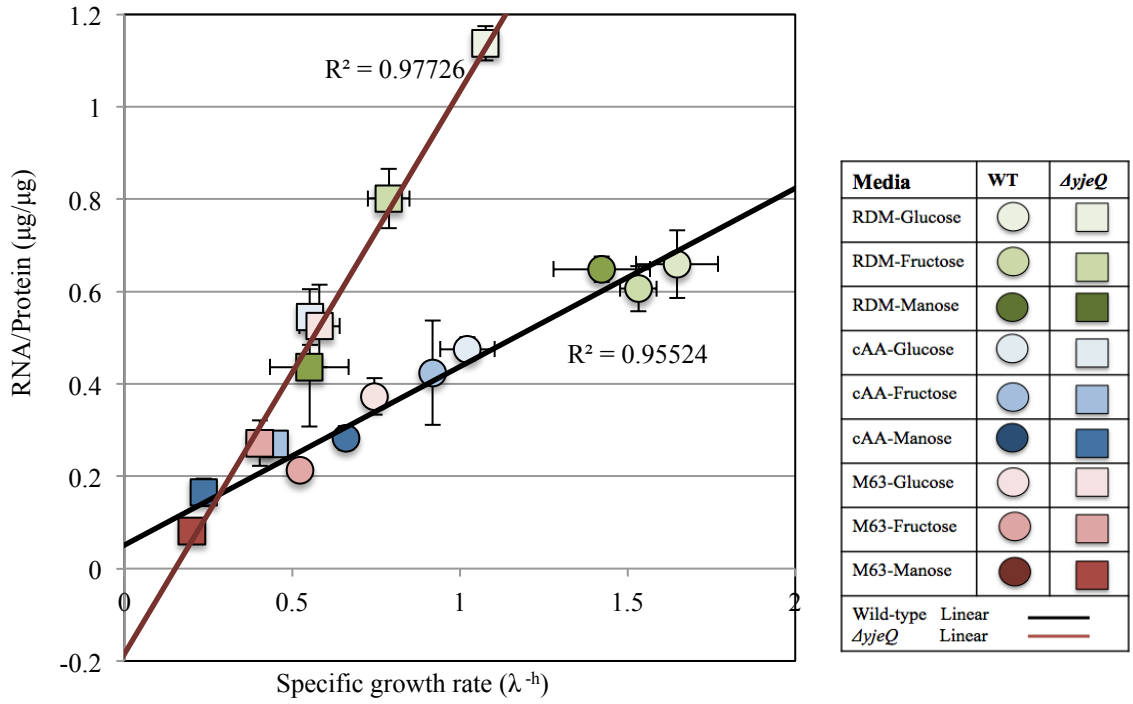

Figure 3.3: Examining the correlation of the RNA/Protein ratio (r) with growth rate (λ) in the ΔyjeQ deletion. *Plot showing λ vs r for wild-type MG1655 and the corresponding ΔyjeQ deletion strain. In this experiment growth rate is modulated using media of different nutritional value (figure legend, top = richest, bottom = poorest). A linear correlation was observed between r and λ for the wild-type (black line). A linear correlation between r and λ was also observed for the ΔyjeQ mutant strain (red line). This correlation varied significantly from that seen for the wild-type strain as it featured a much steeper slope (low k_t) and a negative vertical intercept ($r_o < 0$). The lower k_t indicates that the ΔyjeQ mutant strain has a reduced translational capacity in comparison to the wild-type. Each point was determined by taking the average growth rate and r values for three biological replicates. The plot of individual replicates can be found in Supplemental Figure 3.2.*

RNA/Protein in the ΔyjeQ mutant

It is important to note that for these studies total RNA/total protein is serving as a proxy to measure ribosome levels. Given the aberrant proportion of 17S/16S rRNA seen in the Δ*yjeQ* strain, it would not be surprising if this equivocation no longer holds when

biogenesis is disturbed. The SmR and SmP mutants present an idealized scenario where the rate of translation has been reduced, yet the stoichiometry of rRNA to r-proteins in functional ribosomes remains unchanged. The vast majority of ribosomal material in these strains is contributing directly to protein synthesis. This stands in stark contrast to the *yjeQ*-null strain, in which there is an abundance of free subunits that do not impact a cell's capacity for translation.

Range of Linearity

Previous studies have suggested that the linear trend between ribosomal content breaks down at slow growth rates ($\lambda < 0.5^{-h}$) [89, 146, 175]. In the poorest media tested, the Δ*yjeQ* deletion has specific growth rate approximating ~ 0.2^{-h}. Dennis and Bremer noted that below a certain growth rate, ribosomal content deviates from the linear trend [173]. They suggest that there is some minimal growth rate that serves as the lowest possible point for balanced steady-state growth. Below this rate, some cellular processes (i.e. uptake of nutrients) become limiting, such that ribosome concentration no longer dictates proliferation. We considered the possibility that in poor media the Δ*yjeQ* deletion was no longer in balanced growth: growth rates in the four poorest media used were less than 0.5^{-h}. As such, these values might be skewing the linear trend and misrepresenting the relationship between growth rate and ribosomal content. However, exclusion of values below this specific growth rate ($\lambda < 0.5^{-h}$) had little bearing on the linear trend as it remained substantially steep and continued to intersect the y-axis at a negative value.

Cellular protein concentration

Several studies have demonstrated that total protein quantity per mass of cells (p_{conc}),, as measured by $\mu g_{protein}/OD_{600,}$ remains relatively constant over medium to fast growth rates [181]. At slower growth rates p_{conc} rises modestly with increasing generation time [146, 171]. Cell mass is proportional to growth rate; at slower rates of proliferation, cells are smaller and thus, comprised of less material. However, the proportion of cellular mass that is made up of proteins increases as cell size decreases [89, 146, 173]. As such, at slow growth rates there is a higher concentration of protein in cells (i.e. cells are smaller in poor growth conditions but house more protein per unit of volume) [171].

For our wild-type strain, the majority of growth conditions foster sufficiently rapid growth, such that protein quantity per mass remains approximately equivalent across the various media (Supplemental Figure 3.4 A, B black, circles). In contrast, protein concentration in the Δ*yjeQ* deletion rose significantly with decreasing nutritional quantity (Supplemental Figure 3.4 A, B, squares). This is likely a reflection of the significantly retarded growth rates of the mutant, which are suspected to correspond with a reduction in cell size and increase in p_{conc}.

Cellular RNA concentration

RNA concentration per mass, as measured by μg_{RNA} /OD_{600} (RNA_{conc}), has been shown to be proportional to proliferation rate during balanced growth and is yet another indicator of cellular ribosome levels [171]. In both the wild-type and mutant strains RNA concentration increases linearly with growth rate (Figure 3.4). In the Δ*yjeQ* deletion the level of RNA with respect to mass is significantly elevated in comparison to the wild-type

for a given rate of growth, though less so than the RNA/protein measurements suggest. In addition, the intercept is positive. However, both trends still appear to converge at a growth rate greater than zero (discussed below).

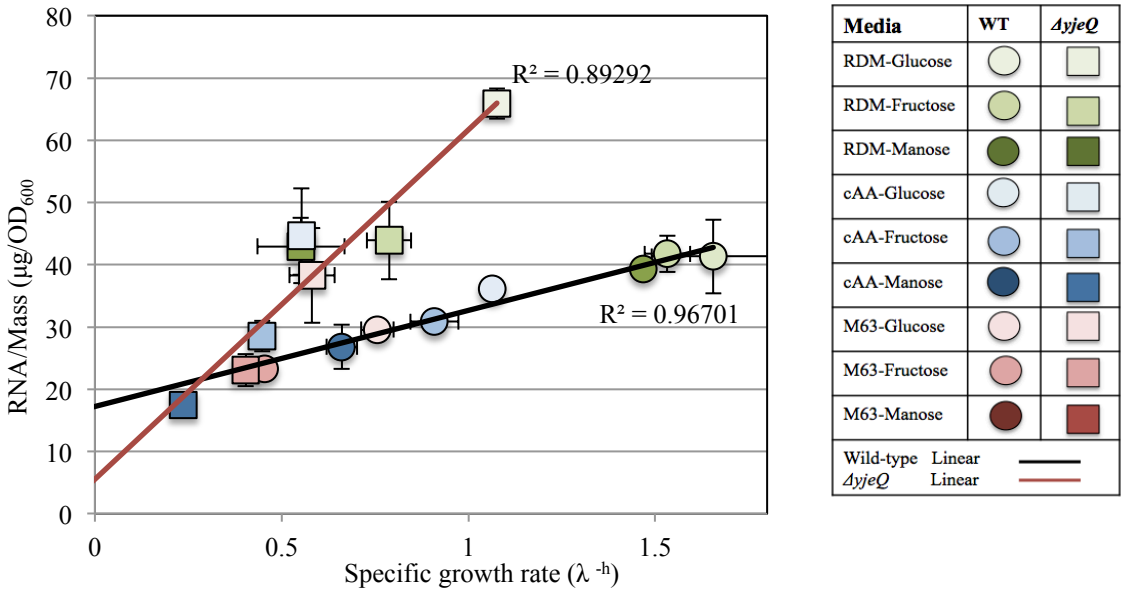

Figure 3.4: Examining the correlation of the RNA/OD$_{600}$ ratio (RNA$_{conc}$) with growth rate (λ) in the ΔyjeQ deletion. *Plot showing λ vs RNA$_{conc}$ for wild-type MG1655 and the corresponding ΔyjeQ null-strain. In this experiment growth rate is modulated using media of different nutritional value (figure legend, top = richest, bottom = poorest). A linear correlation was observed between RNA$_{conc}$ and λ for the wild-type (black line). A linear correlation between RNA$_{conc}$ and λ was also observed for the ΔyjeQ mutant strain (red line). Once again, a steep trendline illustrates that the mutant houses more ribosomal content in comparison to the wild-type at a given growth rate. While neither intercept is negative, the trends still converge at point greater than zero growth.*

RNA/Protein versus RNA/OD$_{600}$

The ratio of RNA/Protein (*r*) is proportional to the number of ribosomes per total amount of cellular protein. As such it signifies the cellular concentration of ribosomes [146]. However, in the Δ*yjeQ* deletion the quantity of protein per cell mass roughly tracks

inversely with growth rate and RNA. As such, RNA/Protein (*r*) is not equivalent to RNA/OD_{600} (RNA_{conc}) in this strain. The latter is likely a more reliable means of determining intracellular RNA levels as the average cell volume per mass (OD_{600}) is largely unaffected by growth rate [146]. Thus, while both methods illustrate growth rate-dependence of ribosomal material, RNA/Protein (*r*) likely over estimates the ribosome quantities as it pegs RNA to protein levels, which fluctuate significantly in the Δ*yjeQ* deletion.

This deviation could be the origin of the negative intercept; RNA levels move inversely with protein levels in the biogenesis mutant, thereby overstating cellular ribosome concentration at fast growth rates and understating them at slow growth rates. However, the RNA/Protein ratio provides unique insight into the translational capacity of the cell as it describes the ratio of ribosomes to total protein in a culture and thus, is an indicator of the translational potential of a population's ribosomal material. For example, at fast growth rates, the protein output per mass of RNA (RNA/Protein) in the Δ*yjeQ* deletion is substantially less than in the wild-type (Supplementary Figure 3.3), indicating that mutant cells are getting less ' bang' for their ribosomal 'buck.' Interestingly, regardless of which approach is used to quantify ribosomal material, the trends converge at a point greater than zero growth, suggesting that in poor nutrient conditions the wild-type and mutant behave in similar fashion. We suggest that the point of intersection represents the point at which perturbation in biogenesis no longer impedes growth rate.

Elevation of Ribosomal Content

While the negative intercept and fluctuating protein levels complicate the interpretation of these trends, it is clear from the data that ribosomal levels are elevated in the Δ*yjeQ* deletion strain, especially in conditions that foster rapid growth. This implies that mutant cells require increased ribosome production to achieve growth rates comparable to the wild-type. Intuitively, this makes sense; approximately 50 % of the ribosomal material in the mutant is non-functional, so twice as much material is required to achieve wild-type translational output. This is similar to the scenario in the translation mutants (SmR, SmP) discussed above where more ribosomes are required to make up for poor translation efficiency. Thus, in the Δ*yjeQ* mutant, the proportion of non-functional material influences ribosome levels, whereas in the translation mutants, ribosome quantity is dictated by the decrease in catalytic efficiency (Supplementary Figure 3.1).

3.3.3 Understanding Ribosomal Growth Rate-Dependence in a *ΔyjeQ* Strain

Steady-state levels of immature rRNA are independent of growth rate

In the absence of YjeQ, assembly of the ribosome still occurs. It is not yet known if this is achieved through alternate parallel pathways or if functional overlap amongst assembly factors ensures that the ribosome is completed. Regardless of the mechanism, maturation proceeds via a YjeQ-independent process, albeit with reduced efficiency. It is worth considering that in media fostering slow growth rates, aberrant biogenesis might be sufficiently fast to keep pace with cell division. Longer generation times provide increased opportunity for maturation and assembly, which could result in a higher

proportion of functional 70S ribosomes in cells. At slow growth rates, a defect in assembly may not be limiting. At faster growth rates, however, a perturbed assembly pathway may be incapable of keeping pace and therefore lead to an accumulation of non-functional material. Thus, at slow growth rates the RNA/Protein ratio may reflect a greater proportion of functionally active ribosomes than at fast growth rates. This variation could potentially account for the convergence of the wild-type and mutant trends, as the correlation between growth and RNA/Protein for the Δ*yjeQ* strain would be non-linear in the mutant with the proportion of functional ribosomes increasing with declining growth rate (Supplementary Figure 3.5). Thus, the Δ*yjeQ* curve would be asymptotic to the wild-type trend with a vertical intercept similar to that seen for the wild-type and translation mutants.

To test this hypothesis, the proportion of 17S (non-functional) to 16S (functional) rRNA in Δ*yjeQ* cells was examined in six different media of varying nutritional quality. (Figure 3.5). Surprisingly, no significant change in the relative levels of 17S and 16S rRNA was observed over the growth rates tested, suggesting that the proportion of immature rRNA in cells is independent of growth rate. While this result was not anticipated, it is consistent with previous observations that the proportion of actively translating ribosomes in wild-type *E. coli* is not affected by environment or growth rate [68, 147, 173]. As this experiment interrogates steady-state levels of rRNA, it only provides a snapshot in time of the ribosome population in a culture. Thus, it yields limited insight into how different growth conditions influence the interplay of assembly and proliferation rates. We next sought to examine this relationship using pulse-chase

methods to examine the kinetics of subunit maturation with respect to growth rate in the in Δ*yjeQ* mutant.

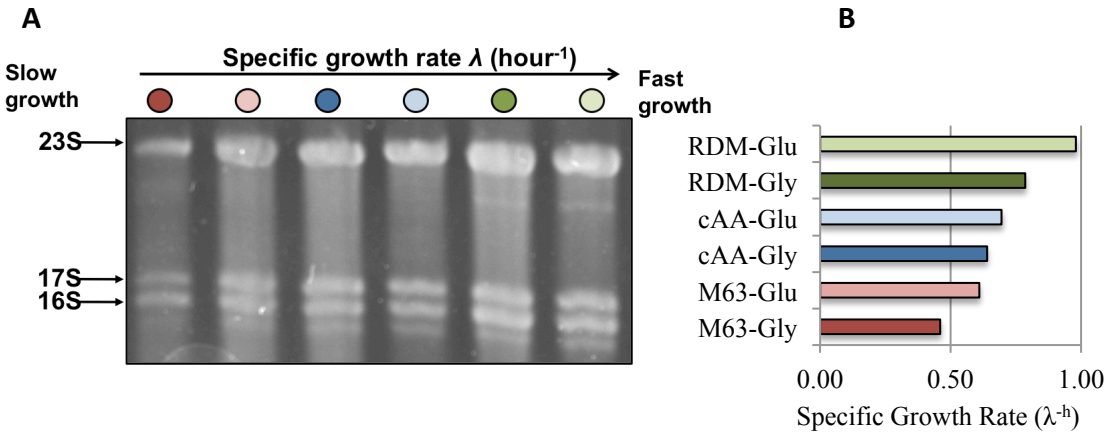

Figure 3.5: Steady-state proportion of precursor rRNA is independent of growth rate in a ΔyjeQ deletion. A) *Analysis of rRNA derived from the ΔyjeQ mutant strain grown in media with varied nutritional content. No significant difference in the proportion of functional to non-functional (16S/17S) rRNA is observed between media.* ***B)*** *Specific growth rates (λ^{-h}) for ΔyjeQ deletion strain grown in media of varying nutritional quality.* ***Acronyms:*** *RDM - Rich Defined Media, cAA - Casamino Acids-Supplemented M63 Media, M63 – Minimal Media, Glu/gly – media supplied with glucose or glycerol.*

Ribosome Maturation Rate versus Growth Rate

Cells lacking YjeQ harbour nearly twice as much ribosomal material as the wild-type. Ribosome profile analysis indicates that nearly half of this material is in the form of free subunits (~43%, Supplementary Figure 1.1. Figure 4.5). Likewise, quantification of rRNA species in the *yjeQ*-null suggests that nearly half of the 30S subunit-derived rRNA is immature 17S (54%) (Figure 4.6). Thus, while the relative amount of non-functional material in the Δ*yjeQ* deletion strain is substantially higher than in the wild-type, the absolute quantity of functional ribosomes in the mutant is roughly equivalent. At first glance, the *yjeQ*-null would then be expected to have a translational capacity similar to

that of the wild-type and arguably, a comparable growth phenotype. However, it is the rate of ribosome accumulation that that limits growth rate when biogenesis is perturbed, not the steady-state level of functional ribosomes.

Studies suggest that the cell division is linked to translational capacity, whereby ribosome production dictates protein synthesis output, which in turn influences the rate of proliferation [182-187]. The precise mechanism governing this connection is not known, but it is clear that regulatory systems enable a cell to tailor ribosomal concentration to suit its environment. Interestingly, it has been suggested that the feedback mechanism regulating ribosome production only accounts for actively translating ribosomes [182-187]. When the level of translating ribosomes is low, synthesis of rRNA is up-regulated to increase the pool of functional ribosomes. This feedback occurs regardless of the level of immature subunits in cells [183]. Thus, a cell will continue to manufacture ribosomes until an optimal concentration is achieved that enables it to maximize growth given the conditions of its environment. Once this threshold is reached, rRNA transcription is down-regulated so that the cell does not needlessly invest resources into ribosome production [183, 188]. This likely explains why a biogenesis mutant would possess vast quantities of ribosomal material and yet still suffer a growth defect. The reduced rate of ribosome assembly extends the time required to synthesize this threshold of active ribosomes, delaying the attainment of maximal output and ultimately, slowing division.

The proportion of functioning 70S within an individual cell requires consideration of both the rate of ribosome synthesis as well division time. In wild-type cells, assembly is rapid (< 5 minutes) and the rate-limiting step in ribosome production is the

transcription of the *rrn* operons [51, 90]. Work by Michaels and others have established that the rate of ribosomal maturation, the time it takes for newly synthesized transcripts to become functional 70S ribosomes, is a constant fraction (*F)* of generation time [51, 90]. That is, the faster cells grow and proliferate, the faster they build ribosomes. When assembly is perturbed, the transcription of rRNA is no longer rate-limiting. Instead, maturation and subunit association become bottlenecks in the biogenesis pathway. As such, we hypothesized that the rate of ribosomal maturation in the Δ*yjeQ* mutant should be consistent across media of varying nutritional quality.

We examined the rate of maturation through pulse-chase monitoring of 17S rRNA processing in rich and poor media (RDM-Glucose and M63-Glucose). The growth rate of the Δ*yjeQ* deletion in RDM-Glucose (doubling time ≈ 40.8 minutes) is approximately 1.9 times that of the growth rate in M63-Glucose (Doubling time ≈ 72.3 minutes). Figure 3.6 depicts the maturation of 17S rRNA in both these conditions. In rich media, ~50% of 17S rRNA was converted to the mature form within 60 minutes as determined by pixel counting with ImageQuant version 5.2. Maturation occurs slightly slower in M63-Glucose: ~40% of 17S rRNA is converted within 60 minutes. Processing is approximately linear for the first 60 minutes of growth in both conditions. The rate of maturation, as measured by the percentage of 17S rRNA processed per minute (*P*), is 0.71% min^{-1} and 0.59% min^{-1} for the rich and poor media respectively.

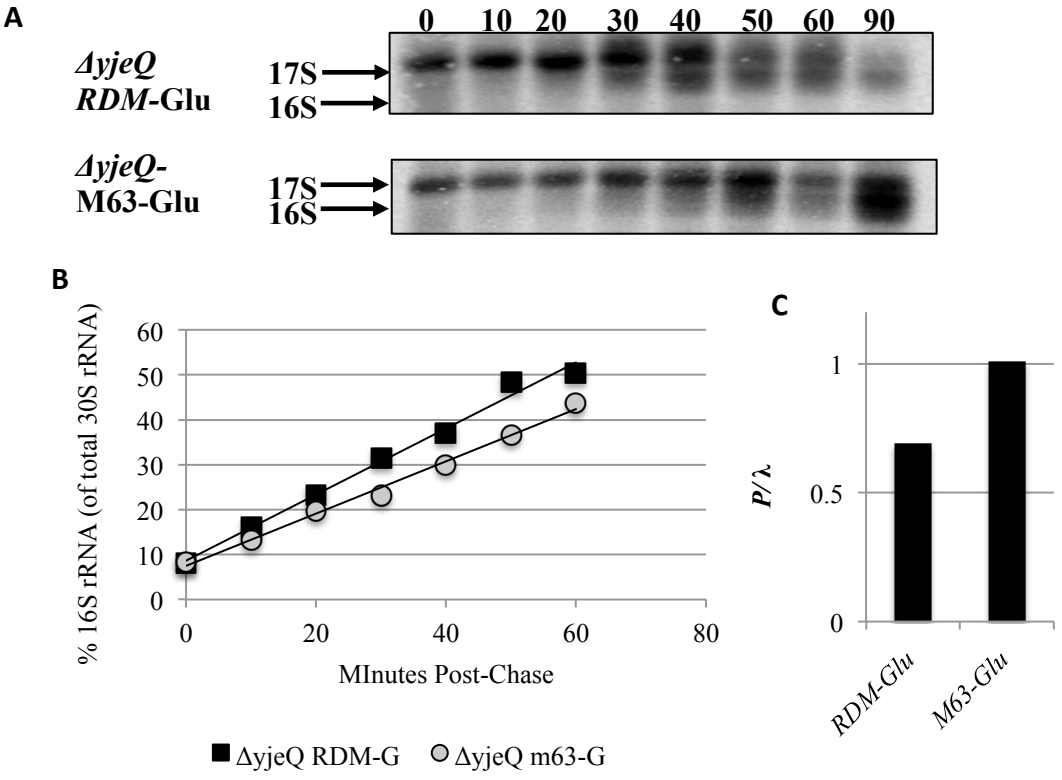

Figure 3.6: Examining the influence of media nutrition on 16S rRNA maturation rate in the ΔyjeQ deletion. A) *Radiogram of labeled 17S rRNA in the ΔyjeQ deletion grown in RDM-Glucose (RDM-Glu) and M63-Glucose (M63-Glu). 17S rRNA is gradually converted to 16S rRNA over the time-course. After 90 minutes, more than 60% of the rRNA is mature in both media.* ***B)*** *Plot showing the level of 16S rRNA (relative to all 30S-derived rRNA) as determined by band quantification using ImageQuant version 5.2. The rate of maturation in RDM-Glu is only slightly faster than the rate in M63-Glu (0.71 % min^{-1} versus .587 % min^{-1}).* ***C)*** *The value of F (P/λ) for the ΔyjeQ deletion is different in the two media tested (RDM-Glu: 0.7, M63-Glu: 1.0)*

The fraction *F,* representing the ratio of rRNA processing rate (*P)* to growth rate (λ), was calculated as:

$$F = \frac{\frac{\Delta\ \%\ 17S\ rRNA\ (P)}{\Delta\ minutes}}{\text{Specific growth rate } (\lambda^{-h})} \qquad \text{eqn. 3.2}$$

F (P/ λ) for the Δ*yjeQ* strain differed substantially between rich and poor media (0.7 and 1.0 respectively). This contrasts previous studies demonstrating that this fraction remains constant across growth rates in wild-type cells [51]. These results support the notion that perturbations in the assembly pathway become the primary determinant of ribosome synthesis rates. Though ribosome maturation rate is slightly faster in rich media (~20% faster), it is small in comparison to the difference in growth rate (~75% faster). As such, in poor media (M63-Glu) a greater proportion of ribosome material is expected to mature per cellular division. Given this decoupling of growth and assembly rates, we suspect that the impact of ribosome biogenesis defects is more pronounced in rich conditions that support rapid growth, where ribosome assembly significantly limits a cell's ability to capitalize on available nutrients. Further study across a broader range of growth rates is required to test this hypothesis and clarify the connection between assembly rate and generation time in the *yjeQ*-null strain.

3.3.4 Growth Rate-Dependence in Additional Biogenesis Mutants

We next examined the growth rate-dependent control of ribosome quantity in two additional biogenesis mutants (Δ*rbfA*, Δ*rimM*) as well as the translation mutant Δ*tufA*. The method employed was the same as above except the strains examined were derived from the Keio collection of non-essential deletions [189]. As such, *E. coli* BW25113 was used as the parent strain for these studies. In addition only six media of varying nutritional content were examined (Figure 3.7, legend).

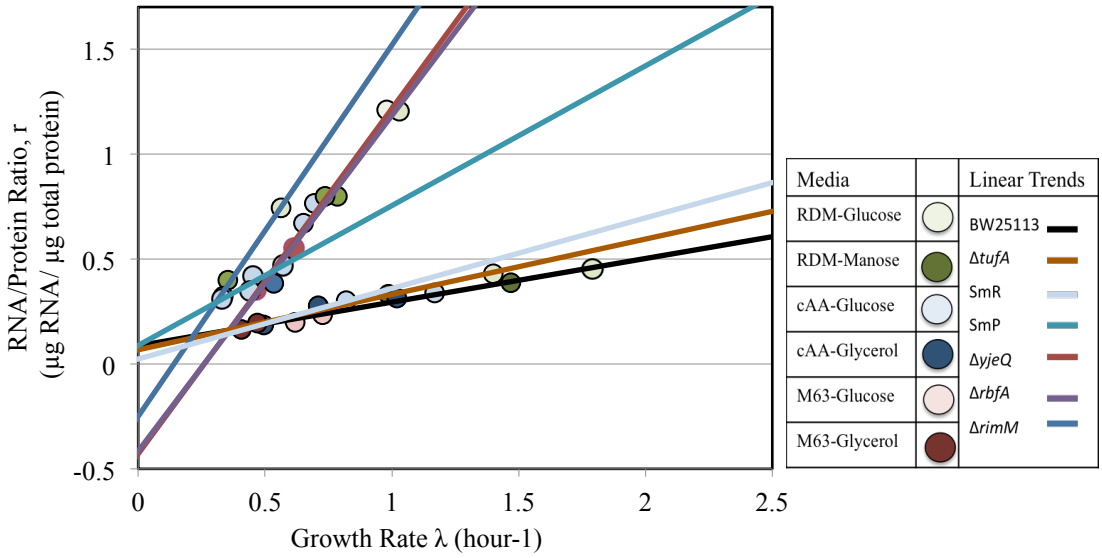

Figure 3.7: Examining the correlation of the RNA/Protein ratio (r) with growth rate (λ) in biogenesis mutants. A) *Plot showing λ vs r values for wild-type BW25113 and a shortlist of deletions. In this experiment growth rate is modulated using media of different nutritional value (figure legend). The plot illustrates the correlation between r and λ in biogenesis and translation mutants. Linear correlations with steep slopes (lower k_t) were observed for biogenesis mutants ΔyjeQ, ΔrbfA, ΔrimM (red, purple, dark blue) and the translation mutants SmR and SmP (data from [179], light blue, teal). A strain lacking tufA, coding the translation aid Elongation Factor Thermo Unstable (EF-Tu, orange), showed a marginal increase in slope with a positive x-intercept ($r_0 \approx 0.1$).*

Biogenesis mutant: ΔrbfA

The plot of *r versus* λ for the Δ*rbfA* deletion yields a linear correlation reminiscent of that seen with Δ*yjeQ*: a steep slope with drastically increased ribosomal content at high growth rates and a linear trend suggesting a negative y-intercept (Figure 3.7, purple line).

Biogenesis mutant: ΔrimM

Deletion of *rimM* severely retards growth and also gives rise to significantly increased ribosomal content at fast growth rates. The slope of the *r*/ λ line for this biogenesis mutant is also increased in comparison to the wild-type (Figure 3.7, dark blue).

For Δ*rimM*, ribosomal content could only be examined for the three richest media. For the poorest media, lengthy incubations were required to allow cultures to reach densities sufficient for the accurate quantification of RNA and protein. Growth rates were inconsistent over these extended time courses and were thus deemed unreliable.

Translation mutant: ΔtufA

To better understand the implications of these observations, efforts were made to examine how direct interference with translation affected the r/λ relation. In the study by Scott et al. mutated ribosomes with reduced translational efficiency were used for this purpose [179]. To further expand on these observations we chose to examine perturbations in translation brought about by disruptions in the function of trans-acting factors. In *E. coli* many trans-acting translation factors are essential. Thus, options for direct interference with translation via a full gene deletion are limited.

EF-Tu is an essential protein involved in the transport and accurate selection of cognate tRNA's. Two genes, *tufA* and *tufB*, encode nearly identical copies of this factor. While deletion of both genes is fatal, strains harboring either single deletion are viable, though they display reduced translational capacity. EF-Tu derived from the *tufA* gene appears to be especially important to full growth in rich media; with strains bearing only *tufB* exhibiting reduced growth rates [190]. As can be seen in Figure 3.7, the *tufA*-null had a specific growth rate (λ) in RDM-Glu approximately 20% slower than the parental wild-type. As expected, a linear correlation between λ and *r* was observed (Figure 3.7, orange). The deletion of *tufA* resulted in a subtle increase in the slope of the trend in comparison to

wild-type. In addition, a positive intercept approximating that of the wild-type was observed.

3.3.5 Towards a Unique Phenotype

The absence of the putative assembly factor YejQ appears to significantly alter the relationship between ribosomal content and growth rate in cells. Likewise, the impediment of translation in the SmR and SmP mutants yields deviation from the wild-type trend. In both cases, the translational capacity (k_t) of the cells is compromised and more ribosomal material is required, relative to the wild-type, to achieve a given growth rate. The degree of elevation seen in the Δ*yjeQ* deletion strain is substantially higher than that associated with the translation mutants examined here. Interestingly, similar trends were observed in strains harboring *rimM* and *rbfA* deletions but not for a strain lacking translation factor EF-Tu (Δ*tufA*). Both strains demonstrated a significantly increased slope in comparison to the wild-type. For the limited collection of mutants we have examined, only deletions in assembly factors gave rise to the enigmatic negative y-intercept. Drawing conclusions about the exclusivity of these phenotypes to disruptions in biogenesis are tempting, but premature. A much broader and comprehensive sample population would be required to solidify the legitimacy of such claims. Nonetheless, these observations suggest that the quantity of ribosomal material in a cell presents a new avenue for identifying disturbances in biogenesis and understanding their affect on cellular fitness.

3.4 DISCUSSION

Growth rate-dependence

The translational capacity of a cell is dictated by the number of functioning ribosomes it houses as well as the efficiency of the individual units. The mutants examined here illustrate this balancing act of quantity and quality in achieving optimal growth; cells with less efficient ribosomes require more of them to achieve the same output as wild-type cells. It is hypothesized that perturbations in biogenesis primarily affect the quantity of functioning units in a cell by decreasing the rate of assembly.

We set out to uncover a readily assayable phenotype unique to perturbations in ribosome assembly by examining growth rate-dependence in biogenesis mutants. While a clear-cut phenotype has evaded us, we believe the approaches outlined here could have utility in the study of assembly. These assays augment the current repertoire of methods available for use in the identification and characterization of biogenesis defects. In the absence of a panacea with which to study this process, diversity in our approaches will enable us to delve deeper into the inner workings of assembly, while maintaining a holistic view of bacterial protein synthesis.

We have demonstrated that cells lacking the YjeQ protein exhibit growth-rate dependence with regards to ribosomal content, as determined by the ratio of RNA/Protein or RNA/OD_{600}. The linear trends illustrate that increased quantities of ribosomes are required for the mutant to achieve growth rates comparable to the wild-type strain for any given media, indicating that cells lacking the YjeQ protein have compromised translational capacity. In addition, the concentration of protein in Δ*yjeQ* cells appears to

be lower than that of the wild-type when grown in fast media. We attribute this to a reduced level of protein synthesis in comparison to the wild-type. We have illustrated that protein concentration increases substantially with generation time in the *yjeQ*-null. This calls into question the accuracy of the RNA/Protein ratio in measuring cytoplasmic ribosome concentration, especially in strains with mutations affecting ribosomal infrastructure. The concentration of RNA per cellular mass (RNA/OD_{600}) is likely a more accurate indicator of ribosomal quantities, especially for slow growing mutants like the Δ*yjeQ* deletion. Nevertheless, both approaches are useful in detecting alterations in ribosome levels and translational output.

Regardless of the method employed to quantify cellular ribosome levels, the linear relationships for the wild-type and Δ*yjeQ* mutants intersect at a growth rate greater than zero. We suggest that this intersection signifies the point at which biogenesis is no longer limiting to growth and as such, is the point at which the Δ*yjeQ* deletion is as efficient as the wild-type at utilizing environmental resources.

Identifying perturbations in biogenesis

The elevated level of ribosomal material seen in the Δ*yjeQ* deletion and other biogenesis mutants presents a new and convenient phenotype that may have utility in identifying perturbations of the assembly process. The ability to characterize this phenotype in high-throughput could enable large-scale genetic and chemical screens for defective biogenesis. Both RNA/Protein (*r*) and RNA/OD_{600} (RNA_{conc}) were useful in recognizing reductions in translational capacity and could have substantial utility in identifying perturbations in ribosome biogenesis or at the very least, protein synthesis.

3.5 MATERIALS AND METHODS

Strains and Media

All strains in this study were sourced from either the Keio collection of non-essential gene-deletions (Wild-type BW25113, Δ*yjeQ,* Δ*rimM,* Δ*rbfA,* Δ*tufA,*) or were previously constructed by Campbell et al. (wild-type MG1655, ΔyjeQ*)* [128, 191]. The nutritional quality of media used in this study was dictated by a combination of a variety of nitrogen and carbon sources. This included MOPS-based EZ Rich Defined Media (RDM, Teknova), M63 media supplemented with casamino acids (cAA), and plain M63 media (M63). Carbon sources in order of nutritional quality were glucose (Glu), glycerol (Gly), fructose (Fru) and manose (Man) [192].

RNA/Protein vs Growth Rate

Growth rates and RNA/Protein ratios were examined for a number of strains grown in media of varied nutritional content. Strains were grown for 16 hours at 37°C with shaking (250 rpm). Cells were then subcultured into one of nine distinct media (RDM-Glu, RDM-Fru, RDM-Man, cAA-Glu, cAA-Fru, cAA-Man, M63-Glu, M63-Fru, M63-Man) and grown to mid-log phase (1 in 10,000 dilution). Cells were subsequently diluted in fresh media, incubated with aeration in a 37°C water bath and grown to early exponential growth phase. Optical density at 600 nm (OD_{600}) was then measured manually throughout exponential growth on a Spectronic^{TM} 200 spectrophotometer (Thermo Scientific). For each growth condition, six OD_{600} readings were taken spanning two doublings of the culture. These values were plotted against time on a semi-log plot and specific growth rates (λ, $hour^{-1}$) were calculated from the slope of a linear trendline

(Supplemental Figure 3.2). A stringent cut-off requiring R^2 values of 0.99 or greater was used to ensure the determination of accurate growth rates. Three biological replicates were performed for each media and strain combination for a total of 27 samples per curve.

Throughout mid-log phase, 1 ml aliquots of each culture were harvested and immediately frozen in a dry ice/ethanol bath. RNA and protein were subsequently extracted from these samples (0.5 ml each). Total RNA was isolated using RNeasy Mini kit (Qiagen) as per the manufacturer's protocol and quantified (μg) by absorbance at 260 nm using a NanoDrop® spectrophotometer. To ensure linearity and accuracy in quantification, RNA was extracted from cells at multiple time-points in exponential growth phase and plotted against OD_{600} (Supplementary figure 3.3). Quantification was only considered accurate if this plot yielded a straight line with an R^2 value greater than 0.95. Total protein was isolated and quantified using the Sigma Total Protein Kit® (a modification of the Lowry assay) as per the manufacturer's protocol using a SpectraMax® Plus 384 plate reader. Once again, reliability of quantification was determined by examining the linear correlation of protein with OD_{600} (cut-off of R^2 = 0.95). The RNA/Protein ratio (r, μg/μg) was plotted against calculated growth rates (λ^{-h}) and a trendline was established.

The same protocol as above was followed when testing strains from the Keio collection except only six distinct media were used including Rich Defined Media supplemented with glucose or glycerol (RDM-Glu, RDM-Gly), M63 minimal

supplemented with casamino acids and glucose or glycerol (cAA-Glu, cAA-Gly), and M63 minimal media supplemented with glucose or glycerol (M63-Glu, M63-Gly).

Steady state levels of rRNA

Steady state levels of rRNA were examined via agarose gel electrophoresis (2.1 %, 4 h at 4.5 V/cm) using RedSafe™ (FroggaBio) in combination with a Typhoon™ multimode imager (GE). The Δ*yjeQ* mutant was assayed in 6 media including Rich Defined Media supplemented with glucose or glycerol (RDM-Glu, RDM Gly), M63 minimal supplemented with casamino acids and glucose or glycerol (cAA-Glu, cAA-Gly), and M63 minimal media supplemented with glucose or glycerol (M63-Glu, M63-Gly).

Maturation Rate

Maturation rate was examined using the pulse-chase methods described in the previous chapter. Δ*yjeQ*-ara was grown overnight at 37°C in LB media. Cells were subsequently diluted (1 in 10,000) in fresh RDM-Glucose or M63-Gluocse media and grown in a 37°C water bath with aeration (250 rpm). At an OD_{600} ~0.1-0.2, carbon-14 labeled uridine was added to the growing culture (final concentration of 0.1 μCi/ml). After five minutes of exposure to this 'pulse,' unlabeled uridine was added to the culture to a final concentration 500 ug/ml (1000-fold greater concentration than the pulse). Cells were harvested (200 μl) at regular intervals (every five minutes) and fast frozen in a dry ice/ethanol bath. Samples were harvested over a full doubling of the cell population. Frozen samples were subsequently pelleted by centrifugation for 10 minutes at 4°C. Total rRNA was extracted from each sample using the Qiagen RNeasy kit as per the

manufactures protocol. Purified RNA was then incubated with custom loading buffer (50% [w/v] urea, 10% [w/v] sucrose, 1× TBE) and resolved via gel electrophoresis. rRNA was subsequently transferred to a charged nitrocellulose membrane (Hybond N+, GE Healthcare) with an alkaline buffer (0.1 M NaOH, 3M NaCl) using the standard capillary method. Membranes were rinsed in 6x SSC buffer (0.3 M sodium citrate, 3M NaCl) and then exposed to a phosphor screen for 72 hours. Following exposure, the radiolabeled samples were imaged on a Typhoon™ multimode imager (GE). Quantification of labeled rRNA bands was performed using ImageQuant, version 5.2 (Molecular Dynamics) with the rolling average of the region surrounding the band used for background correction.

CHAPTER 4. Exploring Genetic Interaction with *yjeQ*

4.1 AUTHOR'S PREFACE

This chapter contains experiments conducted as a part of a manuscript under construction at the time of the writing of this thesis. All experiments were designed and performed by myself in consultation with Dr. Eric Brown with input from my committee. The double-deletion strains used in this study were created previously by Dr. Tracey Campbell [126]. The conditional Δ*yjeQ*Δ*rbfA* clone (Δ*yjeQ*Δ*rbfA*–ara) was created and sequenced by Dr. Jean Philippe Cote, a post-doctoral fellow in the lab of Dr. Eric Brown.

4.2 INTRODUCTION

Despite its role as a model prokaryotic organism for more than a century, there are still enormous gaps in our understanding of the *E. coli* genome. Indeed, of the 4,225 genes encoding proteins, one-third lack any annotated function [193]. Traditionally, efforts to link genes to function focused on deletion phenotypes; the absence of genes leads to obvious cellular defects from which function can be inferred. While this approach has proven fruitful in delineating biology, its utility is limited by the fact that many gene-deletions do not yield discernible phenotypes under standard laboratory conditions. The combination of functional overlap and redundancy tends to make most biochemical pathways substantially robust. Even in cases where deletion phenotypes are evident, this overlap can make it exceedingly difficult to assign specific function to any one gene.

The study of gene-gene interaction has been a powerful tool in exploring the unchartered regions of model genomes and an aid in addressing this dilemma. This approach looks to characterize the function of gene-products by mapping epistasis, the phenomenon in which multiple genes influence a single phenotype. Genetic interaction studies follow the principle that concurrent mutations in two functionally related genes can give rise to a phenotype distinct from those produced by lesions in the individual genes. Depending on the nature of the interaction this can lead to enhancement or suppression (synergy/antagonism) of the individual phenotypes [189]. In this way, genes can be charted to cellular pathways and networks based on their genetic relationship with other genes. This approach has gained momentum in concert with the development of

high-throughput screening techniques that enable rapid large-scale construction and analysis of double-mutants [189].

One of the focuses of our work has been to further understand the functional relationship between YjeQ and other putative assembly factors. Ribosome biogenesis is thought to be a pathway lined with functional overlap and redundancy; hence the dispensability of nearly all the factors involved in what is an absolutely essential process. As such, this arena provides fertile ground for exploration through genetic interaction. While we have investigated the prospect of genome-wide interaction studies, our group elected to take a small-scale directed approach focusing on interactions between gene-products related to ribosome function. Deference to this strategy stemmed from our drive to clarify the cellular role of YjeQ, rather than develop a broad map of factors involved in protein synthesis. With over 100 different ribosome-related factors on the books, there is ample genetic territory with which to take a focused approach.

Genetic map of YjeQ

Previously, Campbell and Brown developed a genetic interaction network for *yjeQ* that highlighted possible functional relationships amongst ribosome-associated proteins [126]. A shortlist of 39 dispensable genes (Supplemental Table 4.1) thought to be involved in ribosome function was examined in the context of a double-deletion screen. Each single gene deletion was introduced into a *yjeQ*-null background and growth of the resulting double mutant was examined. This screen characterized genetic interaction by contrasting the growth of the double mutant with that of the parent Δ*yjeQ* strain; secondary deletions that augmented or suppressed the Δ*yjeQ* phenotype were tagged as

potential interactions [126]. Ribosome profiles of these double-deletion strains were then assessed to further investigate the influence of these genetic interactions on the assembly process. Ultimately, this study yielded an interaction map highlighting functional relationships amongst several ribosome-associated proteins. This included genetic enhancement between *yjeQ* and putative biogenesis factors *rimM*, *ksgA*, and *rluD [126]*. In addition, enhancement interactions were observed with the translation factors *trmE*, *trmU*, *tgt* and *ssrA* [126].

YjeQ interaction map revisited

The connectivity that was observed between YjeQ and several translation/biogenesis proteins fortified the notion of its involvement in biogenesis. However, the phenotypes (growth/ribosome profile) used to examine these interactions provided little insight into the specific role of YjeQ or the mechanisms behind the observed gene-gene interactions. In addition, the gene pairs were qualified via relative growth in comparison to the Δ*yjeQ* deletion strain. This approach assumes that deviation from the single mutant is indicative of genetic interaction. Studies suggest that a multiplicative approach to qualifying defects is most reliable in detecting legitimate interactions (reviewed in [194]). In this model, the fitness defect resulting from the deletion of two functionally unrelated genes is predicted to be the product of the defect resulting from each single-mutant. Deviation from this value represents functional-relatedness in the form of synergy (synthetic sickness) or antagonism (synthetic viability/suppression). We have applied this approach to reexamine this priority list of genes in a double-deletion study by Campbell et al. [126]. Assays discussed in the

previous chapters have been used to further characterize the functional interaction of these factors in the context of the assembly process.

4.3 RESULTS

4.3.1 Double-deletion Screen

Single and double-deletion strains were grown in 96 well plates at 37°C in RDM-Glucose with shaking in an automated plate reader (Tecan Sunrise^{TM}). Optical density (OD_{600}) was read every 10 minutes over a 24-hour period. The resulting curves were used to calculate specific growth rates for each strain (λ^{-h}), with these values reflecting the average rate of three biological replicates grown on separate days. Predicted growth rates (λ_P^{-h}) were then calculated as the product of the relative growth rates of each single deletion with respect to the wild-type (equation 4.1).

$$\lambda_P^{-h} = \frac{\lambda_{deletion}}{\lambda_{wild\text{-}type}} \times \frac{\lambda_{\Delta yjeQ}}{\lambda_{wild\text{-}type}} \qquad \text{eqn 4.1}$$

The predicted and observed (λ_O^{-h}) rates were then contrasted ($\lambda_P^{-h}/\lambda_O^{-h}$) and strains exhibiting substantial deviation from the predicted value were flagged for further study. Of the 37 gene combinations examined only one double-deletion, Δ*ssrA*Δ*yjeQ,* was flagged as demonstrating genetic enhancement of the slow-growth phenotype of the Δ*yjeQ* single-deletion. This was in agreement with the previous study by Campbell et al. [126]. However, the remaining double-deletion mutants did not confirm as enhancers (grey). Four double-mutants (*trmE*, *trmU*, *tgt* and *ksgA)* all demonstrated growth rates in line with values predicted by the multiplicative model. As such, we suspect there is in fact no genetic relationship between these genes and *yjeQ.* In contrast, the double mutants for

rbfA, rimM and *rimI* had significantly faster growth rates than the model predicted (>1.5 fold), suggesting that the simultaneous deletion of *yjeQ* and these genes actually suppress the cumulative effect of their individual mutations. One gene from both of these categories (*trmeE* - non-interacting; *rbfA* - suppressor) was chosen for further study.

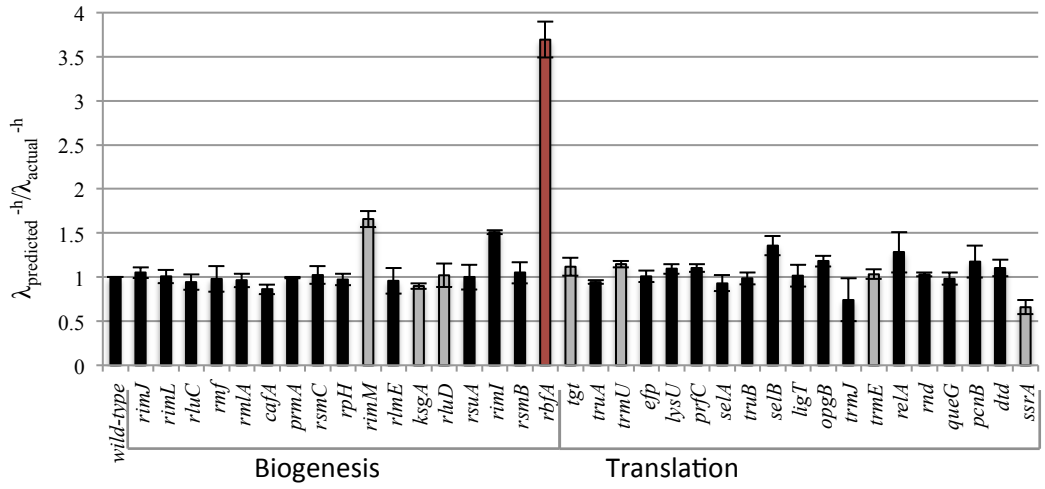

Figure 4.1: Reexamination of double-deletion mutants from Campbell et al. *[126]. The plot shows the ratio of predicted versus actual growth rates for each pair of gene-deletions* ($\lambda_{Predicted}^{-h}/\lambda_{Observed}^{-h}$). *Growth rates were expressed as specific growth rate* λ^{-h} *(ln(2)/doubling time) relative to the wild-type. Predicted growth rates were calculated as the product of growth rates for each individual mutant (relative to the wild-type). Deviation of the predicted and actual values was determined by dividing the former by the later* ($\lambda_P^{-h}/\lambda_O^{-h}$). *A value less than one signifies genetic enhancement while a value greater than one is indicative of suppression. Genes (x axis) are grouped putative function (biogenesis vs translation). Genetic interactions previously identified by Campbell et al. are coloured in grey [126]. Double-mutants featuring deletion of yjeQ and each of rimM, rimI or rbfA all demonstrated* λ_P^{-h} *values greater than 1.5 fold* λ_O^{-h}, *suggesting genetic suppression. rbfA, the gene showing the greatest level of genetic suppression, is highlighted in red. The genetic interaction of yjeQ and ssrA was confirmed (enhancement).*

4.3.2 Δ*rbfA*Δ*yjeQ*

E. coli RbfA is a broadly conserved cold shock protein that is essential for growth at low temperatures and is important for overall cellular fitness [116, 119, 123]. As

discussed in Chapters 1 and 2, there is a growing body of data implicating RbfA in the late stages of 30S subunit maturation. This includes several lines of evidence that suggest RbfA is functionally connected to YjeQ [121].

In the previous screen by Campbell and Brown, RbfA and YjeQ were not classified as an interacting pair. Indeed, the double-deletion exhibited a growth curve nearly identical to both single deletions [126]. However, assessing these genes using the multiplicative approach suggests that there is in fact a genetic interaction. The predicted growth rate of the Δ*yjeQ*Δ*rbfA* strain is significantly lower than the observed rate, suggesting genetic suppression (Figure 4.2). Both the Δ*yjeQ* and Δ*rbfA* single–deletions exhibited equivalent severe growth defects. The growth rate of the double-deletion, however, mirrors that of either single mutant. This suggests some level of genetic interplay in which the presence of one genetic lesion negates the phenotypic influence of the other.

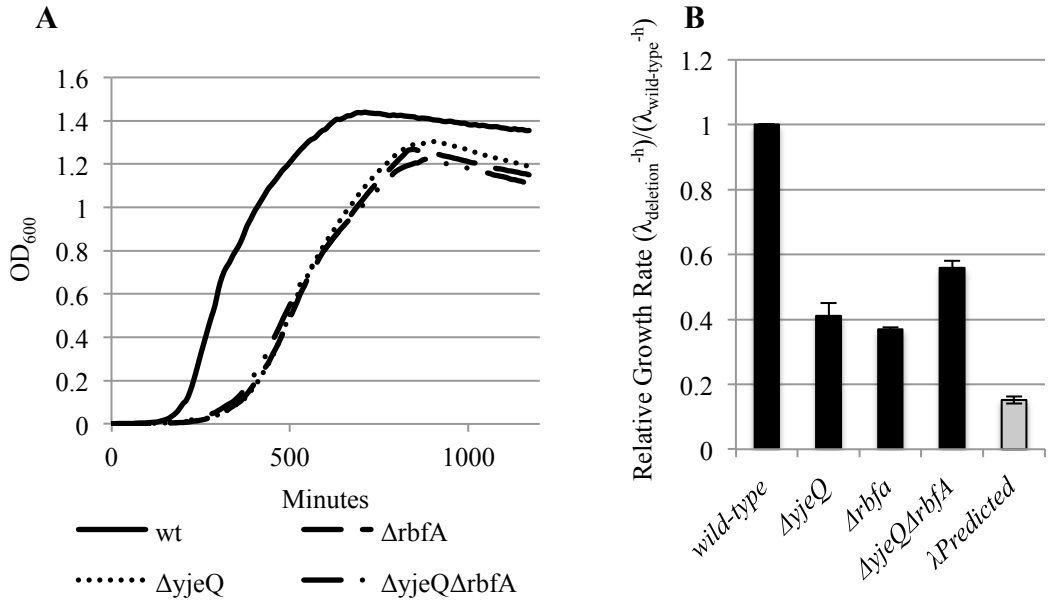

Figure 4.2: Examining the growth phenotype in the ΔyjeQ, ΔrbfA, and ΔyjeQΔrbfA strains. A) *Growth curves for the wild-type, ΔyjeQ, ΔrbfA and ΔyjeQΔrbfA strains* ***B)*** *Specific growth rates (λ^{-h}) for each mutant strain as a fraction of the wild-type growth rate. The ΔyjeQΔrbfA double-deletion grows slightly better than either single mutant (~0.56). The product of the relative growth rates of both single mutants ($\lambda_P{}^{-h}$) was substantially lower (grey bar, ~0.15). This suggests an antagonistic genetic interaction between ΔrbfA and ΔyjeQ that suppresses their combined defect.*

These observations are consistent with reports by Goto et al. that suggest YjeQ and RbfA are functionally related [121, 195]. As discussed in Chapter 1, this work posits that the cellular role of YjeQ is dependent on the presence of RbfA; when the latter is absent the former is completely dispensable. We hypothesized that if this relationship were correct, the rate of 17S rRNA processing should be similar in both the single and double-deletion mutants (Δ*yjeQ*, Δ*yjeQ*Δ*rbfA*). Indeed, pulse-chase analysis of 17S rRNA maturation revealed processing times to be consistent across both strains (Figure 4.3 B, C). These experiments were performed as reported in Chapter 2. We further examined the functional relevance of YjeQ in the absence of RbfA by making use of a double-deletion (Δ*yjeQ*Δ*rbfA*-ara) harboring an arabinose-inducible copy of YjeQ at araBAD (*yjeQ::kan; rbfA*::spec; yjeQ::araBAD-amp). Previously, we demonstrated factor-mediated acceleration of 17S rRNA processing in the *yjeQ*-null using this approach. However, with RbfA absent, reintroduction of YjeQ had no effect on the conversion rate of 17S rRNA (Figures 4.3 B, C).

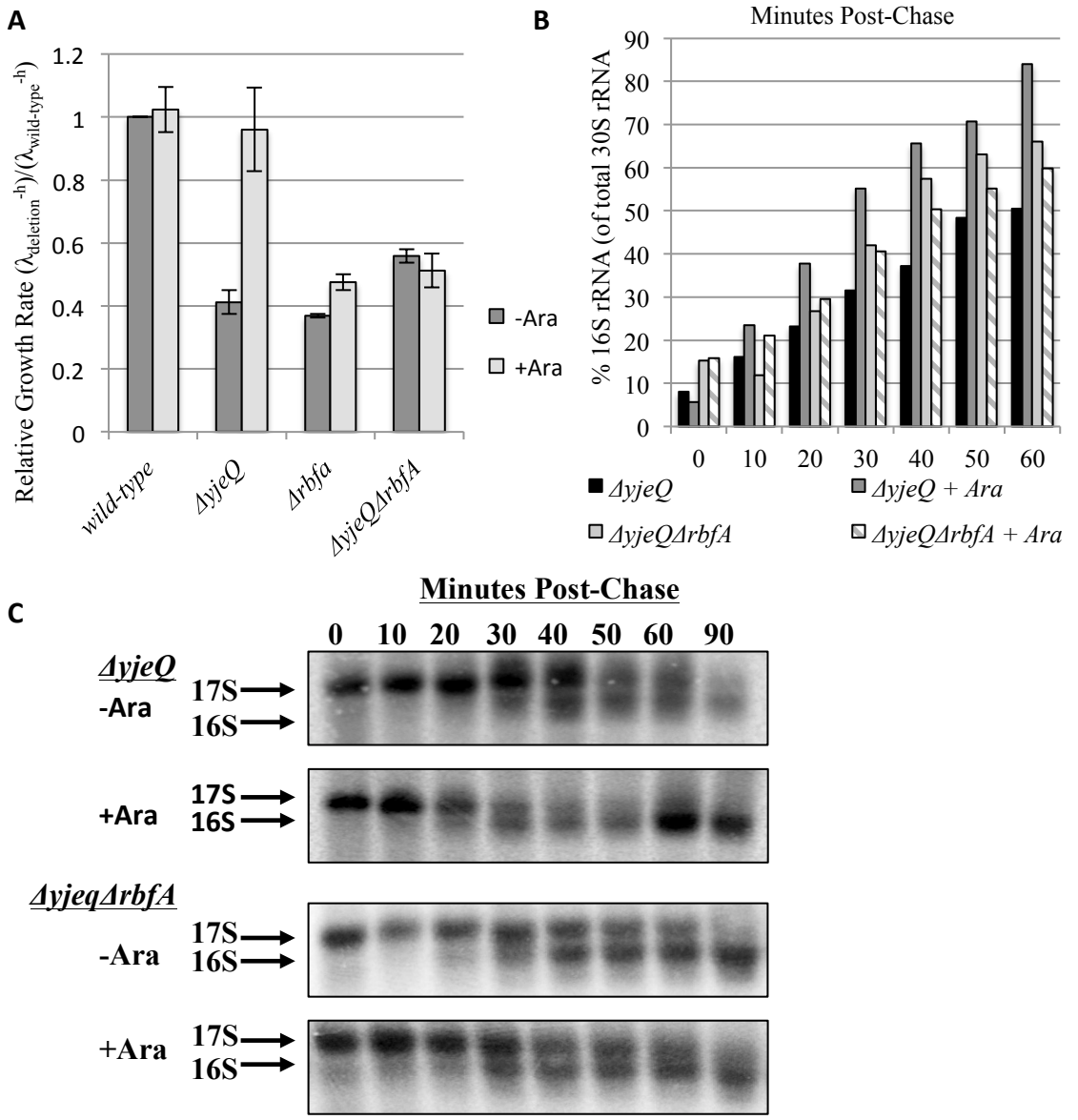

Figure 4.3 Pulse-chase analysis of rRNA processing in the ΔyjeQΔrbfA double-deletion. ***A)*** *Growth rates (+/- arabinose) for wild-type, ΔyjeQ-ara, ΔrbfA and ΔyjeQΔrbfA-ara.* ***B)*** *Plot showing the percentage of 16S rRNA over time. The conversion rate is similar in all strains except for the complemented ΔyjeQ mutant (ΔyjeQ + arabinose). Processing of 17S rRNA in this strain is substantially faster. The same complementation appears to have no effect on maturation when RbfA is absent (ΔyjeQΔrbfA + arabinose).* ***C)*** *The corresponding radiograms tracking rRNA processing over time.*

These observations support the notion that YjeQ only affects ribosome biogenesis if RbfA is present. This is in line with either of the models discussed in Chapter 2: 1) the sole function of YjeQ is to promote dissociation of RbfA from the mature subunit or 2) YjeQ facilitates subunit maturation, but its interaction with the immature 30S species is dependent on RbfA-induced conformational changes. We believe that latter is most likely, given the observation that the presence of YjeQ appears to accelerate 17S rRNA processing.

4.3.4 Δ*trmE*Δ*yjeQ*

A strain lacking both the *trmE* and *yjeQ* genes has been shown to have a growth rate slower than the *yjeQ*-null while simultaneously having a near wild-type ribosome profile [126]. This combination of phenotypes is rather surprising given that the altered ribosome profile of the Δ*yjeQ* deletion is suspected to be the driving force behind its slow growth. These seemingly contradictory changes in phenotype present a unique opportunity to understand how YjeQ influences ribosome assembly, activity and growth rate.

The *trmE* (*mnmE*) gene encodes a 49.6 kDa GTPase that is required for the 5-methylaminomethyl-2-thiouridine modification of tRNA [196]. This modifications aids in correct codon-anticodon pairing. As such, TrmE plays a key role in translational fidelity in *E. coli*, specifically, in maintaining the correct reading frame [197, 198]. Previous studies have illustrated that the dispensability of *trmE* varies in different genetic backgrounds. In certain strains (BW25113, MC1000) the removal of this gene has very little bearing on the overall health and growth rate of cells. However, in other strains

(JC7263, V5701) it is absolutely essential to survival [196]. It is has been hypothesized that the tolerance of mutation in *trmE* is dependent upon the characteristics of other components involved in translation. Additional defects in protein synthesis, in combination with the absence of TrmE, are thought to lead to the synthetic lethality observed in some strains. However, previous work has not ruled out the possibility of a secondary, conditionally essential, function.

The previous gene-gene interaction screen characterized the tandem deletion of *trmE* and *yjeQ* as leading to synthetic sickness [126]. A BW25113 strain lacking both genes showed an increased lag period and protracted growth curve in comparison to either single deletion. In contrast, the single deletion of *trmE* was characterized as having no deleterious effect on growth [126]. To further understand this interaction, the precise growth rates for the strains were determined. As anticipated, the double mutant grew slower than either single deletion (Figure 4.4 A).

Relative growth rates with respect to the wild-type ($\lambda_{deletion}/\lambda_{wild\text{-}type}$) were determined to quantify the impairment of cellular fitness in each deletion strain (Figure 4.4 B). The relative values are as follows: Δ*trmE* =0.87, Δ*yjeQ* = 0.50 and Δ*trmE*Δ*yjeQ* = 0.43. Using the multiplicative approach the $\lambda_{Predicted}^{-h}$ for the double-deletion is 0.44 (0.87 x 0.50). That the predicted value mirrors the experimentally determined rate suggests that *trmE* and *yjeQ* are not, in fact, functionally related. However, the improved ribosome profile of the double mutant previously reported made further inquiry worthwhile.

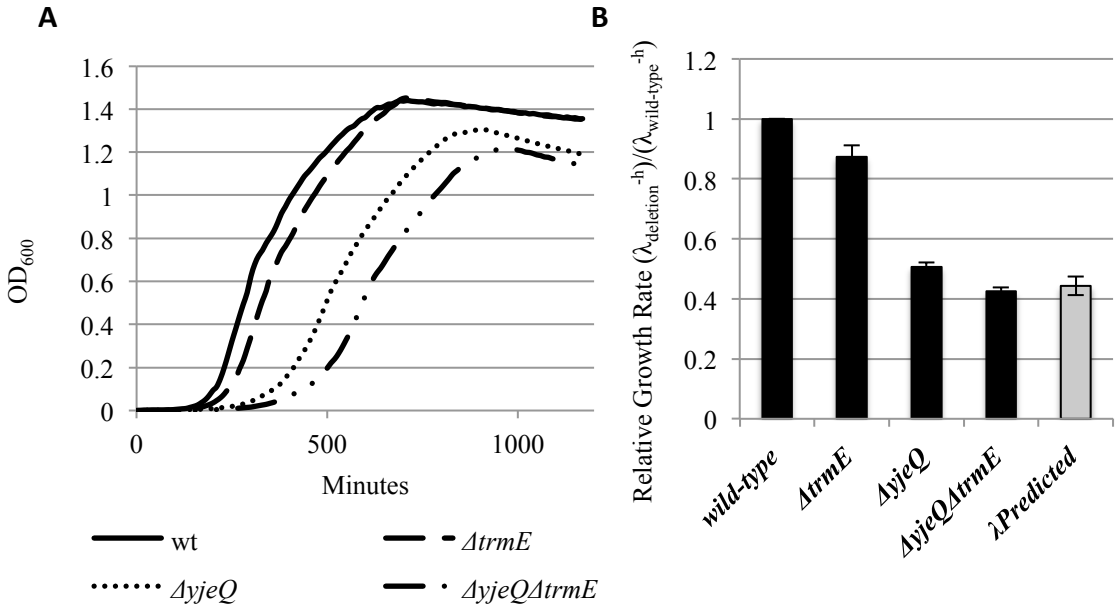

Figure 4.4: Examining the growth phenotype in the ΔyjeQ, ΔtrmE, and ΔtrmEΔyjeQ strains. A) *Growth curves for the wild-type, ΔtrmE, ΔyjeQ and ΔtrmEΔyjeQ strains* ***B)*** *Specific growth rates (λ^{-h}) for each mutant strain as a fraction of the wild-type growth rate. The ΔtrmEΔyjeQ double-deletion grows worse than either single mutant (~0.43). The product of the relative growth rates of both single mutants approximates that of the double deletion (grey bar, ~0.44). This calls into question the validity of the previously established genetic interaction [126].*

Ribosomal phenotypes

The ribosome content of the Δ*trmE*Δ*yjeQ* strain was assessed by ribosome profile and RNA analysis. Phenotypes for the single deletion strains agreed with previous results; the Δ*yjeQ* strain had a significantly altered ribosome profile in conjunction with an abundance of 17S rRNA while the Δ*trmE* strain resembled the wild-type (Figures 4.5 A, B, C) [126, 140]. The ribosome profile of the double mutant was improved in comparison to the *yjeQ*-null strain with an 8% increase in 70S subunits and a concurrent 26.8% decrease in free 50S subunits. Interestingly, the proportion of small 30S subunits remained approximately the same. Analysis of cellular RNA in the double mutant revealed a slight improvement in levels of immature 17S rRNA relative to the Δ*yjeQ* deletion (Figure 4.6). Approximately 50% of 30S-derivived ribosomal RNA is immature

17S precursor in the *yjeQ*-null. However, in the Δ*trmE*Δ*yjeQ* strain 17S rRNA only accounted for 39% of all 30S ribosomal rRNA.

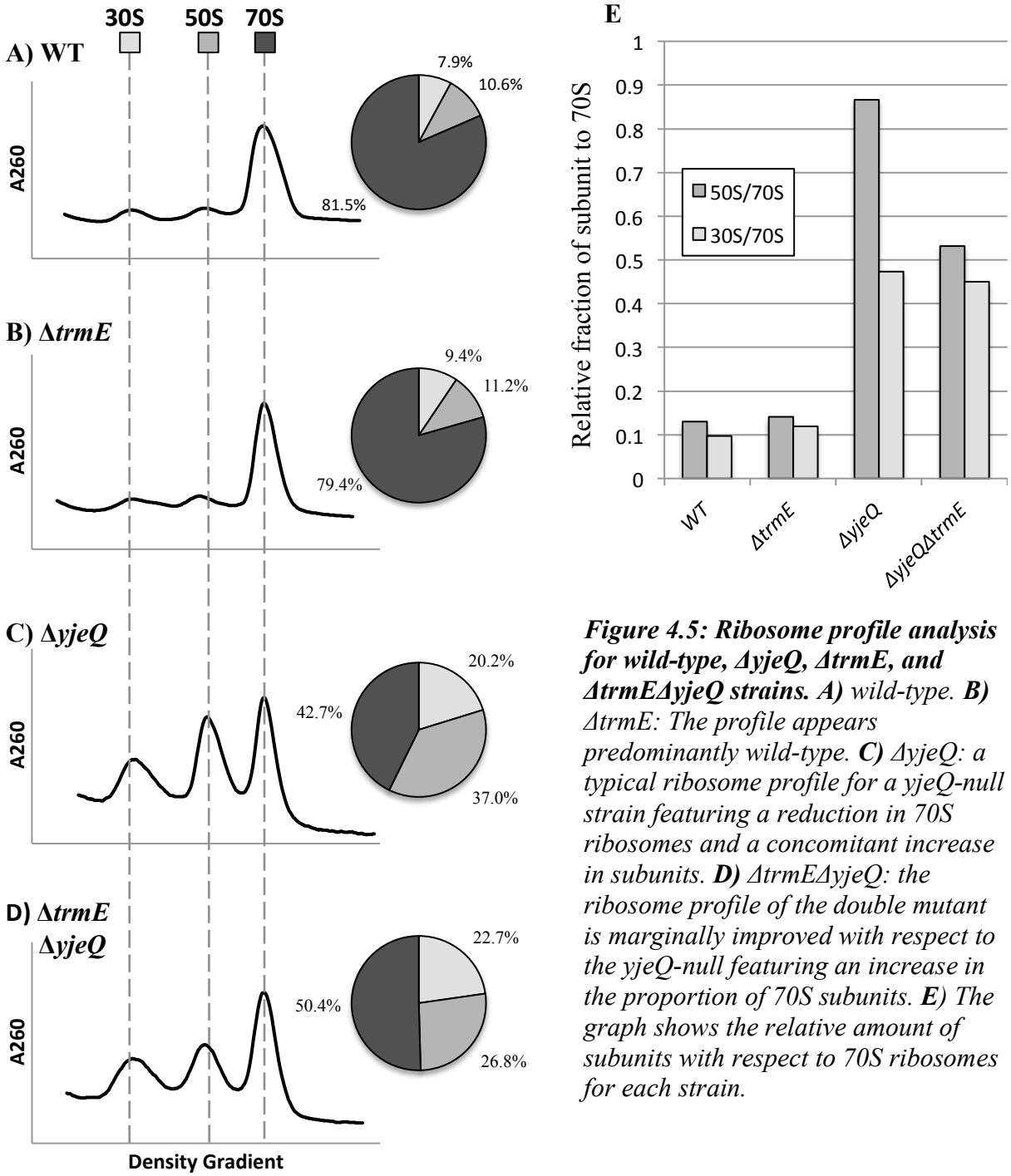

Figure 4.5: Ribosome profile analysis for wild-type, ΔyjeQ, ΔtrmE, and ΔtrmEΔyjeQ strains. ***A)*** *wild-type.* ***B)*** *ΔtrmE: The profile appears predominantly wild-type.* ***C)*** *ΔyjeQ: a typical ribosome profile for a yjeQ-null strain featuring a reduction in 70S ribosomes and a concomitant increase in subunits.* ***D)*** *ΔtrmEΔyjeQ: the ribosome profile of the double mutant is marginally improved with respect to the yjeQ-null featuring an increase in the proportion of 70S subunits.* ***E)*** *The graph shows the relative amount of subunits with respect to 70S ribosomes for each strain.*

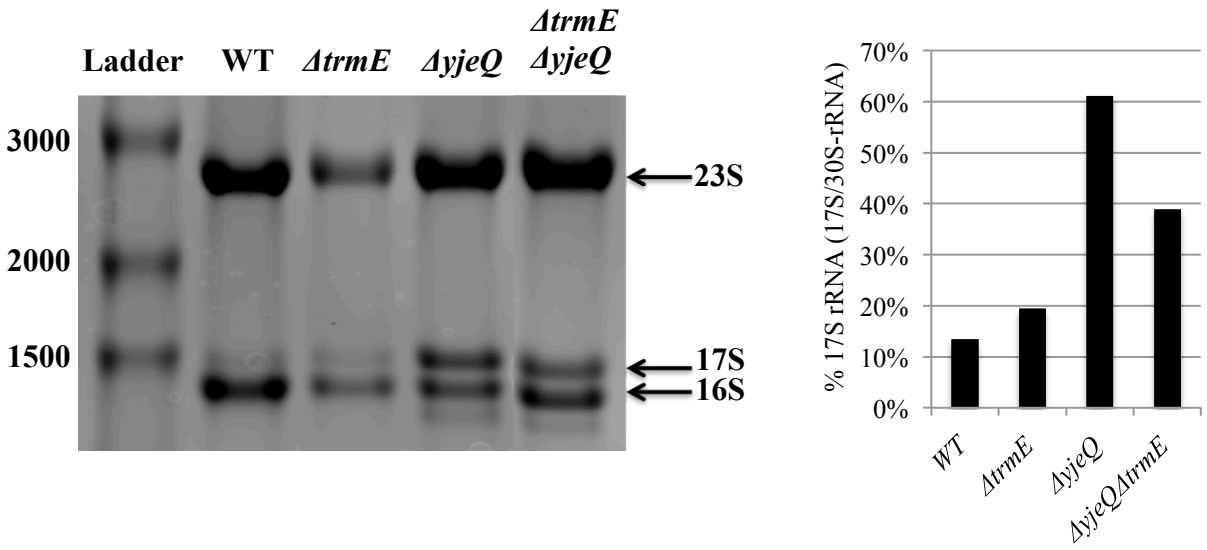

Figure 4.6: RNA analysis for wild-type, ΔyjeQ, ΔtrmE, and ΔtrmEΔyjeQ strains. A) *Electrophoretic analysis of the rRNA makeup of each strain. Lane 1: ladder, Lane 2: Wild-type, Lane 3: ΔtrmE, Lane 4: ΔyjeQ, Lane 5: ΔtrmEΔyjeQ. Both the wild-type and ΔtrmE strains exhibit only trace amounts of 17S rRNA. The ΔyjeQ mutant demonstrates the typical RNA profile associated with the absence of YjeQ. The ΔtrmEΔyjeQ mutant shows a slightly reduced level of 17S rRNA.* ***B)*** *A graph of 17S rRNA levels relative to all 30S-derived rRNA as determined by quantifying the gel bands in* ***A*** *using ImageQuant version 5.2 (GE).*

It has long been suspected that the reduced proportion of 70S ribosomes in the *yjeQ*-null strain is central to its slow-growth phenotype. However, in the case of the Δ*trmE*Δ*yjeQ* double mutant we see an improvement in the number of 70S ribosomes and yet a decreased growth rate. That the growth defect remains as potent despite the repair in ribosome profile suggests the translational capacity of the cell is still compromised as a result of the reduced rate of ribosomal maturation.

We hypothesize that the apparent improvement in ribosome profile and rRNA maturation in the double-mutant is an artifact due to the reduced growth rate of this strain. The work above demonstrates that ribosome assembly times (as indicated by 17S processing) are substantially reduced in the *yjeQ*-null. As YjeQ is absent from the double-

deletion strain it is suspected that ribosomes mature at the same rate as in the *yjeQ*-null strain. It is plausible that the slower division of the Δ*trmE*Δ*yjeQ* cells affords ribosomes the extra time needed for maturation - hence the increase in 70S ribosomes. This is distinct from experiments where growth rate is modulated by manipulating a cells environment (ie. available nutrients). In the case of the double mutant, the translational capacity of the cell is impaired by two simultaneous defects. One affects ribosome quantity (*yjeQ*) and one that affects translational fidelity (*trmE*). The cumulative effect is a reduction in useful protein synthesis, and therefore a reduction in growth rate. The rate of ribosome maturation, however, remains constant and as such, ribosomes are granted an extended window for maturation. In agreement with this hypothesis is the observation that ribosomal defects are corrected by the same degree as the decrease in growth rate (~ 15%).

4.4 DISCUSSION

The intent of this work was not to invalidate the previous interaction map, but rather to add further resolution to the genetic pairings that were identified. That this study uncovered several instances of mischaracterization is a testament to the value of reexamining observations as methodologies improve. By this means, iterative work can both expand and substantiate our view of the genetic landscape surrounding ribosome biogenesis. The methods outlined line here lay the groundwork for broader exploration of epistasis of amongst ribosome-associated factors.

Our results support the hypothesis that YjeQ is fully dispensable at 37°C in rich media when RbfA is absent. The mechanism underlying this phenomenon is not clear, but

it does suggest that RbfA fulfills a critical role upstream of the action of YjeQ. Work by Goto et al. yielded a suppressor of the Δ*yjeQ* deletion by way of a mutation in RbfA that is thought to promote the dissociation of this protein from the 30S subunit [121]. The model put forward suggests that the role of YjeQ is to displace RbfA once the 30S subunit reaches a certain stage in maturation. Thus, the ribosomal defects associated with the absence of YjeQ actually stem from RbfA remaining bound to the precursor 30S (presumably limiting further maturation). If this is true, overexpression of RbfA in a Δ*yjeQ* background should theoretically enhance the slow-growth phenotype, as it would result in an increase in the number of assembling subunits occupied by RbfA.

As YjeQ seems to interact primarily with mature 30S subunits, it would stand to reason that this protein detects elements of the mature ribosome and, upon recognizing certain features, promotes dissociation of RbfA. Our results provide corroborating evidence for this hypothesis. However, the Δ*yjeQ* strain harbours small subunits that are clearly not mature. If YjeQ does indeed serve to promote the exit of RbfA from the 30S subunit then it must interact with the immature species. Therefore, we suspect that YjeQ binds these intermediates and participates in maturation events beyond the dissociation of RbfA.

Interestingly, both Δ*yjeQ* and Δ*rbfA* single deletions are suppressed by the overexpression of Era [123, 126]. This lends credence to the notion that they are functionally related. It is possible that Era fills in for YjeQ in promoting the dissociation of RbfA. However, the mechanism of suppression for the Δ*rbfA* deletion is in all likelihood distinct. Overexpression of the translation factor IF2, another GTPase, has also

been shown to suppress defects in a Δ*yjeQ* deletion strain [126]. It will be worth examining this suppression in the Δ*yjeQ*Δ*rbfA* double knockout. If the proposed model for YjeQ-RbfA function is correct, the over expression of IF2 should have little bearing on phenotype. Reexamining these genetic interactions will prove useful in further clarifying the functional relationship between YjeQ and RbfA. In addition, it will provide insight as to whether or not epistasis amongst these factors is the result of direct and compensatory functional overlap or general improvements in the translational capacity of cells.

The case of *trmE* sheds light on an interesting caveat when studying ribosome biogenesis: steady-state phenotypes can be deceiving. In certain circumstances, perturbations in assembly do not manifest in obvious ribosomal phenotypes such as the prevalence of 17S rRNA or free 50S subunits. In the case of Δ*trmE*Δ*yjeQ*, it is thought that the deceleration of cell division accompanying the secondary deletion partially masks ribosome immaturity. Steady-state levels of 17S rRNA in the double mutant appear to be closer to those found in wild-type cells, effectively conveying an improvement in ribosome assembly when TrmE is absent. Thus, the value of steady-state phenotypes is dependent on the conditions under which they are examined. Strict reliance on these phenotypes has the potential to mislead interpretation of genetic or chemical lesions disrupting the assembly process. This will be especially true when lesions have pleiotropic effects that influence growth rate by different means, such as in the case of the Δ*trmE*Δ*yjeQ* double-deletion.

4.5 MATERIALS AND METHODS

Strains

A total of 37 single gene deletions were selected for analysis in our initial screen. These were sourced from the BW25113-based Keio collection (K-12 in-frame single-gene knockout mutants), which features a kanamycin cassette in place of the target gene [191]. The shortlisted genes represent a broad cross-section of ribosome-associated proteins including factors involved in biogenesis and translation. Campbell and Brown created the double-deletion strains used in this screen in in a previous study [126]. Here, we provide a brief overview of the method used for creating these strains.

Secondary deletions were introduced into a Keio-derived *ΔyjeQ* parental strain that lacked a kanamycin marker. The kanamycin cassette was removed from this strain using pCP20, a plasmid carrying the FLP recombinase that is able to excise the deletion region marker. Chromosomal DNA was purified from each Keio deletion strain. Primers flanking the target gene (500-1000 bp upstream and downstream) were used to PCR amplify the deletion region. These products were then transformed into the Keio-derived Δ*yjeQ* deletion strain harbouring pKD46, a plasmid featuring the λ red recombinase system that mediates homologous recombination.

We also created a version of the Δ*yjeQ*Δ*rbfA* double-deletion strain that featured an ectopic copy of yjeQ at araBAD. To make this strain, the chromosomal copy of *rbfA* was removed from the previously created Δ*yjeQ*-ara strain using the above method. A spectinomycin cassette was used as a resistance marker in place of kanamycin.

Growth Rates

Each single deletion and corresponding Δ*yjeQ* double-deletion was grown overnight in 5 ml of EZ Rich Defined Media media (Teknova) supplemented with glucose (37°C with shaking 250 rpm). Cells were then taken from saturated overnight cultures, diluted in fresh media (1:10000 dilution) and grown under optimal conditions (37°C shaking at 250 rpm) in 96-well in a Tecan Sunrise^{TM} plate reader. The optical density of each culture was read every ten minutes and growth was monitored for 16 hours. Specific growth rates (λ^{-h}) were determined by calculating the exponential rate of change during early growth phase (OD_{600}= 0.1-0.2). Each strain was tested in triplicate and growth rates were reported as an average of all 3 replicates.

Analysis of genetic interaction

A multiplicative approach was taken to qualify genetic interaction amongst gene pairs [194]. In this method, relative growth rates of each individual mutant were calculated in reference to the wild-type strain ($\lambda_{deletion}/\lambda_{wild\text{-}type}$). The product of these values represented the predicted growth rate of non-interacting pairs. The observed growth rates were then contrasted against these values and expressed as a multiple of the predicted rate (fold-predicted). Strains that deviated by more than 50% of the predicted value were flagged for further investigation. In addition, previously identified gene deletions that did not qualify in this screen were shortlisted for examination.

RNA Analysis

Analysis of rRNA was performed as described in previous chapters with slight modification. Cell cultures (5ml, wild-type or deletion) were grown under optimal

conditions (RDM-Glucose, 37°C and shaking at 250 rpm) and harvested in early exponential growth phase (0.1-0.2) by centrifugation for 10 minutes at 3000 g in an Eppendorf 5424 microcentrifuge. Total RNA was extracted using a QIAGEN RNeasy kit as per the manufactures protocol. The purified material was incubated with RNA loading buffer (50% [w/v] urea, 10% [w/v] sucrose, 1× TBE) for 10 minutes at 75°C and then resolved via agarose gel electrophoresis (2%, 4 h at 4.5 V/cm.). The gel was subsequently visualized with RedSafe™ (FroggaBio) in combination with a Typhoon™ multimode imager (GE). Quantification of rRNA bands was performed using ImageQuant, version 5.2 (Molecular Dynamics) with the local average of the region surrounding the band used for background correction.

Ribosome Profiles

Ribosome Profiles were performed as described in Chapter 2 and in [140]. Briefly, 50 ml cultures of each strain were grown in RDM-Glucose at 37°C with shaking (250 rpm) to an optical density of ~ 0.2 from a saturated seed culture. All proceeding steps were performed at 4°C. Cells were harvested by centrifugation at 3000 g in a Sorvall™ Legend tabletop centrifuge for 10 minutes and resuspended in 5 ml of buffer A (20 mM Tris pH 7.0, 10mM magnesium acetate, 100 mM NH_4Cl). Samples where then lysed by mechanical disruption using a cell disruptor operating at 10,000 psi (Constant Systems, Kennesaw, GA). Cellular debris was removed by pelleting at 24,000 rpm for 45 minutes using a Beckman Coutler ultracentrifuge in combination with an MLA 80 rotor. The resulting supernatant, the S30 extract, was loaded onto 35 ml sucrose gradients (linear, 10-40%), which were subsequently spun at 18,700 rpm in Thermo Sorvall™ WX90

ultracentrifuge using a Surespin 630/36 rotor. Gradients were prepared using a BioComp Gradient Station with two solutions of 10% and 40% sucrose in Buffer A. Following centrifugation, gradients were fractionated by upward displacement with 80% glycerol using a Brandel gradient fractionator in combination with an AktaPrime system (Amersham, GE). Profiles were recorded using the corresponding PrimeView software (Amersham, GE).

Pulse-Chase Studies

Strains were grown overnight at 37°C in RDM-Glucose media with appropriate selection. Cells were subsequently diluted (1 in 10,000) in fresh media and grown in a 37°C water bath with aeration (270 rpm). At an OD_{600} ~0.1-0.2, carbon-14 labeled uridine was added to the growing culture (final concentration of 0.1 μCi/ml). Following five minutes of exposure to this 'pulse,' unlabeled uridine was added to the culture to a final concentration 500 ug/ml (1000-fold greater concentration than the pulse). Cells were harvested (200 μl) at regular intervals (WT every two minutes, Δ*yjeQ* every five minutes) and fast frozen in a dry ice/ethanol bath. Samples were harvested over a full doubling of the cell population. Frozen samples were subsequently pelleted by centrifugation for 10 minutes at 4°C. Total rRNA was extracted from each sample using the Qiagen RNeasy kit as per the manufactures protocol. Purified RNA was then incubated with loading buffer (50% [w/v] urea, 10% [w/v] sucrose, 1× TBE) and resolved via gel electrophoresis. RNA was subsequently transferred to a charged nitrocellulose membrane (Hybond N+, GE Healthcare) with an alkaline buffer using the standard capillary method (0.1 M NaOH, 3M NaCl). Membranes were rinsed in 6x SSC buffer (0.3 M sodium citrate, 3M

NaCl) and then exposed to a phosphor screen for 72 hours. Following exposure, the radiolabeled samples were imaged on a Typhoon™ multimode imager (GE). Quantification of labeled rRNA bands was performed using ImageQuant, version 5.2 (Molecular Dynamics) with the local average of the region surrounding the band used for background correction

CHAPTER 5. Concluding Remarks

5.1 THE FUNCTION OF YJEQ

There is now considerable evidence supporting the role of YjeQ in ribosome biogenesis, specifically in the terminal stages of 30S subunit maturation. When this factor is absent, immature 30S subunits accumulate that lack several late stage proteins and house unprocessed rRNA [121, 129, 140]. The cryo-EM structure of this ribosomal species suggests that these subunits are nearly complete, but nonetheless house a non-native, and presumably non-functional, decoding center. Our pulse-chase studies illustrate that this population of ribosomes is in fact competent for maturation and that this process can be accelerated *in vivo* by the reintroduction of YjeQ. Taken together, these observations support the hypothesis that YjeQ takes part in the final events of small subunit maturation, likely facilitating development of the regions surrounding the decoding center.

Model

The co-structures of YjeQ in complex with mature 30S subunits indicate that this protein interacts with functionally important locales surrounding the A-site and decoding center [130]. This further emphasizes the probability that YjeQ influences the maturation of this region. How it does do so, however, is unclear. While numerous studies document this factor's interaction with mature subunits, there is little evidence of this protein interacting with immature ribosomes [121, 132, 138, 195]. Indeed, studies examining this interaction report that immature subunits are less effective at stimulating the GTPase activity of YjeQ than their mature counterparts [121, 132]. This does not preclude the

possibility that YjeQ associates with immature subunits, but rather, suggests that features unique to fully mature 30S subunits stimulate GTP catalysis and product release. As such, one can envision this factor serving as both a maturation factor and checkpoint protein. In this scenario, the GTP-bound form of YjeQ would bind the immature subunit and facilitate one or more maturation events. These changes to the ribosome would in turn trigger product release (GDP and Pi) and lead to the dissociation of YjeQ.

Binding with the 30S subunit

The model alluded to above is largely consistent with the canon of research surrounding this proteins involvement in ribosome function. However, it hinges on an as of yet unobserved interaction of YjeQ with the immature species. One of the obstacles preventing efforts to probe this interaction is the inability to purify immature subunits to homogeneity. All of the work documented herein relied on sucrose gradient profiling to parse out free 30 subunits from those housed in 70S ribosomes, thereby enriching the number of immature 30S subunits collected [140]. This approach, however, did not completely eliminate mature 30S ribosomes from the free subunit population. Examining the interaction of YjeQ with the immature subunit will require samples purified to near homogeneity, as any contaminating wild-type 30S subunits will affect YjeQ binding and stimulation. Our efforts to develop a system to purify immature subunits were ultimately unsuccessful. Fortunately, several groups have recently developed new approaches to isolating assembly intermediates [117, 199]. These protocols will make it possible to purify immature subunit species from strains lacking ribosome biogenesis factors and

thus, will augment future efforts to reliably examine factor interaction with precursor species using in *vitro* assays.

Functional relationships amongst trans-acting factors

In ruminating on the function and mechanism of YjeQ, it is important to consider the action of other small subunit biogenesis factors (i.e. RbfA, RimM). The observation that all of these proteins appear to influence 30S maturation suggests that their activities may impact the function of one another, regardless of whether they act in sequence or in concert. As such, an accurate understanding of their individual functions requires a holistic view of the *in vivo* assembly process.

The absence of either RbfA or RimM leads to a collection of typical biogenesis defects mirroring that of the *yjeQ* deletion (accumulation of 17S rRNA, elevated levels of free subunits) [114, 116, 119-123, 125, 129, 133]. These common phenotypes are high-level indicators of perturbation and should not be taken to necessarily reflect functional overlap. Indeed, these three factors bind distinct regions of the 30S subunit: YjeQ appears to interact with helix 44 and both the head and platform of the 30S subunit, RimM is thought to bind to the head and RbfA has been shown to bind the neck in the vicinity of the mature 5' end of 16S rRNA [114, 120, 130, 133]. Thus, it has been suggested that all three of these factors can occupy the subunit simultaneously [117, 195].

Cryo-EM structures of immature subunits derived from both Δ*yjeQ and ΔrimM* strains depict precursors with common defects, including malformed decoding centers and missing tertiary proteins [129, 140]. These in turn look remarkably similar to the immature 30S subunits derived from a Δ*yjeQΔrbfA* strain [129, 195]. It has been

suggested that all of these immature species are in fact one and the same [117, 129, 195]. That deletion of each of these factors seems to lead to a common assembly intermediate suggests that they may all partake in a global maturation event [195]. Thus, the immature subunit we have isolated and characterized in our work may represent this critical, perhaps rate-limiting, stage of assembly, before the action of trans-acting biogenesis factors can facilitate its conversion to a mature subunit.

The classical view of biogenesis posited that ribosomes were built in a linear fashion, proceeding through a number of sequential intermediates and maturation steps [21, 52, 58, 65]. Recent work, however, has laid bare the dynamics of this process and illustrated that assembly in cells is fluid, with folding and conformational rearrangements occurring simultaneously at multiple sites on the rRNA [69-71]. As such, the assembly process is now viewed as a multidimensional landscape rather than a progressive pathway. This model suggests that multiple, parallel routes exist by which a subunit can form [69-71]. An important question to now address is whether or not these parallel pathways eventually converge on the common immature species discussed above. If so, what role does this trio of trans-acting factors play in the transition to the mature state? Do they act in series or all at once?

At the outset of this work, the field was undergoing a paradigm shift towards examining ribosome assembly *in vivo*. Much of the early insight into this process was gained from *in vitro* studies examining ribosome reconstitution and protein binding. However, assembly in a tube is only a loose approximation of the process in cells [11, 21, 52]. This realization provided the impetus to develop the means to examine ribosome

construction i*n vivo*. The first ribosome crystal structures provided new tools with which to examine assembly by characterizing the structure and composition of intermediates purified from strains with perturbed biogenesis. These structures, however, only provide a snapshot of assembly in time.

The next great frontier in studying biogenesis will center on methodologies that can track *in vivo* assembly over time. Several groups have already unveiled time-resolved approaches for characterizing subunit structures as they assemble [69, 70]. Using *in vivo* X-Ray footprinting Clatterbuck Soper et al. were able to examine the progression of 30S precursors in Δ*rimM* and Δ*rbfA* deletion strains [117]. In agreement with our published structure, the absence of both of these factors was found to produce precursors with conformational aberrations in vicinity of helix 44 and lacking tertiary r-proteins S2 and S21. However, comparison of the footprints for precursors in both strains revealed subtle differences in their composition and structure, informing on the specific roles of these proteins [117].

5.2 RIBOSOME BIOGENESIS AS A DRUG TARGET

Protein synthesis drives cellular proliferation. Thus, any means of compromising this process should ultimately reduce growth. Complete cessation of the assembly process should effectively arrest translational activities. Ribosome biogenesis, however, is both robust and intricately regulated [11, 21, 51, 52]. As such, it is not clear what the impact of inhibition will be within a cell or if total blockage is even feasible.

Work by Maguire and Wild provide some insight into the mechanics and consequences of inhibiting ribosome assembly in prokaryotes [51, 200]. Experiments

using conditional copies of the r-proteins L28 and L33 have demonstrated that disruption of ribosome production has a bacteriostatic effect [51, 200]. *In vivo* assembly requires at least one of these proteins. If both are absent, ribosome biogenesis is completely stalled. However, cells can continue to divide for several generations following the removal of these proteins, getting by on the ribosome supply that existed prior to the arrest of assembly. Eventually, this population of ribosomes is sufficiently diluted such that proliferation is no longer possible. Thus, Maguire argues, an inhibitor of biogenesis will, at best, be a weak bacteriostatic agent [51].

The implications of this work suggest that a successful inhibitor of ribosome biogenesis needs to stop assembly entirely. Merely slowing down the process may not be sufficient to deter bacterial growth. Likewise, partial disruption will not be an effective means of abolishing translation, as cells will continue to synthesize proteins with those ribosomes that do reach maturity. This calls into question strategies to target non-essential biogenesis factors, as the process of assembly proceeds even when they are absent. In opposition to this, work by Campbell et al. demonstrated that the absence of YjeQ drastically reduced the virulence of *Staphylococcus aureus* in mouse models [128]. Thus, partial disruption of assembly can be sufficient to impair cell growth, such that an infectious population can be readily cleared by a host immune system.

Strategies to uncover small molecules that specifically target this process are still limited by the inherent challenges of recognizing perturbations in assembly. Our work in Chapter 3 three lays the foundation for a convenient phenotype by which to identify impaired ribosome biogenesis, or at the very least, disruptions in protein synthesis. While

this assay is somewhat crude, its simplicity makes it highly amendable to high-throughput screening. A campaign to identify inhibitors of biogenesis could use this phenotype as a primary filter for all perturbations affecting ribosome concentration. Follow-up studies (biochemical, structural) could then be used to further classify molecules directly affecting ribosome biogenesis. Stokes et al. executed such a screen, relying on the cold sensitivity phenotype associated with ribosome biogenesis factors to identify molecules that inhibit the process directly [201]. A second option will be to take a factor-focused approach to search out molecules that inhibit the function of assembly proteins. To this end, those factors with obvious enzymatic activity (i.e the GTPases) and critical cellular functions may make excellent candidates for screening campaigns.

Despite the caveats, ribosome assembly still offers new biological terrain worthy of exploration. The suite of assembly factors governing this process represents a pool of untapped targets that may yet prove relevant to clinical efforts. Many of these proteins are broadly conserved, specific to bacteria and serve functions of vital cellular importance. The fact that this catalogue also includes a number of essential proteins is especially encouraging (Era, EngA, ObgE, YihA) [51]. Regardless of therapeutic utility, the pursuit of inhibitors of this process should be a top priority for the field. Our understanding of the process of translation evolved alongside the discovery and development of ribosome-targeting antibiotics [18, 20]. Indeed, many important regions of the ribosome were charted using inhibitors as molecular probes of function. By extension, inhibitors could now prove a game changer to study of assembly, improving upon the relatively slow and clumsy genetic approaches currently used to perturb biogenesis. The ability to rapidly and

selectively disrupt components of this process, combined with new time-resolved approaches for *in vivo* study, will no doubt serve as a formidable pairing in the continued exploration of this remarkable biological process.

REFERENCES

1. Domagk, G. (1935) Ein Beitrag zur Chemotherapie der kateriellen Infektionen, *Dsch Med Wochenschr.* **61**, 250.

2. Fleming, A. (1929) On antibacterial action of culture of *Penicillium*, with special reference to their use in isolation of *B.* influenzae *Br J Exp Pathol.* **10**, 226-236.

3. Aminov, R. (2010) A brief history of the antibiotic era: lessons learned and challenges for the future, *FMICB.* **1**, 1.

4. Walsh, C., Wencewicz, TA. (2014) Prospects for new antibiotics: a molecule-centered perspective, *J Antibiot.* **67**, 7-22.

5. Butler, M., Blaskovich, MA., Cooper, MC. (2013) Antibiotics in the clinical pipeline in 2013, *J Antibiot.* **66**, 571-591.

6. Bozdogan, B., Appelbaum, PC. (2004) Oxazolidinones: activity, mode of action, and mechanism of resistance, *Int J Antimicrob Agents.* **23**, 113-119.

7. Laxminarayan, R., Duse, A., Wattal, C., Zaidi, AKM., Wertheim, HFL., Sumpradit, N., Vlieghe, E., Levy Hara, G., et al. (2013) Antibiotic resistance - the need for global solutions, *The Lancet Infect Dis.* **13**, 1057-1089.

8. Blair, J., Webber, MA., Baylay, AJ., Ogbolu, DO., Piddock, LJV. (2015) Molecular mechanisms of antibiotic resistance, *Nat Rev Microbiol.* **12**, 42-51.

9. D'Costa, V., McGrann, KM., Hughes, DW., Wright, GD. (2006) Sampling the antibiotic resistome, *Science.* **311**, 374-377.

10. Clardy, J., Fischbach, M., Currie, C. (2009) The natural history of antibiotics, *Curr Biol.* **9**, R437-R441.

11. Nierhaus, K., Wilson, DN. (2004) *Protein synthesis and ribosome strucutre: translating the genome* WILEY-VCH Verlag GMbH&Co.

12. Cannone, J., Subramanian, S., Schnare, MN., Collett, JR., D'Souza, LM., Du, Y., Feng, B., Lin, N., adbus, LV., Iler, KM. Pande, N., Shang, Z., Yu, N., Gutell, RR. (2002) The Comparative RNA web (CRW) Site: an online database of comparative sequence and structure information for ribosomal, intron and RNAs, *BMC Bioinformatics* **3**, 1-31.

13. Agmon, I., Bashan, A., Yonath, A. (2006) On ribosome conservation and evolution, *Isr J Ecol Evol.* **52**, 359-379.

14. Mears, J., Cannone, JJ., Stagg, SM., Gutell, RR., Agrawal, RK., Harvey, SC. (2002) Modeling a minimal ribosome based on comparative sequence analysis, *J Mol Biol.* **321**, 215-234.

15. Lambert, T. (2012) Antibotics that affect the ribosome, *Rev sci tech Off int Epiz.* **31**, 57-64.

16. Wittmann, H. (1983) Achitecture of Prokaryotic Ribosomes, *Annu Rev Biochem.* **52**, 35-65.

17. Garreau de Loubresse, N., Prokhorova, I., Holtkamp, W., Rodina, MV., Yusupova, G., Yusupov, M. (2014) Structural basis for the inhibition of the eukaryotic ribosome, *Nature.* **513**, 517-522.

18. Wilson, D. (2014) Ribosome-targeting antibiotics and mechanisms of bacterial resistance, *Nat Rev Microbiol.* **12**, 35-48.

19. Davies, J. (2006) Where have all the antibiotics gone?, *C J Infect Dis Med Microbiol.* **17**, 287-290.

20. Blanchard, S., Cooperman, BS., Wilson, DN. (2010) Probing translation with smal-molecule inhibitors, *Chem Biol.* **17**, 633-645.

21. Wilson, D., Nierhaus, NH. (2007) The Weird and Wonderful World of Bacterial Ribosome Regulation, *Crit Rev Biochem Mol Biol.* **42**, 187-219.

22. Ban, N., Nissen, P., Hansen, J., Moore, PB., Steitz, TA. (2000) The complete atomic structure of the large ribosomal subunit at 2.4 A resolution, *Science.* **289**, 905-920.

23. Schluenzen, F., Tocilj, A., Zaariach, R., Harms, J., Gluehmann, M., Janell, D., Bashan, A., Bartels, H. Agmon, I., Franceschi, F., Yonath, A. (2000) Structure of functionally activated small ribosomal subunit at 3.3 angstroms resolution, *Cell.* **102**, 615-623.

24. Wimberly, B., Brodersen, DE., Clemons, WM, Jr., Morgan-Warren, RJ., Carter, AP., Vonrhein, C., Hartsch, T., Ramakrishnan, V. (2000) Structure of the 30S ribosomal subunit, *Nature.* **407**, 327-339.

25. Harms, J., Schluenzen, F., Zarivach, R., Bashan, A., Gat, S., Agmon, I., Bartels, H., Francesch,i F., Yonath, A. (2001) High resolution structure of the large ribosomal subunit from a mesophilic eubacterium, *Cell.* **107**, 679-688.

26. Yusupov, M., Yusupova, GZ., Baucom, A., Lieberman, K., Earnest, TN., Cate, JH., Noller, HF. (2001) Crystal structure of the ribosome at 5.5 A resolution, *Science.* **292**, 883-896.

27. Schuwirth, B., Borovinskaya, MA., Hau, CW., Zhang, W., Vila-Sanjurjo, A., Holton, JM., Cate, JH. (2005) Structures of the bacterial ribosome at 3.5 A resolution, *Science.* **310**, 827-834.

28. Lata, K., Agrawal, RK., Penczek, P., Grassucc,i R., Zhu, J., Frank, J. (1996) Three-dimensional reconstruction of the Escherichia coli 30 S ribosomal subunit in ice., *J Mol Biol.* **262**, 43-52.

29. Agalarov, S., Zheleznyakova, EN., Selivanova, OM., Zheleznaya, LA., Matvienko, NI., et al. (1998) In vitro assembly of a ribonucleoprotein particle corresponding to the platform domain of the 30S ribosomal subunit, *Proc Natl Acad Sci USA.* **95**, 999-1003.

30. Samaha, R., O'Brien, B., O'Brien, TW., Noller, HF. (1994) Independent in vitro assembly of a ribonucleoprotein particle containing the 3′ domain of 16S rRNA, *Proc Natl Acad Sci USA.* **91**, 7884-7888.

31. Weitzmann, C., Cunningham, PR., Nurse, K., Ofengand, J. (1993) Chemical evidence for domain assembly of the *Escherichia coli* 30S ribosome, *FASEB J.* **7**, 177–180.

32. Adilakshmi, T., Ramaswamy, P., Woodson, SA. (2005) Protein-independent folding pathway of the 16S rRNA 5' domain, *J Microbiol.* **251**, 508-519.

33. Noller, H., Kop, J., Wheaton, V., Brosius, J., Gutell, RR., Kopylov, AM., Dohme, F., Herr, W., Stahl, DA., Gupta, R., Woese, CW. (1981) Secondary structure model for 23S ribosomal RNA, *Nucl Acid Res.* **9**, 6167-6189.

34. Monro, R. (1967) Catalysis of peptide bond formation by 50 S ribosomal subunits from *Escherichia coli J Mol Biol.* **26**, 147-151.

35. Traut, R., Monro, RE. (1964) The Puromycin Reaction and Its Relation to Protein Synthesis, *J Mol Biol.* **10** 63-72.

36. Steitz, T., Moore, PB. (2003) RNA, the first macromolecular catalyst: the ribosome is a ribozyme, *Trends Biochem Sci.* **28**, 411-418.

37. Rheinberger, H., Sternbach, H., Nierhaus, KH. (1981.) Three tRNA binding sites on *Escherichia coli* ribosomes, *Proc Natl Acad Sci U S A.* **78**, 5310-5314.

38. Shine, J., Dalgarno, L. (1974) The 3'-terminal sequence of Escherichia coli 16S ribosomal RNA: complementarity to nonsense triplets and ribo- some binding sites, *Proc Natl Acad Sci USA.* **71**, 1342-1346.

39. Crick, F. (1966) Codon-Anticodon Pairing: The Wobble Hypothesis, *J mol Biol.* **19**, 548-555.

40. Matthaei, H., Jones, OW., Martin, RG., Nirenber, MW. (1962) Characterstics and composition of RNA coding units, *Proc Natl Acad Sci U S A.* **48**, 666-677.

41. Nirenberg, M., Matthaei, HJ. (1961) The dependence of cell-free protein synthesis in *E. coli* upon naturally occuring or synthetic polyribonucleotides, *Proc Natl Acad Sci U S A.* **47**, 1580-1588.

42. Ogle, J., Murphy, FV., Tarry, MJ., Ramakrishnan, V. (2002) Selection of tRNA by the ribosome requires a transition from an open to a closed form, *Cell.* **111**, 721-732.

43. Jenner, L., Demeshkina, N.,Yusupova, G., Yusupov, M. (2010) Structural rearrangements of the ribosome at the tRNA proofreading step, *Nat Strut Mol Biol.* **17**, 1072-1078.

44. Ogle, J., Brodersen, DE., Clemons, WM. Jr., Tarry, MJ., Carte,r AP., Ramakrishnan, V. (2001) Recognition of cognate transfer RNA by the 30S ribosomal subunit *Science.* **292**, 897-902.

45. Moazed, D., Noller, HF. (1990) Binding of tRNA to the ribosomal A and P sites protects two distinct sets of nucleotides in 16 S rRNA, *J Mol Biol.* **211**, 135-145.

46. Yoshizawa, S., Fourmy, D., Puglisi, JD. (1999) Recognition of the codon-anticodon helix by ribosome RNA, *Science.* **285**, 1722-17225.

47. Shimizu, Y., Inone, A., Tomari, Y., Suzuki, T., Yokogawa, T., Nishikawa, K., Ueda, T. (2001) Cell-free translation reconstituted with purified components, *Nat Biotechnol.* **19**, 751-755.

48. Margus, T., Remm, M., and Tenson, T. (2007) Phylogenetic distribution of translational GTPases in bacteria, *BMC Genomics.* **8**, 15.

49. Ganoza, M., Aoki, H. (2000) Peptide bond synthesis: function of the efp gene product, *Biol Chem.* **381**, 533-559.

50. Swaney, S., McCroskey, M., Shinabarger, D., Wang, Z., Turner, BA., Parker, CN. (2006) Characterization of a high-throughput screening assay for inhibitors of elongation factor P and ribosomal peptidyltransferase activity, *J Biochem Screen.* **11**, 736-742.

51. Maguire, B. (2009) Inhibition of bacterial ribosome assembly: a suitable drug target?, *Microbiol Mol Rev.* **73**, 739-755.

52. Nierhaus, K. (1991) The assembly of prokaryotic ribosomes, *Biochimie.* **73**, 739–755.

53. Nomura, M. (1999) Regulation of ribosome biosynthesis in *Escherichia coli* and *Saccharomyces cerevisiae*: diversity and common principles, *J Bacteriol.* **181**, 6857-6864.

54. Nomura, M., Gourse, R., Baughman, G. (1984) Regulation of the synthesis of ribosomes and ribosomal components, *Annu Rev Biochem.* **53**, 75-117.

55. Mizushima S., N., M. (1970) Assembly mapping of 30S ribosomal proteins from *E. coli*, *Nature.* **226**, 214–218.

56. Held, W., Mizushima, S., Nomura, M. (1973) Reconstitution of Escherichia coli 30S ribosomal subunits from purified molecular components, *J Biol Chem.* **248**, 5720–5730.

57. Traub, P., Nomura, M. (1968) Structure and function of *E.coli* ribosomes.V.Reconstitution of functionally active 30S ribosomal particles from RNA and proteins, *Proc Natl Acad Sci U S A.* **59**, 777-784.

58. Nierhaus, K., Dohme, F. (1974) Total reconstitution of functionally active 50S ribosomal subunits from Escherichia coli, *Proc Natl Acad Sci U S A.* **71**, 4713-4717.

59. Herold, M., Nowotny, V., Dabbs, ER., Nierhaus, KH. (1986) Assembly analysis of ribosomes from a mutant lacking the assembly-initiator protein L24: lack of L24 induces temperature sensitivity, *Mol Gen Genet* **203**, 281-287.

60. Herold, M., Nierhaus, KH. (1987) Incorporation of six additional proteins to complete the assembly map of the 50 S subunit from Escherichia coli ribosomes, *J Biol Chem.* **262**, 8826-8833.

61. Held, W., Ballou, B., Mizushima, S., Nomura, M. (1974) Assembly mapping of 30 S ribosomal proteins from *Escherichia coli*. Further studies., *J Biol Chem.* **25**, 3103-3111.

62. Talkington, M., Siuzdak, G., et al. (2005) An Assembly Landscape of the 30S Ribosomal Subunit, *Nature.* **438**, 628-632.

63. Grondek, J., Culver, GM. (2004) Assembly of the 30S ribosomal subunit: positioning ribosomal protein S13 in the S7 assembly branch, *RNA.* **10**, 1861-1866.

64. Powers, T., Daubresse, G., Noller, HF. (1993) Dynamics of *in vitro* assembly of 16S rRNA into 30S ribosomal subunits., *J Mol Biol.* **232**, 362-374.

65. Rohl, R., Nierhaus, KH. (1982) Nierhaus, Assembly map of the large subunit (50S) of *Escherichia coli* ribosomes., *Proc Natl Acad Sci U S A.* **79**, 729-733.

66. Roth, H., Nierhaus, KH. (1980) Assembly map of the 50-S subunit from Escherichia coli ribosomes, covering the proteins present in the first reconstitution intermediate particle, *Eur J Biochem.* **103**, 95-98.

67. Spillmann, S., Dohme, F., Nierhaus, KH. (1977) Assembly in vitro of the 50 S subunit from *Escherichia coli* ribosomes: proteins essential for the first heat- dependent conformational change, *J Mol Biol.* **115**, 512-523.

68. Kaczanowska, P., Ryden-Aulin, M. (2007) Ribosome Biogenesis and the Translation Process in *Escherichia coli*, *Microbiol Mol Rev.* **71**, 477-494.

69. Bunner, A., Williamson, JR. (2009) Stable isotope pulse-chase monitored by quantitative mass spectrometry applied to *E. coli* 30S ribosome assembly kinetics, *Methods.* **49**, 136-141.

70. Bunner, A., Nord, S., Wikstrom, M., Williamson, JR. (2010) The effect of ribosome assembly cofactors on in vitro 30S subunit reconstitution, *J Mol Biol.* **398**, 1-7.

71. Shajani, Z., Skykes, MT., Williamson, JR. (2011) Assembly of Bacterial Ribosomes, *Annu Rev Biochem.* **80**, 501-526.

72. Sykes, M., Williamson, JR. (2009) A complex assembly landscape for the 30S ribosomal subunit, *Annu Rev Biophys.* **38**, 197-215.

73. Paul, B., Ross W., Gaal, T., Gourse, RL. (2004) rRNA transcription in *Escherichia coli*, *Annu Rev Genet.* **38**, 749-770.

74. Gourse, R., Gaal, T., Bartlett, MS., Appleman, JA., Ross, W. (1996) rRNA transcription and growth rate-dependent regulation of ribosome synthesis in *Escherichia col*i, *Annu Rev Microbiol.* **50**, 645-677.

75. Rainey, F., Ward-Rainey, NL., Janssen, PH., Hippe, H. (1996) Clostridium paradoxum DSM 7308(T) contains multiple 16S rRNA genes with heterogeneous intervening sequences, *Microbiology.* **142**, 2087-2095.

76. Murray, H., Appleman, J.A., Gourse, RL. (2003) Regulation of the *Escherichia coli rrnB* P2 promoter, *J Bacteriol.* **185**, 28-34.

77. Sarmientos, P., Cashel, M. (1983) Carbon starvation and growth rate-dependent regulation of the *Escherichia coli* ribosomal RNA promoters: differential control of dual promoter, *Proc Natl Acad Sci U S A.* **80**, 7010-7013.

78. Sarmientos P., S., JE., Contente, S., Cashel, M. (1983) Differential stringent control of the tandem *E. coli* ribosomal RNA promoters from the rrnA operon expressed in vivo in multicopy plasmids, *Cell.* **32**, 1337-1346.

79. Sulthana, S., Deutscher, MP. (2013) Multiple exoribonucleases catalyze maturation of the 3' terminus of 16S ribosomal RNA (rRNA), *J Biol Chem.* **288**, 12574-12579.

80. Li, Z., Pandit, S., Deutscher, MP. (1999) RNase G (CafA protein) and RNase E are both required for the 5′ maturation of 16S ribosomal RNA., *EMBO J.* **18**, 2878-2885.

81. Young, R., Steitz, JA. (1978) Complementary sequences 1700 nucleotides apart form a ribonuclease III cleavage site in *Escherichia coli* ribosomal precursor RNA., *Proc Natl Acad Sci U S A.* **75**, 3593-3597.

82. Ginsburg, D., Steitz, JA. (1975) The 30 S ribosomal precursor RNA from *Escherichia coli*. A primary transcript containing 23 S, 16 S, and 5 S sequences, *J Biol Chem.* **250**, 5647-5654.

83. King, T., Sirdeshmukh, E., Schlessinger, D. (1984) RNase III cleavage is obligate for maturation but not for function of *Escherichia coli* pre-23S rRNA, *Proc Natl Acad Sci U S A.* **8**, 185-188.

84. Wachi, M., Umitsuki, G., Shimizu, M., Takada, A., Nagai, K. (1999) Escherichia coli cafA gene encodes a novel RNase, designated as RNase G, involved in processing of the 5′ end of 16S rRNA, *Biochem Biophys Res Commun.* **259**, 483-488.

85. Sirdeshmukh, R., Schlessinger, D. (1985) Why is processing of 23S ribosomal RNA in *Escherichia coli* not obligate for its function?, *J Mol Biol.* **186**, 669-672.

86. Sirdeshmukh, R., Schlessinger, D. (1985) Ordered processing of *Escherichia coli* 23S rRNA in vitro, *Nucl Acid Res.* **13**, 5041-5054.

87. Li, Z., Pandit, S., Deutscher, MP. (1999) Maturation of 23S ribosomal RNA requires the exoribonuclease RNase T, *RNA.* **5**, 139-146.

88. Zengel, J., Lindahl, L. (1994) Diverse mechanisms for regulating ribosomal protein synthesis in *Escherichia coli*, *Prog Nucleic Acid Res Mol Biol.* **47**, 331-370.

89. Dennis, P., Ehrenberg, M., Bremer, H. (2004) Control of rRNA synthesis in *Escherichia coli*: a systems biology approach, *Microbiol Mol Rev.* **68**, 639-668.

90. Michaels, G. (1972) Ribosome maturation of *Escherichia coli* growing at different growth rates, *J Bacteriol.* **110**, 889-894.

91. Hage, A., Tollervey, D (2005) A surfeit of factors: why is ribosome assembly so much more complicated in eukaryotes than bacteria?, *RNA Biol.* **1**, 10-15.

92. Alix, J. (1993) Extrinsic factors in ribosome assembly, *Transl Appar Proc Int Conf*, 173-184.

93. Bryant, R., Sypherd, PS. (1974) Genetic analysis of cold-sensitive ribosome maturation mutants of *Escherichia coli*, *J Bacteriol.* **117**, 1082-1092.

94. Iost, I., Dreyfus, M. (2006) DEAD-box RNA helicases in Escherichia coli, *Nucl Acid Res.* **34**, 4189-4197.

95. Comartin, D., Brown, ED. (2006) Non-ribosomal factors in ribosome subunit assembly are emerging targets for new antibacterial drugs, *Curr Opin Pharmacol.* **6**, 453-458.

96. Alix, J., Nierhaus, KH. (2003) DnaK-facilitated ribosome assembly in *Escherichia coli* revisited, *RNA.* **9**, 787-793.

97. Maki, J., Schnobrich, DJ., Culver, GM. (2002) The DnaK chaperone system facilitates 30S ribosomal subunit assembly, *Mol Cell.* **10**, 129-138.

98. Decatur, W., Fournier, MJ. (2002) rRNA modifications and ribosome function, *Trends Biochem Sci.* **27**, 244-351.

99. Brown, E. (2005) Conserved P-loop GTPases of unknown function in bacteria: an emerging and vital ensemble in bacterial physiology, *Biochem Cell Biol.* **83**, 738-746.

100. Britton, R. (2009) Role of GTPases in bacterial ribosome assembly, *Annu Rev Biochem.* **63**, 155-176.

101. Del Campo, M., Kaya, Y., Ofengand, J. (2001) Identification and site of action of the remaining four putative pseudouridine synthases in *Escherichia coli*, *RNA.* **7**, 1603-1615.

102. Gutgsell, N., Deutscher, MP., Ofengand, J. (2005) The pseudouridine synthase RluD is required for normal ribosome assembly and function in *Escherichia coli.* **11**, 1141-1152.

103. Liu, M., Novotny, GW., Douthwaite, S. (2004) Methylation of 23S rRNA nucleotide G745 is a secondary function of the RlmAI methyltransferase, *RNA.* **10**, 1713–1720.

104. Cameron, D., Gregory, S., Thompson, J., Suh, M., Limbach, P., Dahlberg, A. (2004) Thermus thermophilus L11 methyltransferase, PrmA, is dispensable for growth and preferentially modifies free ribosomal protein L11 prior to ribosome assembly, *J Bacteriol.* **186**, 5819-5825.

105. Roy-Chaudhuri, B., Kirthi, N., Kelley, T., Culver, GM. (2008) Suppression of a cold-sensitive mutation in ribosomal protein S5 reveals a role for RimJ in ribosome biogenesis., *Mol Microbiol.* **68**, 1547-1549.

106. Lhoest, J., Colson, C. (1981) Cold-sensitive ribosome assembly in an *Escherichia coli* mutant lacking a single methyl group in ribosomal protein L3, *Eur J Biochem.* **121**, 33-37.

107. Cumberlidge, A., Isono, K. (1979) Ribosomal protein modification in *Escherichia coli.* I. A mutant lacking the N-terminal acetylation of protein S5 exhibits thermosensitivity, *J Mol Biol.* **131**, 169-189.

108. Pan, C., Russell, R. (2010) Roles of DEAD-box proteins in RNA and RNP folding, *RNA Biol.* **7**, 667-676.

109. Charollais, J., Pflieger, D., Vinh, J., Dreyfus, M., Iost, I. (2003) The DEAD-box RNA helicase SrmB is involved in the assembly of 50S ribosomal subunits in *Escherichia coli*, *Mol Microbiol.* **48**, 1253-1265.

110. Charollais, J., Dreyfus, M., Iost, I. (2004) CsdA, a cold-shock RNA helicase from *Escherichia coli*, is involved in the biogenesis of 50S ribosomal subunit, *Nucl Acid Res.* **32**, 2751-2759.

111. Trubetskoy, D., Proux, F., Allemnd, F., Dreyfus, M., Iost, I. (2009) SrmB, a DEAD-box helicase involved in *Escherichia coli* ribosome assembly, is specifically targeted to 23S rRNA in vivo, *Nucl Acid Res.* **37**, 6540-6549.

112. Al Refaii, A., Alix, JH. (2009) Ribosome biogenesis is temperature-dependent and delayed in *Escherichia coli* lacking the chaperones DnaK or DnaJ, *Mol Microbiol.* **71**, 748-762.

113. El Hage, A., Sbai, M., Alix, JH. (2001) The chaperonin GroEL and other heat-shock proteins, besides DnaK, participate in ribosome biogenesis in *Escherichia coli*, *Mo Gen Genet.* **264**, 796-808.

114. Lo¨vgren, J., Bylund, G., Srivastava, M., Lundberg, L., Persson, O., Wingsle,G., Wikstro¨m, P. (2004) The PRC-barreldomainofthe ribosome maturation protein RimM mediates binding to ribosomal protein S19 in the 30S ribosomal subunits, *RNA.* **10**, 1798-1812.

115. Bylund, G., Persson, BC., Lundberg, LAC., Wikstrom, PM. (1997) A novel ribosome-associated protein is important for efficient translation in *Escherichia coli*, *J Bacteriol.* **179**, 4567-4574.

116. Bylund, G., Wipemo, L., Lundberg, L., Wikstrom, P. (1998) RimM and RbfA are essential for efficient processing of 16S rRNA in *Escherichia coli*, *J Bacteriol.* **180**, 73-82.

117. Clatterbuck Soper, S., Dator, RP., Limbac, PA., Woodson, SA. (2013) In vivo X-ray footprinting of pre-30S ribosomes reveals chaper- one-dependent remodeling of late assembly intermediates., *Mol Cell.* **52**, 506-516.

118. Dammel, C., Noller, HF. (1993) A cold-sensitive mutation in 16S rRNA provides evidence for helical switching in ribosome assembly, *Genes Dev.* **7**, 660-670.

119. Dammel, C., Noller, HF. (1995) Suppression of a cold-sensitive mutation in 16S rRNA by overexpression of a novel ribosome- binding factor, RbfA, *Genes Dev.* **9**, 626-637.

120. Datta, P., Wilson, DN., Kawazoe, M., Swami, NK., Kaminishi, T., Sharma, MR., Booth, TM., Takemoto, C., Fucini, P., Yokoyama, S., Agrawal, RK. (2007) Structural aspects of RbfA action during small ribosomal subunit assembly, *Mol Cell.* **28**, 434-445.

121. Goto, S., Kato, S., Kimura, T., Muto, A., Himeno, H. (2011) RsgA releases RbfA from 30S ribosome during a late stage of ribosome biosynthesis, *EMBO J.* **30**, 10114.

122. Xia, B., Ke, H., Shinde, U., Inouye, M. (2003) The role of RbfA in 16S rRNA processing and cell growth at low temperature in *Escherichia coli*, *J Mol Biol.* **332**, 575-584.

123. Inoue, K., Alsina, J., Chen, J., Inouye, M. (2003) Suppression of defective ribosome assembly in a rbfA deletion mutant by overexpression of Era, an essential GTPase in *Escherichia coli*, *Mol Microbiol.* **48**, 1005-1016.

124. Sharma, M., Barat, C., Wilson, DN., Booth, TM., Kawazoe, M., Hori-Takemoto, C., Shirouzu, M., Yokoyama, S., Fucini, P., Agrawal, RK. (2005) Interaction of Era with the 30S ribosomal subunit implications for 30S subunit assembly, *Mol Cell.* **18**, 319-329.

125. Inoue, K., Chen, J., Tan, Q., Inouye, M. (2006) Era and RbfA have overlapping function in ribosome biogenesis in *Escherichia coli*, *J Microbiol Biotechnol.* **11**, 41-52.

126. Campbell, T., Brown, ED. (2008) Genetic interaction screens with ordered overexpression and deletion clone sets implicate the *Escherichia coli* GTPase YjeQ in late ribosome biogenesis, *J Bacteriol.* **190**, 2537-2545.

127. Daigle, D., Brown, ED. (2002) YjeQ, an essential, conserved, uncharacterized protein from Escherichia coli, is an unusual GTPase with circularly permuted G-motifs and marked burst kinetics, *Biochemistry.* **41**, 11109-11117.

128. Campbell, T., Henderson, J., Heinrichs, DE., Brown, ED. (2006) The yjeQ gene is required for virulence of *Staphylococcus aureus*, *Infect Immun.* **74**, 4918-4921.

129. Leong, V., Kent, M., Jomaa, A., Ortega, J. (2013) *Escherichia coli* rimM and yjeQ null strains accumulate immature 30S subunits of similar structure and protein complement., *RNA.* **19**, 789-802.

130. Jomaa, A., Stewart, G., Mears, JA., Kireeva, I., Brown, ED., Ortega, J. (2011) Cryo-electron microscopy structure of the 30S subunit in complex with the YjeQ biogensis factor, *RNA.* **17**, 2026-2038.

131. Nord, S., Bylund, Go., Lovgren, JM., Wikstrom. (2009) The RimP protein is important for maturation of the 30S ribosomal subunit, *J Mol BIol.* **27**, 742-753.

132. Himeno, H., K, Hanawa-Suetsugu, K., Kimura, T., Takagi, K., Sugiyama, W., Shirata, S., Mikami, T., Odagir, F., Osania, Y., Watanave, D., Goto, S., Kalacynyuk, L., Ushida, C., Muta, A. (2004) A novel GTPase activated by the small subunit of ribosome, *Nucleic Acids Res.* **32**, 5303-5309.

133. Guo, Q., Yuan, Y., Feng, B., Liu, L., CHen, K., Sun, M., Yang, Z., Lei, J., Gao, N. (2013) Dissecting the in vivo assembly of the 30S ribosomal subunit reveals the role of RimM and general features of the assembly process, *Nucl Acid Res.* **41**, 2609-2620.

134. Arigoni, F., Talabot, F., Peitsch, M., Edgerton, MD., Meldrum, E., Allet, E., Fish, R., Jamotte, T., Curchod, ML., Loferer, H. (1998) A genome-based approach for the identification of essential bacterial genes, *Nat Biotechnol.* **16**, 851-856.

135. Leipe, D., Wolf, YI., Koonin, EV., Aravind, L. (2002) Classificaiton and evolution of P-loop GTPases and related ATPases, *J mol Biol.* **317**, 41-72.

136. Bourne, H., Sanders, DA., McCormick, F. (1991) The GTPase super-family: conserved structure and molecular mechanism, *Nature.* **349**, 117-127.

137. Shin, D., Lou, Y., Jancarik, J. Yokota, H., Kim, R., Kim, SH. (2004) Crystal structure of YjeQ from *Thermotoga maritima* contains a circularly permuted GTPase domain, *Proc Natl Acad Sci U S A.* **101**, 12198-13203.

138. Daigle, D., Brown, ED. (2004) Studies of the Interaction of *Escherichia coli* YjeQ with the Ribosome In Vitro, *J Bacteriol.* **186**, 1381-1387.

139. Campbell, T., Daigle, DM., Brown, ED. (2005) Characterization of the *Bacillus subtilis* GTPase YloQ and its role in ribosome function, *Biochem J.* **289**, 843-852.

140. Jomaa, A., Stewart, GFS., Martin-Benito, J., Zielke, R., Campbell, T., Maddock, JR., Brown, ED, Ortega, J. (2011) Understanding ribosome assembly: the structure of *in vivo* assembled immature 30S subunits revealed by cryo-electron microscopy, *RNA.* **17**, 697-709.

141. Hase, Y., Yokoyama, S., Muto, A., Himeno, H. (2009) Removal of a ribosome small subunit-dependant GTPase confers salt restance of *Eschericia coli* cells, *RNA*. **15**, 1766-1774.

142. Ross, P., Huang, YN., Marchese, JN., Williamson, B., Parker, K., Hattan, S., Khainovski, N., Pillai, S., Dey, S., Daniels, S., Purkayastha, S., Juhasz, P., Martin, S., Bartlet-Jones, M., He, F., Jacobson, A., Pappin, DJ. (2004) Multiplexed protein quantitation in Saccharomyces cerevisiae using amine-reactive isobaric tagging reagents, *Mol Cell Proteomics*. **3**, 1154-1169.

143. Valle, M., Sengupta, J., Swami, NK., Grassucci, RA., Burkhardt, N., Nierhaus, KH., Agrawal, RK., Frank, J. (2002) Cryo-EM reveals an active role for aminoacyl-tRNA in the accommodation process, *EMBO J.* **21**, 3557-3567.

144. Gao, H., , Valle, M., Ehrenberg, M., Frank, J. (2004) Dynamics of EF-G interaction with the ribosome explored by classification of a heterogeneous cryo-EM dataset, *J Struct BIol.* **147**, 283-290.

145. Mangiarotti, G., Turoc, E., Ponzetto, A., Altruda, F. (1974) Precursor 16S RNA in active 30S ribosomes, *Nature.* **247**, 147-148.

146. Bremer, H., Dennis, PP. (1996) Modulation of chemical composition and other param- eters of the cell by growth rate in *Escherichia coli and Salmonella* (FC, N., ed) pp. 1553-1569, AM Soci Microbiol, Washington, DC.

147. Lindahl, L. (1975) Intermediates and time kinetics of the *in viv*o assembly of *Escherichia coli* ribosomes, *J Mol Biol.* **92**, 15-37.

148. Spedding, G. (1990) *Isolation and analysis of ribosome from prokaryotes, eukaryotes and organelles*, IRL Press, New York.

149. Sengupta, J., Agrawal, RK., Frank, J. (2001) Visualization of protein S1 within the 30S ribosomal subunit and its interaction with messenger RNA, *Proc Natl Acad Sci USA*. **98**, 11991-11996.

150. Kimura, T., Takagi, K., Kyoko, HS., Kalachnyuk, L., Muto, A., Himeno, H. (2007) Interaction between RsgA and the ribosome, *Nucl Acids Symp Ser (Oxf)*. **51**, 375-376.

151. Guo, Q., Yuan, Y., Xu, Y., Feng, B., Liu, L., Chen, K., Sun, M., Yang, Z., Lei, J., Gao, N. (2011) Structural basis for the function of a small GTPase RsgA on the 30S ribosomal subunit maturation revealed by cryoelectron microscopy, *Proc Natl Acad Sci USA*. **108**, 13100-13105.

152. Davies, B., Kohrer, C., Jacob AI., Simmons, LA., Zhu, J. Aleman, LM. Rajbhandary, UL., Walker, GC. (2010) Role of *Escherichia coli* YbeY, a highly conserved protein, in rRNA processing, *Mol Microbiol.* **78**, 506-518.

153. Pardon, B., Wanger, R. (1995) The *Eschericia coli* ribosomal RNA leader nut region interacts with mature 16S RNA, *Nucl Acid Res.* **23**, 932-941.

154. Besanacon, W., Wagner, R. (1999) Characterization of transient RNA-RNA interactions improtant for the facilitated structure formation of bacterial ribosomal 16S RNA, *Nucl Acid Res.* **27**, 4353-4362.

155. Schaferkordet, J., Wagern, R. (2001) Effects of base change mutations within an *Eschericia coli* ribosomal RNA leader region on rRNA mautration and ribosome formation, *Nucl Acid Res.* **29**, 3394-3403.

156. Jiang, M., Datta, K., Walker, A., Strahler, J., Bagamasbad, P., Andrews, PC., Maddock, JR. (2006) The *Escherichia coli* GTPase CgtAE is involved in late steps of large ribosome assembly, *J Bacteriol.* **188**, 6757-6770.

157. Jiang, M., Sullivan, SM., Walker, AK., Strahler, JR., Andrews, PC., Maddock, JR. (2007) Identification of novel *Escherichia coli* ribosome-associated proteins using isobaric tags and multidimensional protein identification techniques, *J Bacteriol.* **189**, 3434-3444.

158. Aebi, U., Pollard, TD. (1987) A glow discharge unit to render electron microscope grids and other surfaces hydrophilic, *J Electron Microsc Tech.* **7**, 29-33.

159. Ludtke, S., Baldwin, PR., Chiu, W. (1999) EMAN: semiautomated software for high- resolution single-particle reconstructions, *J Struct BIol.* **128**, 82-97.

160. Mindell, J., Grigorieff, N. (2003) Accurate determination of local defocus and specimen tilt in electron microscopy, *J Struct BIol.* **142**, 334-347.

161. Scheres, S., Nuñez-Ramirez, R., Sorzano, COS., Carazo, JM., Marabini, R. (2008) Image processing for electron microscopy single-particle analysis using Xmipp, *Nat Protoc.* **3**, 977-990.

162. Scheres, S., Valle, M., Nunez, R., Sorzano, CO., Marabini, R., Herman, GT., Carazo, JM. (2005) Maximum-likelihood multi-reference refinement for electron microscopy images, *J Mol Biol.* **348**, 139-149.

163. Scheres, S., Gao, H., Valle, M., Herman, GT., Eggermont, PP., Frank, J., Carazo, JM. (2007) Disentangling conformational states of macromolecules in 3D-EM through likelihood optimization, *Nat Methods.* **4**, 27-29.

164. Borovinskaya, M., Pai, RD., Zhang, W., Schuwirth, BS., Holton, JM., Hirokawa, G., Kaji, H., Kaji, A., Cate, JH. (2007) Structural basis for aminoglycoside inhibition of bacterial ribosome recycling, *Nat Strut Mol Biol.* **14**, 727-732.

165. Wriggers, W., Agrawal, RK., Drew, DL., McCammon, A., Frank, J. (2000) Domain motions of EF-G bound to the 70S ribosome: insights from a hand-shaking between multi- resolution structures, *Biophys J.* **79**, 1670-1678.

166. Pettersen, E., Goddard, TD., Huang, CC., Couch, GS., Greenblatt, DM., Meng, EC., Ferrin, TE. (2004) UCSF Chimera--a visualization system for exploratory research and analysis, *J Comput Chem.* **25**, 1605-1612.

167. Nichols, C., Johnson, C., Lamb, HK., Lockyer, M., Charles, IG., Hawkins, AR., Stammers, DK. (2007) Structure of the ribosomal interacting GTPase YjeQ from the enterobacterial species *Salmonella typhimurium*, *Acta Crystallogr Sect F Struct Biol Cryst Commun.* **63**, 922-928.

168. Tan, R., Devkota, B., Harvey, SC. 2008. (2008) YUP.SCX: coaxing atomic models into medium resolution electron density maps, *J Struct BIol.* **163**, 163-174.

169. Tan, R., Petrov, AS., Harvey, SC. (2006) YUP: A molecular simulation program for coarse-grained and multi-scale models, *J Chem Theory Comput* **2**, 529-540.

170. Harvey, R., Koch, AL. (1980) How partially inhibitory concentrations of chloramphenicol affect the growth of *Escherichia coli*, *Antimicrob Agents Chemother.* **18**, 323-337.

171. Klumpp, S., Zhang, Z., Hwa, T. (2009) Growth rate-dependent global effects on gene expression in bacteria, *Cell.* **139**, 1366-1375.

172. Schaechter, M., Maaloe, O., Kjeldgaard, NO. (1958) Dependency on medium and temperature of cell size and chemical composition during balanced grown of *Salmonella typhimurium*, *J Gen Microbiol.* **19**, 592-606.

173. Dennis, P., Bremer, H. (1974) Macromolecular composition during steady-state growth of *Escherichia coli* B/r, *J Bacteriol.* **119**, 270-281.

174. Young, R., Bremer, H. (1976) Polypeptide-chain-elongation rate in *Escherichia coli* B/r as a function of growth rat, *Biochem J.* **160**, 185-194.

175. Dennis, P., Bremer, H. (1974) Differential rate of ribosomal protein synthesis in *Escherichia coli* B/r, *J mol BIol.* **84**, 407-422.

176. Dennis, P., Nomura, M. (1974) Stringent control of ribosomal protein gene expression in *Eschericia coli*, *Proc Natl Acad Sci U S A.* **71**, 3819-3823.

177. Forchhammer, J., Lindahl, L. (1971) Growth rate of polypeptide chains as a function of the cell growth rate in a mutant of *Escherichia coli* 15, *J Mol Biol.* **55**.

178. Ehrenberg, M., Brem, H., Dennis, PP. (2013) Medium-dependent control of the bacterial growth rate, *Biochime.* **95**, 643-658.

179. Scott, M., Gunderson, CW., Mateescu, EM., Zhang, Z., Hwa, T. (2010) Interdependence of cell growth and gene expression: orgins and conseuqences, *Science.* **330**, 1099-1102.

180. Ruusala, T., Andersson, D., Ehrenberg, M., Kurland, CG. (1984) Hyper-accurate ribosomes inhibit growth, *EMBO J.* **3**, 2575-2580.

181. Churchward, G., Estiva, E., Bremer, H. (1981) Growth rate-dependent control of chromosome replication initiation in *Escherichia coli*, *J Bacteriol.* **145**, 1232-1238.

182. Jinks-Robertson, S., Gourse, RL., Nomura, M. (1983) Expression of rRNA and tRNA genes in *Escherichia coli*: evidence for feedback regulation by products of rRNA operons, *Cell.* **33**, 865-876.

183. Takebe, Y., Miura, A., Bedwell, DM., Tam, M., Nomura, M. (1985) Increased expression of ribosomal genes during inhibition of ribosome assembly in *Escherichia coli*, *J Mol Biol.* **184**, 23-30.

184. Condon, C., French, S., Squires, C., Squires, CL. (1993) Depletion of functional ribosomal RNA operons in *Escherichia coli* causes increased expression of the remaining intact copies, *EMBO J.* **12**, 4305-4315.

185. Cole, J., Olsson, CL., Hershey, JWB., Grunberg-Manago, M., Nomura, M. (1987) Feedback regulation of rRNA synthesis in *Escherichia coli*. Requirement for initiation factor IF2, *J Mol BIol.* **198**, 383-392.

186. Yamagishi, M., De Boer, HA., Nomura, M. (1987) A mutattional alteration in the anti-Shine-Dalgarno region of the 16S rRNA gene abolishes regulation, *J Mol Biol.* **198**, 547-550.

187. Mikkola, R., Kurland, CG. (1991) Evidence for demand-regulation of ribosome accumulation in *E. coli*, *Biochime.* **73**, 1551-1556.

188. Slater, M., Schaechter, M. (1974) Control of cell division in bacteria, *Bacteriol Rev.* **38**, 199-221.

189. Butland G, B. M., Díaz-Mejía JJ, Bohdana F, Phanse S, Gold B, Yang W, Li J, Gagarinova AG, Pogoutse O, et al. (2008) eSGA: *E. coli* synthetic genetic array analysis, *Nat Methods.* **5**, 789-795.

190. Zuurmond, A., Rundlöf, AK., Kraal, B. (1999) Either of the chromosomal tuf genes of *E. coli* K-12 can be deleted without loss of cell viability, *Mol Gen Genet.* **260**, 603-607.

191. Baba, T., Ara T., Hasegawa M., Takai, Y., Okumura, Y., Baba, M., Datsenko, KA., Tomita, M., Wanner, BL., Mori, H. (2006) Construction of *Escherichia coli* K-12 in-frame, single-gene knockout mutants: the Keio collection, *Mol Syst Biol.* **2**, 2006-2008.

192. Bettenbrock, K., Sauter, T., Jahreis, K., Kremling, A., Lengeler, J., Gilles, ED. (2007) Correlation between growth rates, EIIACrr phosphorylation, and intracellular cyclic AMP levels in *Escherichia coli* K-12, *J Bacteriol.* **189**, 6891-6900.

193. Hu, P., Janga, SC., Babu, M., Diaz-Mejia, JJ., Butland, G., Yang, W., et al. (2009) Global functional atlas of *Escherichia coli* encompassing previously uncharacterized proteins, *PLoS Biol 2009.* **7**, e96.

194. Mani, R., Onge, RP., Hartman, JL 4th., Giaever, G., Roth, FP. (2008) Defining Genetic Interaction, *Proc Natl Acad Sci U S A.* **109**, 3461-3466.

195. Yang, Z., Guo, Q., Goto,S. Chen, Y., Li, N., Yan, K., Zhang, Y., Muta, A., Den, H., Himeno, H., Lei, J., Gao, N. (2014) Structural insights into the assembly of the 30S ribosomal subunit in vivo: functional role of S5 and location of the 17S rRNA precursor sequence, *Protein Cell.* **5**, 394-407.

196. Cabedo, H., Macián, F., Villarroya, M., Escudero, JC., Martínez-Vicente, M., Knecht, E., Armengod, ME. (1999) The *Escherichia coli trmE* (*mnmE*) gene, involved in tRNA modification, codes for an evolutionarily conserved GTPase with unusual biochemical properties, *EMBO J.* **18**, 7063-7076.

197. Brégeon, D., Colot, V., Radman, M., Taddei, F. (2001) Translational misreading: a tRNA modification counteracts a +2 ribosomal frameshift, *Genes Dev.* **15**, 2295-2306.

198. Urbonavicius, J., Stahl, G., Durand, JM., Ben Salem, SN., Qian, Q., Farabaugh, PJ., Björk, GR. (2003) Transfer RNA modifications that alter +1 frameshifting in general fail to affect -1 frameshifting, *RNA.* **9**, 760-768.

199. Gupta, N., Culver, GM. (2014) Multiple in vivo pathways fo *Eschericia coli* small ribosomal subunit assembly occur on one pre-rRNA, *Nat Struct Mol Biol.* **21**, 937-943.

200. Maguire, B., Wild, DG. (1997) The roles of proteins L28 and L33 in the assembly and function of *Escherichia coli* ribosomes in vivo, *Mol Microbiol.* **23**, 237-245.

201. Stokes, J., Davis, JH., Mangat, CS., Willaimson, JR., Brown, ED. (2014) Discovery of a small moleculte that inhitivts bacterial ribosome biogenesis, *Elife.* **18**, e03574.

202. Isono, S., Isono, K (1981) Ribosomal protein modification in *Escherichia coli.* III. Studies of mutants lacking an acetylase activity specific for protein L12, *Mol Gen Genet.* **183**, 473-477.

203. Conrad, J., Sun, D., Englund, N., Ofengand, J. (1998) The *rluC* gene of *Escherichia coli* codes for a pseudouridine synthase that is solely responsible for synthesis of pseudouridine at positions 955, 2504, and 2580 in 23 S ribosomal RNA, *J Biol Chem.* **273**, 18562-18566.

204. Wada, A., Yamazaki, Y., Fujita, N., Ishihama, A. (1990) Structure and probable genetic location of a "ribosome modulation factor" associated with 100S ribosomes in stationary-phase *Escherichia coli* cells, *Proc Natl Acad Sci U S A.* **87**, 2657-2661.

205. Tscherne, J., Nurse, K., Popienick, P., Ofengand, J. (1999) Purification, cloning, and characterization of the 16 S RNA m2G1207 methyltransferase from Escherichia coli, *J Biol Chem.* **274**, 924-929.

206. Ost, K., Deutscher, MP. (1991) *Escherichia coli orfE* (upstream of *pyrE*) encodes RNase PH, *J Bacteriol.* **173**, 5589-5591.

207. Caldas, T., Binet, E., Bouloc, P., Costa, A., Desgres, J., Richarme, G. (2000) The FtsJ/RrmJ heat shock protein of *Escherichia coli* is a 23 S ribosomal RNA methyltransferase, *J Biol CHem.* **275**, 16414-16419.

208. Poldermans, B., Roza, L., Van Knippenberg, PH. (1979) Studies on the function of two adjacent N6,N6-dimethyladenosines near the 3' end of 16 S ribosomal RNA of *Escherichia coli.* III. Purification and properties of the methylating enzyme and methylase-30 S interactions, *254.* **18**, 9100.

209. Connolly, K., Rife, JP., Culver, G. (2008) Mechanistic insight into the ribosome biogenesis functions of the ancient protein KsgA, *Mol Microbiol.* **70**, 2062-1075.

210. Conrad, J., Niu, L., Rudd, K., Lane, BG., Ofengand, J. (1999) 16S ribosomal RNA pseudouridine synthase RsuA of Escherichia coli: deletion, mutation of the conserved Asp102 residue, and sequence comparison among all other pseudouridine synthases, *RNA.* **5**, 751-763.

211. Isono, K., Isono, S (1980) Ribosomal protein modification in *Escherichia coli*. II. Studies of a mutant lacking the N-terminal acetylation of protein S18, *Mol Gen Genet.* **177**, 645-651.

212. Curnow, A., Garcia, GA. (1994) tRNA-guanine transglycosylase from *Escherichia coli*: recognition of dimeric, unmodified tRNA(Tyr), *Biochimie.* **76**, 1183-1191.

213. Reuter, K., Chong, S., Ullrich, F., Kersten, H., Garcia, GA. (1994) Serine 90 is required for enzymic activity by tRNA-guanine transglycosylase from *Escherichia coli*, *Biochemistry.* **33**, 7041-7046.

214. Kammen, H., Marvel, CC., Hardy, L., Penhoet, EE. (1988) Purification, structure, and properties of *Escherichia coli* tRNA pseudouridine synthase I, *263.* **5**.

215. Kambampati, R., Lauhon, CT. (2003) MnmA and IscS are required for in vitro 2-thiouridine biosynthesis in *Escherichia coli*, *Biochemistry.* **42**, 1109-1117.

216. Glick, B., Ganoza, MC. (1975) Identification of a soluble protein that stimulates peptide bond synthesis, *Proc Natl Acad Sci U S A.* **72**, 4257-4260.

217. Ude, S., Lassak, J., Starosta, AL., Kraxenberger, T., Wilson, DN., Jung K. (2013) Translation elongation factor EF-P alleviates ribosome stalling at polyproline stretches, *Science.* **339**, 82-88.

218. Jakubowski, H. (1999) Misacylation of tRNALys with noncognate amino acids by lysyl-tRNA synthetase, *Biochemistry.* **38**, 8088-8093.

219. Capecchi, M., Klein, HA. (1969) Characterization of three proteins involved in polypeptide chain termination, *Cold Sping Harb Symp Quant Biol.* **34**, 469-477.

220. Freistroffer, D., Pavlov, MY., MacDougall, J., Buckingham, RH., Ehrenberg, M. (1997) Release factor RF3 in *E. coli* accelerates the dissociation of release factors RF1 and RF2 from the ribosome in a GTP-dependent manner, *EMBO J.* **16**, 4126-4133.

221. Vanet, A., Plumbridge, JA., Guérin, MF., Alix, JH. (1994) Ribosomal protein methylation in *Escherichia coli*: the gene *prmA,* encoding the ribosomal protein L11 methyltransferase, is dispensable, *Mol Microbiol.* **14**, 947-958.

222. Forchhammer, K., Leinfelder, W., Boesmiller, K., Veprek, B., Böck, A. (1991) Selenocysteine synthase from *Escherichia coli.* Nucleotide sequence of the gene (*selA*) and purification of the protein, *J Biol Chem.* **266**, 6318-6323.

223. Nurse, K., Wrzesinski, J., Bakin, A., Lane, BG., Ofengand, J. (1995) Purification, cloning, and properties of the tRNA psi 55 synthase from *Escherichia coli*, *RNA.* **1**, 102-112.

224. Heider, J., Baron, C, Böck, A. (1992) Coding from a distance: dissection of the mRNA determinants required for the incorporation of selenocysteine into protein, *EMBO J.* **11**, 3759-3766.

225. Remus, B., Jacewicz A., Shuman, S. (2014) Structure and mechanism of *E. coli* RNA 2',3'-cyclic phosphodiesterase, *RNA.* **20**, 1697-1705.

226. Jackson, B., Kennedy, EP. (1983) The biosynthesis of membrane-derived oligosaccharides. A membrane-bound phosphoglycerol transferase, *J Biol Chem.* **258**, 2394-2398.

227. Purta, E., van Vliet, F., Tkaczuk, KL., Dunin-Horkawicz, S., Mori, H., Droogmans, L., Bujnicki, JM. (2006) The yfhQ gene of Escherichia coli encodes a tRNA:Cm32/Um32 methyltransferase, *BMC Mol Biol.* **7**, 23.

228. Haseltine, W., Block, R. (1973) Synthesis of guanosine tetra- and pentaphosphate requires the presence of a codon-specific, uncharged transfer ribonucleic acid in the acceptor site of ribosomes, *Proc Natl Acad Sci U S A.* **70**, 1564-1568.

229. Payoe, R., Fahlman, RP. (2011) Dependence of RelA-mediated (p)ppGpp formation on tRNA identity, *Biochemistry.* **50**, 3075-3083.

230. Cudny, H., Deutscher, MP. (1980) Apparent involvement of ribonuclease D in the 3' processing of tRNA precursors, *Proc Natl Acad Sci U S A.* **77**, 837-841.

231. Miles, Z., McCarty, RM., Molnar, G., Bandarian, V. (2011) Discovery of epoxyqueuosine (oQ) reductase reveals parallels between halorespiration and tRNA modification
, *Proc Natl Acad Sci USA.* **108**, 7368-7362.

232. Mohanty, B., Kushner, SR. (2006) The majority of Escherichia coli mRNAs undergo post-transcriptional modification in exponentially growing cells, *Nucl Acid Res.* **34**, 5695-5704.

233. Soutourina, J., Plateau, P., Delort, F., Peirotes, A., Blanquet S. (1999) Functional characterization of the D-Tyr-tRNATyr deacylase from *Escherichia coli*, *J Biol Chem.* **274**, 19109-19114.

234. Muto, A., Sato, M., Tadaki, T., Fukushima, M., Ushida, C., Himeno, H. (1996) Structure and function of 10Sa RNA: trans-translation system, *Biochimie.* **78**, 985-991.

SUPPLEMENTARY FIGURES

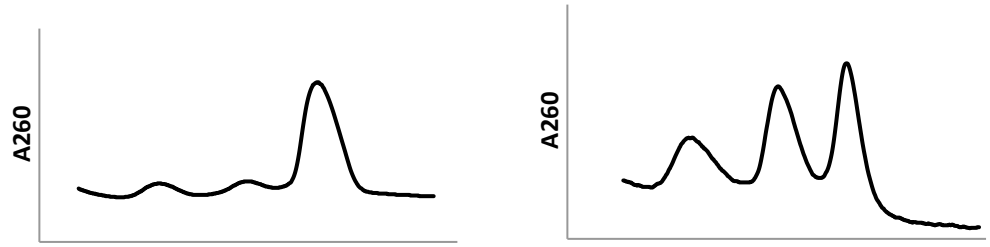

Supplementary Figure 1.1: Ribosome profile for the ΔyjeQ deletion. *The mutant shows an elevated level of free 30S and 50S subunits relatives to 70S ribosomes.*

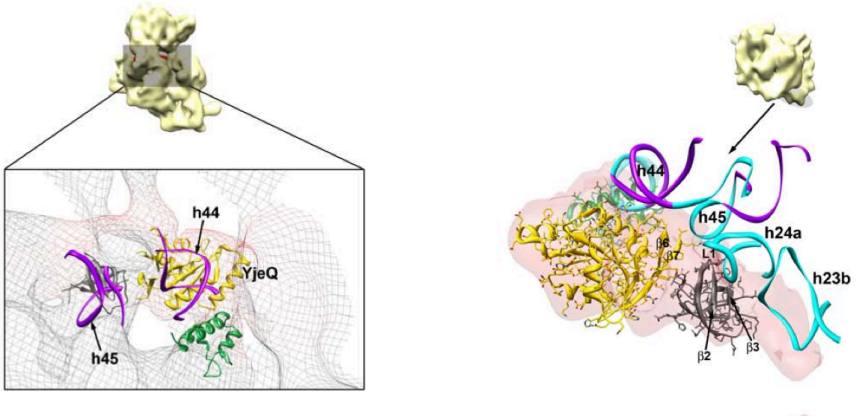

Supplementary Figure 1.2: Interaction of YjeQ with the 30S subunit. A) *View of the 30S:YjeQ complex (see orientation aid in panel above) after a clipping plane orthogonal to the direction of view was applied to the cryo-EM map removing the blocking densities on the back. The panel shows the density map of the 30S:YjeQ complex as a mesh. The OB-fold, GTPase and zinc-finger domains of the YjeQ structure are shown fitted into this density and colored in grey, yellow and green, respectively. The nucleotides in helix 44 and helix 45 for which a corresponding density in the 30S:YjeQ complex EM map does not exist are colored in purple.* ***B)*** *Interactions of the OB-fold and GTPase domain of YjeQ with the 16S rRNA helices 24a and 23b in the platform and helix 45 in the 3' minor domain of the 30S subunit. Important loops and b strands in YjeQ for the interaction with the 30S subunit are labeled. The OB-fold, GTPase and zinc-finger domains of the YjeQ structure are colored in grey, yellow and green, respectively. The extra density attributed to YjeQ is displayed as a red semitransparent surface. The rRNA is displayed in cyan except for the nucleotides for which a corresponding density in the 30S:YjeQ complex EM map does not exist that are colored in blue. Adapted from Jomaa et al. [130]*

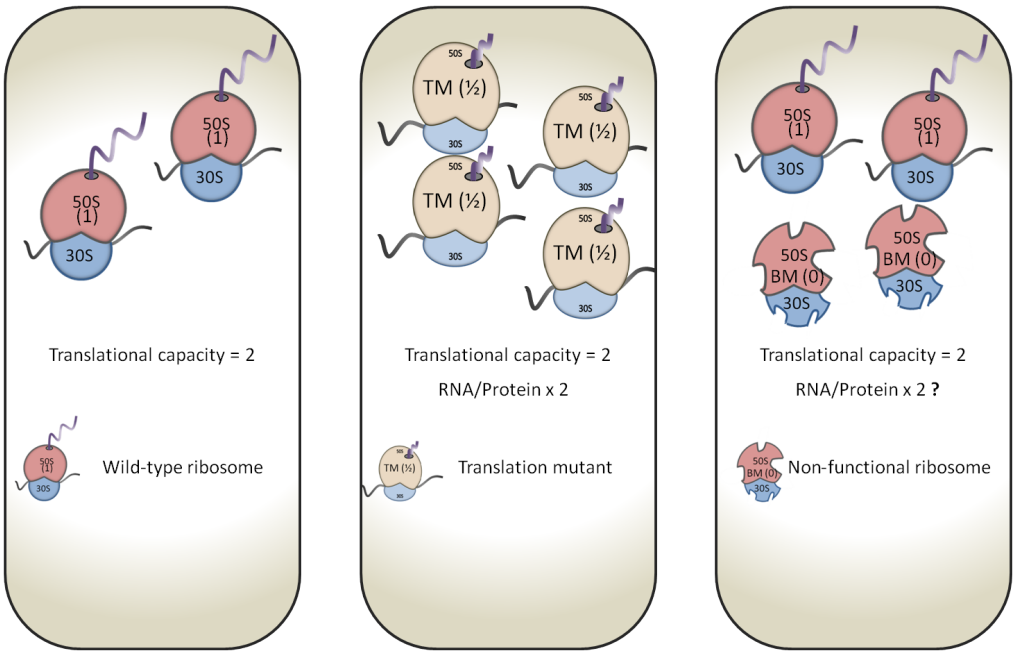

Supplementary Figure 3.1: Understanding the effects of perturbations in biogenesis on growth rate-dependent ribosomal content. *A schematic illustrating the relationship between translational capacity and RNA/protein ratio in various cell types. In wild-type strains and translation mutants, the non-functional portion of ribosomal material is minor and anticipated to be constant regardless of growth rate. Thus, translational capacity is reflective of the translational efficiency of the ribosome population. In contrast, non-functional material makes up a significant portion of the ribosomal content in cells with disrupted biogenesis and thus, translational capacity is instead determined by the proportion of functional to non-functional ribosomal material.* ***A)*** *Wild-type cells with a theoretical translational capacity (k_t) of 2. The value k_t is determined by the quantity of ribosomes reflected by the RNA/Protein ratio (r).The values in parentheses (1) indicate hypothetical values of translational output for individual ribosomes.* ***B)*** *A translation mutant with a theoretical k_t of 2. Because the translational output of the mutant ribosomes is reduced (½), more units (4) are required to achieve the same translational capacity as the wild-type. Thus, r is twice that of the wild-type.* ***C)*** *A biogenesis mutant with a theoretical k_t of 2. Only a fraction (½) of the total ribosomal material is functional, with each unit having an output of 1. Immature subunits are non-functional and thus, have an output of 0. In this scenario, the RNA/Protein ratio of the cell would be twice that of the wild-type (2 functional, 2 non-functional).*

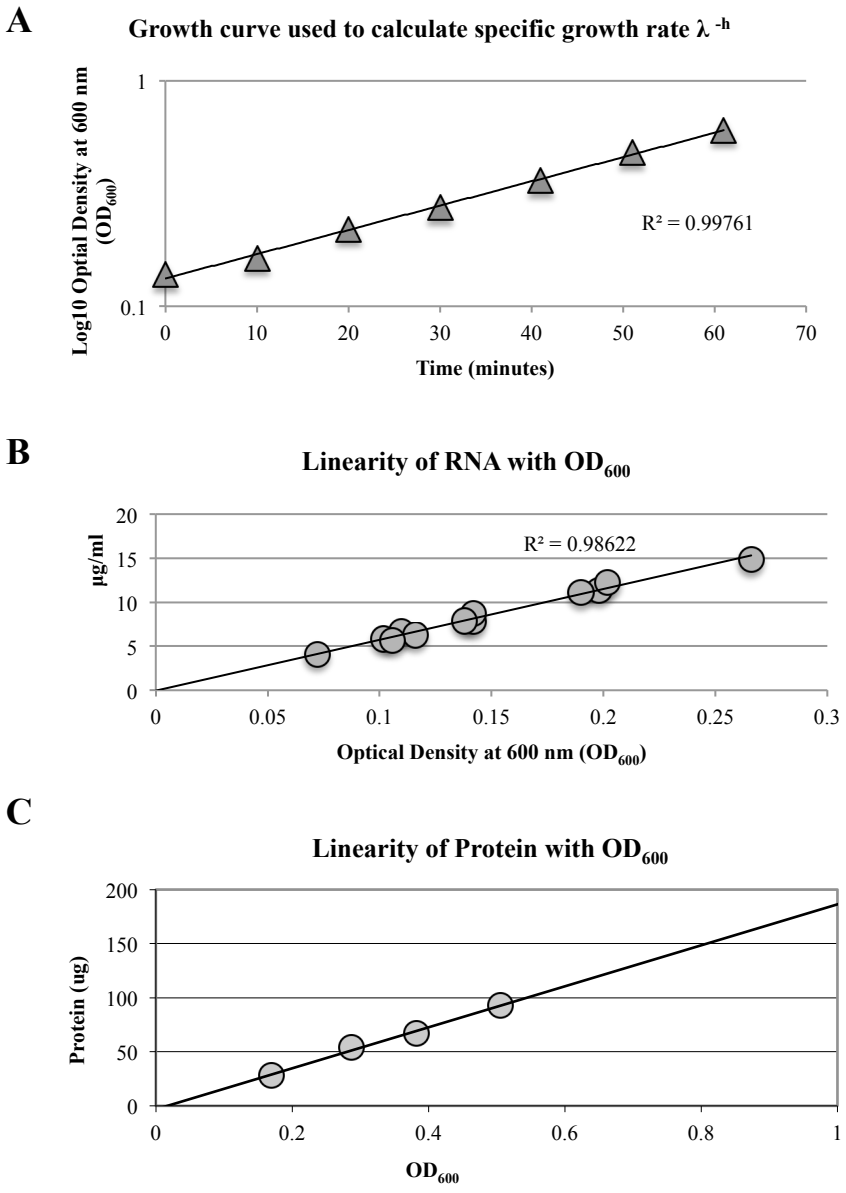

Supplementary Figure 3.2: Examples of growth rate, rRNA and protein curves for determining the RNA/Protein versus λ^{-h}. ***A)*** *Growth rates. Only growth rates with an R^2 value greater than 0.99 were used for calculation of the linear trend.* ***B)*** *RNA versus OD_{600}. The linearity of RNA quantity was verified for each sample to ensure accurate quantification.* ***C)*** *Protein versus OD_{600}. The linearity of protein quantity was verified for each sample to ensure accurate quantification.*

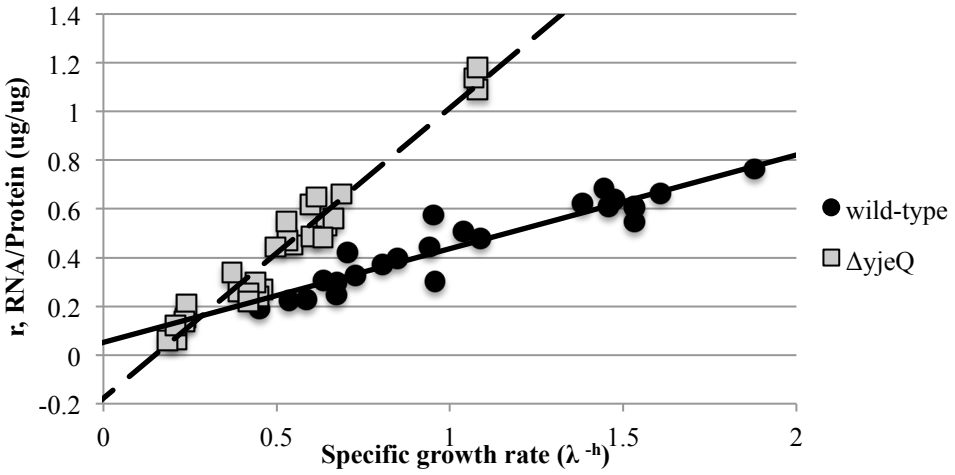

Supplementary Figure 3.3: RNA/Protein (µg/µg) as a function of specific growth rate λ^{-h} for the wild-type and ΔyjeQ. *Each plot contains >20 distinct samples for which growth rate and RNA/Protein (r,) are calculated.*

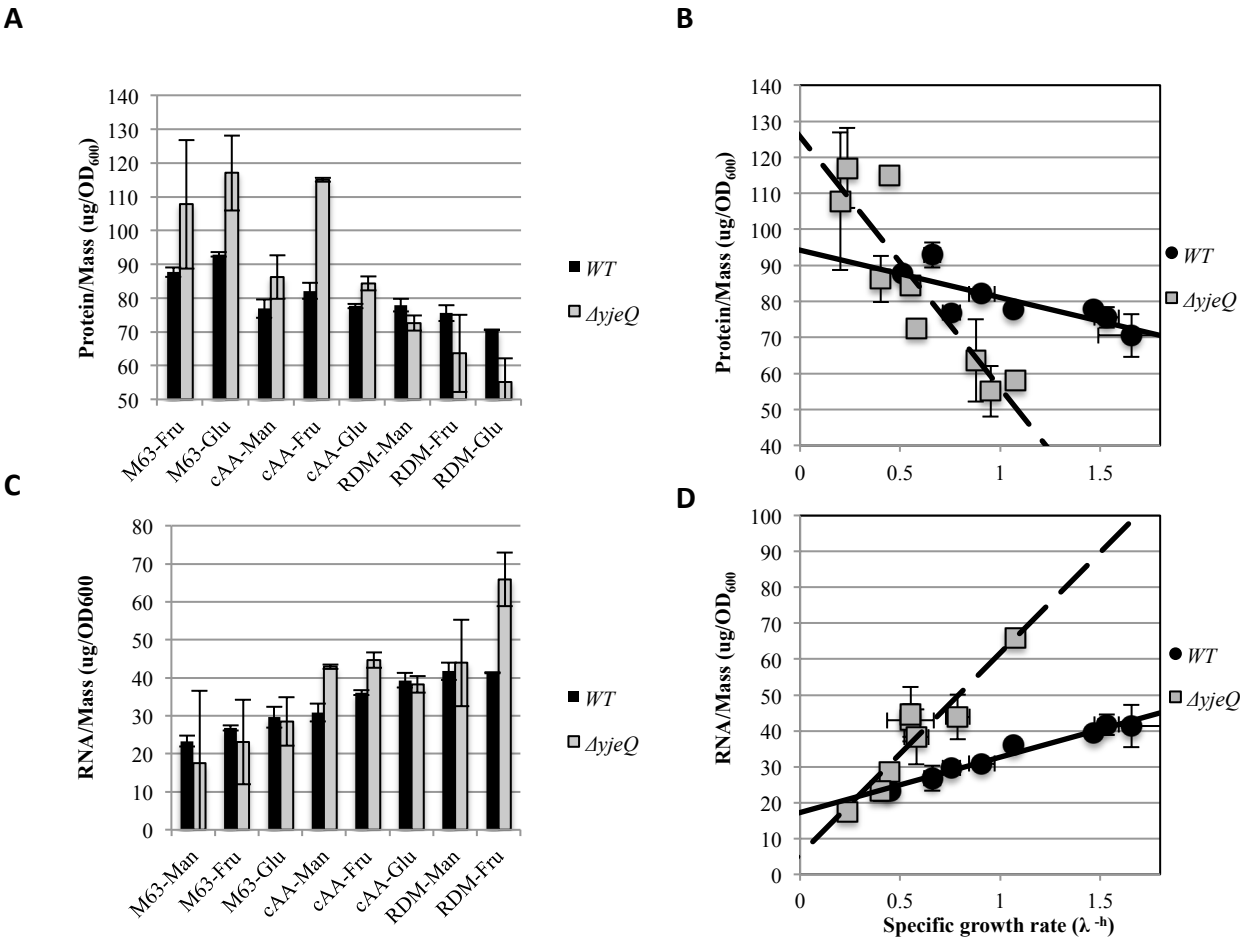

Supplementary Figure 3.4: RNA and protein concentration in the ΔyjeQ deletion. A) *Bar graph showing the concentration of protein (μg/OD_{600}) for the wild-type and ΔyjeQ mutant in each media. Media has been ordered from poorest to richest.* ***B)*** *Plot showing the concentration of protein (μg/OD_{600}) versus specific growth rate λ^{-h} for the wild-type and ΔyjeQ mutant. Protein concentration in the wild-type is approximately constant over the range of growth/media, rising modestly. Protein concentration in the ΔyjeQ increases sharply as growth rate decreases.* ***C)*** *Bar graph showing the concentration of RNA (μg/OD_{600}) for the wild-type and ΔyjeQ mutant in each media. Media has been ordered from poorest to richest to poorest.* ***D)*** *Plot showing the concentration of RNA (μg/OD_{600}) versus specific growth rate λ^{-h} for the wild-type and ΔyjeQ mutant. The RNA concentration in both strains exhibits growth rate-dependence in the form of a linear trend. Collectively, this illustrates that while RNA/Protein is not an equivalent treatment of ribosome content for both strains, ribosomal material is indeed elevated in the mutant for any given growth rate. In addition, the ratio of RNA/Protein is substantially higher in the mutant at fast growth rates.*

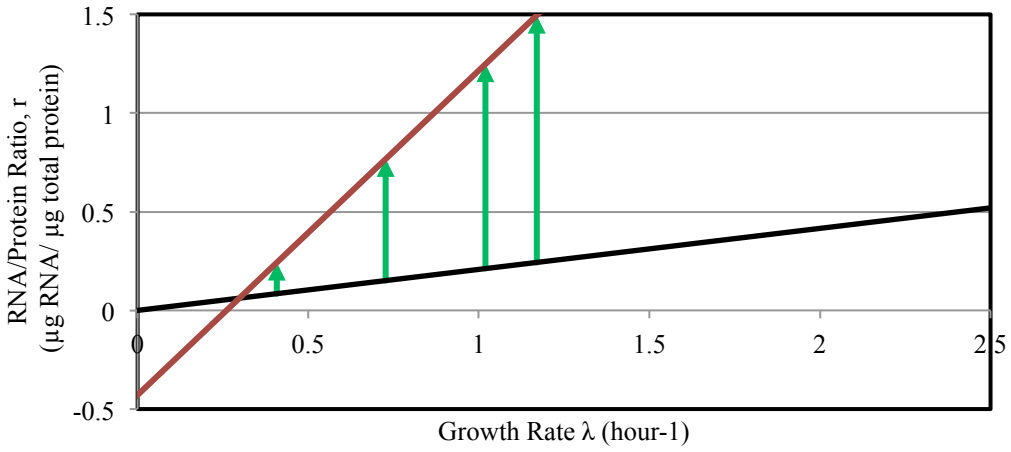

Supplementary Figure 3.5: Model for growth rate-dependence in yjeQ-null cells. *Total ribosomal material (r) in the ΔyjeQ strain is shown in red with respect to growth rate. The assumption in this model is that actively translating ribosomes in ΔyjeQ cells have the same translational efficiency as those in wild-type cells. As such, the number of functional ribosomes in the ΔyjeQ deletion at any given growth rate can be extrapolated from the slope of λ vs r curve for wild-type cells (black line). As this does not include any non-functional ribosomal material the linear trend passes through the origin. The non-functional ribosomal material in the cell is difference between total and functional ribosomal material (r_{nf} green). The value of r_{nf} has a minimum value, as seen in wild-type cells (dashed black line). As growth rate decreases, the value of r approaches this basal amount of non-functional ribosomal material beyond which it cannot decrease. Thus, the λ vs r trend for the yjeQ-null is asymptotic to the minimum level of non-functional material seen in wild-type and translation mutants. We hypothesize that this point represents growth conditions in which biogenesis is no longer limiting to growth rate. At this point the yjeQ-null would behave essential like the wild-type.*

Gene	**Biogenesis Factors**
rimJ	Maturation of 30S/ alanine acetyltransferase [105, 107]
rimL	r-protein modification [202]
rluC	RNA modification [203]
rmf	70S dimerization [204]
rmlA	RNA modification [103]
cafA	RNase G 16S, [80, 84]
prmA	RNA modification [104]
rsmC	RNA modification [205]
rpH	RNase PH, 16S RNA processing [206]
rimM	30S maturation [114, 116, 129, 133]
rlmE	RNA modification [207]
ksgA	RNA modification [208, 209]
rluD	RNA modification [102]
rsuA	RNA modification [210]
rimI	r-protein modification [211]
rsmB	RNA modification [205]
rbfA	30S maturation [116, 119, 122, 123]
	Translation and tRNA Modification Factors
tgt	tRNA transglycosolyase [212, 213]
truA	tRNA pesudouridine synthase [214]
trmU	tRNA modification, 2-thiouridine synthesis [215]
efp	Peptide synthesis, anti-stalling mechanism [216, 217]
lysU	tRNA synthetase [218]
prfC	Release factor 3 [219, 220]
prmA	tRNA modification [221]
selA	tRNA modification [222]
truB	tRNA modification [223]
selB	Translation factor for selenocysteine incorporation [224]
ligT	Phosphoesterase [225]
opgB	Phosphoglycerol transferase [226]
trmJ	tRNA nethyltransferase [227]
trmE	tRNA modification, 2-thiouridine synthesis [196]
relA	(p)ppGpp synthase [228, 229]
rnd	RNase D, tRNA processing [230]
queG	Epoxyqueeuosine reductase [231]
pcnB	Poly(A) polymerase I [232]
dtd	tRNA deacylase [233]
ssrA	10Sa RNA, prevents ribosomal stalling [234]

Supplementary Table 4.1: Shortlist of gene-deletions for 37 putative ribosome-associated factors. *Genes were sourced from the Keio deletion collection and confirmed by sequencing.*